AD NUMBER

ADC017835

CLASSIFICATION CHANGES

TO: unclassified

FROM: secret

LIMITATION CHANGES

TO:

Approved for public release, distribution unlimited

FROM:

Controlling DoD Organization. Commanding Officer, Naval Ocena Systems Center, San Diego, CA.

AUTHORITY

ONR ltr, 3 Dec 2003; ONR ltr, 3 Dec 2003

SECRET

NOSC

LEVEL II

NOSC TR 394

Technical Report 394

HORIZONTAL DIRECTIONALITY OF AMBIENT NOISE DURING THE CHURCH OPAL EXERCISE (U)

R. A. Wagstaff

October 1978

"NATIONAL SECURITY INFORMATION"

"Unauthorized Disclosure Subject to Criminal Sanctions"

Classified by: OPNAVINST S5510.72D of 7 February 1977
Review on: 7 February 1997

NAVAL OCEAN SYSTEMS CENTER
SAN DIEGO, CALIFORNIA 92152

SECRET

NAVAL OCEAN SYSTEMS CENTER, SAN DIEGO, CA 92152

AN ACTIVITY OF THE NAVAL MATERIAL COMMAND

RR GAVAZZI, CAPT USN
Commander

HL BLOOD
Technical Director

ADMINISTRATIVE INFORMATION (U)

(U) The work reported herein was sponsored by the Long Range Acoustic Propagation Project (LRAPP), Naval Ocean Research and Development Activity Code 600 under Program Element 63795N.

(U) Mr. L. K. Arndt was the technical reviewer for this report.

(U) Contributions to this work by Robert B. Marusich and Associates were provided under Contract No. N66001-77-M-9295.

Released by
M. R. AKERS, Head
System Concepts and Analysis
Division

Under authority of
H. A. SCHENCK, Head
Undersea Surveillance
Department

ACKNOWLEDGMENTS (U)

(U) Acknowledgment of Mr. J. W. Aitkenhead's contributions to the work reported herein is especially appropriate. Mr. Aitkenhead assisted in collecting data during the at-sea portion of the exercise, helped develop the computer programs necessary for data analysis activities and processed much of the data, both aboard ship and during the post-exercise analysis.

(U) Dr. Gordon Martin's analysis of the high-frequency artifacts and the eventual explanation of these unusual phenomena are similarly acknowledged.

(This page is unclassified)

UNCLASSIFIED

SECURITY CLASSIFICATION OF THIS PAGE (When Data Entered)

SECRET

REPORT DOCUMENTATION PAGE

READ INSTRUCTIONS BEFORE COMPLETING FORM

1. REPORT NUMBER: NOSC TR-394	2. GOVT ACCESSION NO. ✓
3. RECIPIENT'S CATALOG NUMBER	
4. TITLE (and Subtitle): HORIZONTAL DIRECTIONALITY OF AMBIENT NOISE DURING THE CHURCH OPAL EXERCISE (U)	5. TYPE OF REPORT & PERIOD COVERED: Research Report Oct 75 – Oct 78
	6. PERFORMING ORG. REPORT NUMBER
7. AUTHOR(s): R. A. Wagstaff	8. CONTRACT OR GRANT NUMBER(s)
9. PERFORMING ORGANIZATION NAME AND ADDRESS: Naval Ocean Systems Center, San Diego, CA 92152	10. PROGRAM ELEMENT, PROJECT, TASK AREA & WORK UNIT NUMBERS: 63795N
11. CONTROLLING OFFICE NAME AND ADDRESS: Naval Ocean Research and Development Activity, NSTL Station, MS 39529	12. REPORT DATE: October 1978 13. NUMBER OF PAGES: 82
14. MONITORING AGENCY NAME & ADDRESS (if different from Controlling Office) 12 75	15. SECURITY CLASS. (of this report): SECRET 15a. DECLASSIFICATION/DOWNGRADING SCHEDULE: Review on 7 February 1997

16. DISTRIBUTION STATEMENT (of this Report)

17. DISTRIBUTION STATEMENT (of the abstract entered in Block 20, if different from Report)

18. SUPPLEMENTARY NOTES

19. KEY WORDS (Continue on reverse side if necessary and identify by block number)

Underwater sound propagation
Noise propagation
Sonar
Noise measurement
Towed array

20. ABSTRACT (Continue on reverse side if necessary and identify by block number)

(U) Ambient noise horizontal directionality was measured in the Northeast Pacific Ocean during the CHURCH OPAL exercise of September 1975. Results obtained from the analysis of data acquired by a towed line-array are reported. The results for frequencies dominated by shipping (below 200 Hz) indicate a definite north-south bias in excess of 15 dB at some frequencies. The results are similar to the CHURCH ANCHOR results obtained at the same location 2 years previously, supporting the idea that the pseudo-stationary background noise is repeatable and hence, predictable.

393 159

DD FORM 1 JAN 73 1473 EDITION OF 1 NOV 65 IS OBSOLETE
S/N 0102-LF-014-6601

UNCLASSIFIED

SECURITY CLASSIFICATION OF THIS PAGE (When Data Entered)

SECRET

(This page is unclassified)

CONTENTS (U)

ILLUSTRATIONS (U)

ILLUSTRATIONS (U) (Continued)

TABLES (U)

SECTION 1. (U) SUMMARY

1.1 (U) OBJECTIVES

(U) The objectives of the CHURCH OPAL exercise pertaining to the ambient noise horizontal directionality measurements were:

- Measure the horizontal directionality of ambient noise in the Northeast Pacific with a long-aperture array and report the results for a wide range of frequencies.
- Compare the measured directionality patterns with those obtained two years previously during CHURCH ANCHOR to determine whether they are repeatable and hence predictable.
- Obtain a data base to support regional assessment and regional assessment objectives.

1.2 (U) CONCLUSIONS

(C) In the frequency regime between 10 Hz and approximately 200 Hz, the ambient noise field at Sofar channel depths in the Northeast Pacific Ocean has persistent directional properties. The noise levels are 5 dB to 15 dB higher in the north and northwesterly directions toward the Aleutian Islands arc and in the east or northeasterly directions toward the west coast of the United States than along southerly azimuths. Shipping along the basin boundary is believed responsible for the observed directional characteristics. Shipping noises are introduced into the Sofar channel through downslope propagation (and possibly other means). Once in the Sofar channel, the noise travels throughout the Northeast Pacific by way of the favorable (low-loss, continuously refracted) propagation paths. Consequently, any model used to calculate low-frequency noise at Sofar channel depths within the Northeast Pacific Ocean must include the noise which arrives from distant sources in order to agree with measured data for noise depth dependence and vertical and horizontal directionality.

(U) CHURCH OPAL and CHURCH ANCHOR measurements, separated by 2 years, suggest that the gross characteristics of the spatially and temporally smoothed horizontal directionality patterns are repeatable year after year, provided that shipping along the basin boundaries does not change radically. The noise in the Northeast Pacific is, therefore, predictable and modelable with reasonably high confidence.

(C) Most of the noise at 19 Hz is attributed to biological sources, the main contribution believed due to the fin whale. The horizontal directionality of this noise is similar to that for shipping, (i.e., high levels toward the Aleutian Islands arc, where the fin whale population density is expected to be large). Relatively high noise levels toward the west coast of the United States below the Mendocino Escarpment were also observed. However, since the contribution from these azimuths to the total noise is minor, the relative amounts that are due to whales and shipping is uncertain.

(C) Narrow-beam systems (i.e., those with beamwidths of 1°-2°) can achieve minimum beam noise levels on one or more beams which are surrounded by high noise level beams. In the present measurements, the level of the null below the omnidirectional noise level closely corresponds to the array's side-lobe suppression level. This suggests that arrays

with narrower beams and greater side-lobe suppression levels (in excess of 24 dB) may measure deeper nulls and, hence, have increased detection capabilities.

1.3 (U) RECOMMENDATIONS

(C) The increased understanding of directional noise properties obtained in recent years is just beginning to impact fleet operational systems. Since LRAPP measurements are responsible for much of the knowledge obtained, it is strongly recommended that the measurement program be continued. End results from the program should be focused on assessments of environmental conditions in various geographic areas in order to provide guidance in the tactical use of fleet systems.

(U) The directionality of the ambient noise field in the Sofar channel of the Northeast Pacific Ocean has been measured at approximately two different depths (180 and 500 m) during September 1973 and September 1975. Measurements should be made at other depths and other times of the year in order to obtain a more complete understanding of the temporal variability and depth dependence of the directional noise properties.

(U) Horizontal directionality measurements should also be made below the critical depth, where the noise along a given azimuth is strongly influenced by the ocean's bathymetry. This type of data would greatly enhance the Navy's noise modeling capability.

(U) Measurements of the horizontal directionality characteristics at widely distributed locations in the Northeast Pacific Ocean are desirable. Such measurements would help confirm the hypothesis that basin boundary shipping is responsible for the majority of the noise anticipated at other geographic locations.

(U) Simultaneous measurements acquired by two horizontal line arrays at nearly the same location are also desired. Such data could be used to estimate noise field directionality without the delays arising from the single array heading changes. High-resolution, instantaneous directionality estimations could be obtained from these data.

(C) Certain results indicate that noise levels toward southerly azimuths were below the measurement capability of the LAMBDA configuration deployed during CHURCH OPAL. It would be most interesting to perform similar measurements using a system which achieves side-lobe suppression levels in excess of 40 dB. This, perhaps, could be accomplished with the LAMBDA array if the exact positions of the elements are known during the measurement and a modified binomial spatial shading scheme is employed.

SECTION 2. (U) INTRODUCTION

2.1 (U) BACKGROUND

(C) Acoustic and environmental properties of the Northeast Pacific Ocean have been studied in considerable detail during the last decade. Of the scientific investigations conducted during this time frame, the CHURCH ANCHOR Exercise (September 1973) is by far the most comprehensive and detailed. The extensive data base acquired during CHURCH ANCHOR encouraged the scientific community to examine acoustic/environmental properties of the water mass in a level of detail that was heretofore not possible. Consequently, the detailed analyses of the CHURCH ANCHOR data base gave rise to a number of hypotheses and questions concerning the acoustic characteristics that, in turn, led to the definition of a new set of acoustic data collection/measurement requirements.

(C) Horizontal directionality characteristics of the ambient noise field were examined in considerable detail during CHURCH ANCHOR, since these properties have a strong influence on towed array system design parameters. Results indicated that ambient noise levels were from 5 to 15 dB greater in directions toward the Aleutian Islands arc and the west coast of the United States than in other directions. The anisotropic character of the noise field was attributed, primarily, to the uneven distribution of surface shipping traffic within the basin. Extending this line of reasoning, it was hypothesized that many of the ambient noise field properties would be repeatable from year to year if the surface shipping pattern did not change drastically from one September to the next. If this hypothesis is correct, then much of the ambient noise field (at least in the frequency regime from 10 Hz to 200 Hz) could be modeled with relatively high confidence levels.

(C) The CHURCH OPAL Exercise was intended to satisfy many of the data requirements arising from the analysis of CHURCH ANCHOR measurements, including those pertaining to the directional nature of the ambient noise field. Consequently, planning for CHURCH OPAL centered on supplementing the CHURCH ANCHOR data base, not repeating the earlier exercise in its entirety. Although the scope and extent of the CHURCH OPAL Exercise were smaller than those of CHURCH ANCHOR, it was nonetheless a major undertaking. Resources committed to the CHURCH OPAL Exercise included the following:

- The Large Aperture Marine Basic Data Array (LAMBDA) deployed from M/V SEISMIC EXPLORER at sites λ_1, λ_A and λ_B (see Fig. 1).
- Acoustic data capsules (ACODAC's), the Delta horizontal drift array and the HX-231F acoustic projector deployed from R/V MOANA WAVE.
- A VIBROSEIS acoustic projector deployed from AMERICAN DELTA II.
- P-3A aircraft from U. S. Navy Squadron VXN-8.
- WARF and SEA ECHO over-the-horizon (OTH) radars.

Since the intent was to acquire acoustic measurements that were directly comparable to corresponding CHURCH ANCHOR data, at-sea operations were limited to the same seasonal time frame and geographic locations as the previous exercise. Thus, at-sea operations were conducted during September 1975 at several sites in the Northeast Pacific Ocean that were occupied during the CHURCH ANCHOR Exercise. The detailed plan for the exercise is contained in Ref. 1. References 2 and 3 summarize overall results of the exercise and contain a bibliography of related documentation.

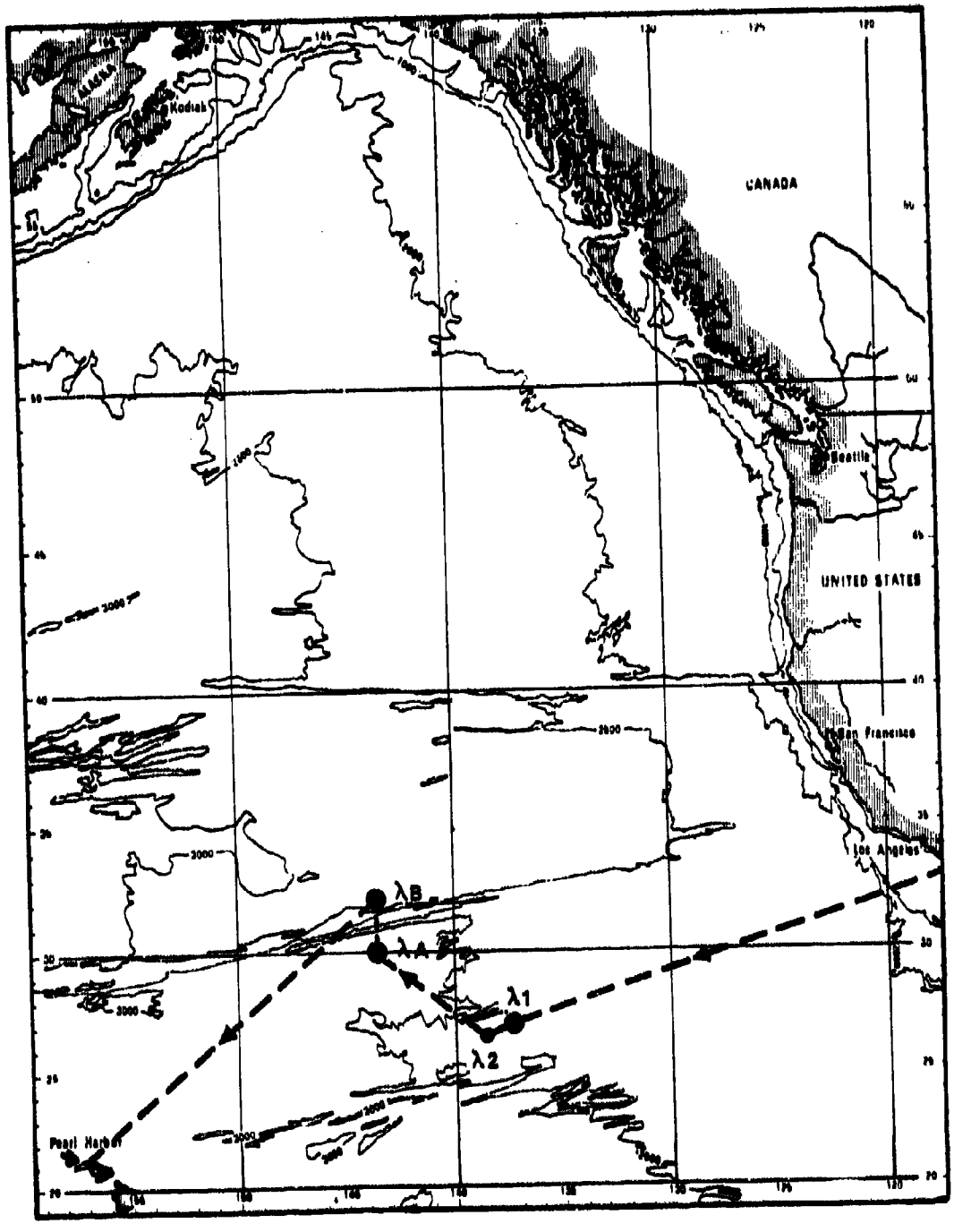

Figure 1. (C) LAMBDA measurement sites and M/V SEISMIC EXPLORER's track during the CHURCH OPAL Exercise. (U)

2.2 (U) SCOPE OF REPORT

(C) This document presents ambient noise field characteristics that were determined from acoustic measurements acquired with LAMBDA. The primary emphasis in this report is placed on the horizontal directionality of the ambient noise field. However, other characteristics such as omnidirectional levels, beam noise levels, and related statistics are also addressed. Complete analytical results from the LAMBDA measurements are presented whenever possible (e.g., horizontal directionality characteristics and omnidirectional levels). Where presentation of the complete results would be impractical (e.g., beam noise levels, array gain estimates, etc.), representative selections have been included to illustrate the key features or the primary characteristics. More detailed information concerning the LAMBDA ambient noise measurements acquired during CHURCH OPAL and the analyses thereof are available from the Naval Ocean Systems Center (Code 714).

(U) Ambient noise characteristics that were determined from acoustic measurements acquired with other devices (e.g., ACODAC, DELTA, etc.) are beyond the scope of this report. Similarly, the results of other investigations with LAMBDA during the CHURCH OPAL Exercise are not addressed herein. All such information has been or will be published separately (see Ref. 3).

2.3 (U) ORGANIZATION OF REPORT

(U) This report consists of five numbered sections and three appendixes. The first section summarizes the main findings and conclusions drawn from the data acquisition and analysis activities. The conduct of LAMBDA operations during CHURCH OPAL and a brief description of the data processing/analysis techniques are presented in Section 3. Analytical results are presented in Section 4 together with a discussion of the observed ambient noise characteristics. Project documentation and technical references are listed in Section 5.

(U) Appendix A contains a technical description of the LAMBDA array and associated shipboard electronics. Representative environmental information for the Northeast Pacific Ocean is included as Appendix B, while Appendix C presents certain analytical results in more detail.

SECTION 3. (U) LAMBDA AMBIENT NOISE MEASUREMENTS

3.1 (U) EXERCISE OBJECTIVES AND EXPERIMENT DESIGN

(C) Ambient noise measurements were acquired with the Large Aperture Marine Basic Data Array (LAMBDA) in support of three specific objectives delineated in the CHURCH OPAL Exercise plan (Ref. 1):

- Inter-array coherent processing;
- Horizontal directionality of ambient noise; and
- Towed array performance.

In general, the CHURCH OPAL Exercise was structured to investigate each objective individually and, for the most part, the duration of the experimental period was partitioned among the various technical objectives. Each principal investigator was allowed to specify the disposition and geometry of the available assets during his allocated measurement time periods. As a result, the LAMBDA measurements are usually applicable to only one of the exercise's technical objectives even though there may be considerable overlap between several of the technical objectives.

(C) The LAMBDA configuration deployed during the CHURCH OPAL Exercise contained three different 64-element arrays within the towed streamer. LAMBDA was particularly well suited for ambient noise directionality investigations since its multi-array design provided a high degree of azimuthal resolution (i.e., narrow beamwidths) over a relatively broad frequency range. LAMBDA's multi-array configuration also allowed the directional character of the noise field to be determined with varying amounts of spatial smoothing (i.e., different beamwidths) at several discrete frequencies. A more complete description of the LAMBDA system is included as Appendix A and should be consulted for additional information and/or operational characteristics.

(C) Acoustic measurements for noise directionality investigations were acquired during CHURCH OPAL in much the same manner as in previous exercises. M/V SEISMIC EXPLORER's tracks during the data acquisition intervals followed the usual polygon pattern that evolved from CHURCH ANCHOR and similar exercises (see Refs. 1 and 2 for detailed run geometries). Two and one-half hours were required to complete each leg of the polygon. Approximately 1.75 hours were allowed to change course and stabilize the LAMBDA arrays on the new heading. The remaining 45 min constituted the data acquisition window which, in turn, was further subdivided into three 15-min data-sampling intervals. Measurements were taken during the three 15-min periods with the LAMBDA HF, MF, and LF arrays (in that order) to allow the longer arrays more time for stabilization after a turn. M/V SEISMIC EXPLORER's speed during a typical polygon leg was on the order of 2 knots; however, turns were executed occasionally at somewhat higher speeds.

(C) Array depths during the measurements were planned for approximately 550 and 150 m. The larger of these, near the deep sound channel axis, was chosen to facilitate the comparison of CHURCH OPAL results with like data from the CHURCH ANCHOR Exercise (September 1973). Measurements at the shallower depth were accomplished to satisfy both the inter-array coherent processing and the ambient noise field characterization objectives.

(C) Noise polygon maneuvers provided independent measurements of time-averaged beam noise levels on several headings. Since the LAMBDA beamformer supplied for this exercise had full azimuthal coverage, three sets of measurements on headings approximately 120 deg apart were necessary to resolve the ambiguities due to the horizontal line array's symmetrical beam patterns. However, five sets of measurements (or more) are preferred in order to increase the confidence levels applicable to the results.

3.2 (U) OPERATIONS SUMMARY

(U) The LAMBDA system was made available for noise directionality measurements periodically throughout the exercise. The six time periods allocated for this purpose are listed in Table 1 together with the approximate coordinates of the actual measurement sites.

(U) At CHURCH OPAL Sites λ_1 and λ_A the allocated time periods were only long enough to obtain data on two different headings. Since an acoustic projector was not available to provide a heading reference during either set of measurements, they were of limited value and were used mainly to test the ambiguity-resolution algorithm. Data acquired with the HF array at the first site (λ_1) were characterized by high-level noise measurements on the aft endfire beam, and it appeared that some noisy source was following the array. It was soon discovered that the inputs to the Three Array Processor were connected backwards (inverted). The improper connections caused an inversion in the beam steering angles and the high-level noise source that appeared to be following the array was, in fact, the tow ship preceding the array. This problem was eliminated by changing the sign convention for the beam steering angles (i.e., negative angles forward of broadside and positive angles aft).

(C) The four time periods allocated for noise directionality measurements at CHURCH OPAL Site λ_B are also given in Table 1. These measurement periods were sufficient to obtain data on 4, 6, 11, and 5 different array headings, respectively. Acoustic data acquired at CHURCH OPAL Site λ_B with the LAMBDA system constitute the entire set of measurements used in the ambient noise directionality analysis reported in Section 4.

Table 1. (C) LAMBDA deployment parameters for CHURCH OPAL ambient noise directionality investigations. (U)

Date/Time September 1975/ZULU)		Site	Location		Array Depth (meters)
Start	Finish		Latitude	Longitude	
081919	082231	λ_1	26° 11′N	137° 47′W	152
110702	111107	λ_A	29° 50′N	143° 58′W	610
131206	132210	λ_B	31° 54′N	143° 46′W	182
141851	150900	λ_B	31° 45′N	142° 54′W	518
232038	242215	λ_B	32° 00′N	143° 04′W	488
250015	251030	λ_B	32° 03′N	143° 31′W	182

(C) About half-way through the measurements at Site λβ, leaks developed in two modules used in both the MF and LF arrays. The two defective array modules ("B" sections) were removed but could not be replaced since spares were not available aboard the ship. After removal of the two defective array modules, the LAMBDA MF and LF arrays contained 58 and 62 hydrophone groups, respectively. To account for these changes, appropriate spatial shading coefficients were set to zero in the Three-Array Processor. The HF array remained unchanged throughout the exercise with 63 operable hydrophone groups; HF hydrophone group number 42 was inoperative from the beginning of the exercise.

(U) A number of minor problems occurred during the acquisition of the noise directionality data. Most of these were either due to operator errors or equipment malfunctions. They had no effect on the results since the contaminated data were discarded upon discovery and the data retaken.

(U) Only a limited amount of data processing and analysis could be accomplished aboard M/V SEISMIC EXPLORER during the conduct of the exercise as opposed to the extensive data analysis effort that had been planned. Data processing software for the noise directionality analyses had been developed to utilize the output of a Double Fast Fourier Transform (DFFT) beamformer which was anticipated to be operational for CHURCH OPAL. However, this unit was not operational until approximately 6 months after the exercise. As a result, the Three Array Processor (TAP) became the primary unit for spectral analysis and beamforming of the LAMBDA array outputs. Since the TAP's outputs were not compatible with most of the data analysis software (especially the statistical tests intended for quality control purposes), the majority of the data were processed and analyzed ashore during the post-exercise period.

3.3 (U) DATA ACQUISITION

3.3.1 (U) Analysis Frequencies and Bandwidths

(S) Analysis frequencies and bandwidths selected for the LAMBDA horizontal directionality measurements are presented in Table 2. As shown therein, the highest analysis frequency for each LAMBDA array corresponds to the approximate design (half-wavelength) frequency for that array (i.e., 19, 57 and 320 Hz for the LF, MF, and HF arrays, respectively). The analysis frequencies shown in Table 2 are ordered in columns of approximately equal beamwidths. For example, the LF, MF and HF arrays have nearly identical beam patterns at 6.5, 19 and 100 Hz, respectively. Frequencies of 11, 19, and 50 Hz are common to more than one array and allow the effects of different beamwidths to be investigated. Since the LAMBDA wet end did not include heading sensors during this exercise, an acoustic projector was located on a known azimuth and used as a beacon for accurate estimates of the array's heading. The projector's beacon frequencies are also noted in Table 2. Unfortunately, the projector operated below expectations and was detectable only about half the time during the noise measurements. When the projector was not detectable, the array heading was, by default, assumed equal to ship's heading. It should also be noted that the analysis bandwidths given in Table 2 correspond to the spectral analysis bin widths used in the discrete Fourier transform (DFT) algorithm. Since the DFT inputs (in the time domain) were amplitude weighted by a Hann window, the actual spectral analysis bandwidths (-3 dB points) are 0.8 Hz and 1.6 Hz instead of the 0.5 and 1.0 Hz values shown.

Table 2. (S) Spectral analysis frequencies and bandwidths for CHURCH OPAL ambient noise directionality investigations. (U)

LAMBDA Array	Analysis Frequencies[1] (Hz)								Analysis Bandwidth (Hz)
Low Frequency			6.5	9.5	11	12[2]		19	1.0
Mid Frequency		11	19			36	50	57[2]	0.5
High Frequency	50		100	156[2]	192			320	0.5
Broadside Beamwidth Multiplier[3]	6.4	5.2	3.0	2.0	1.7	1.6	1.1	1.0	

Notes:

(1) Analysis frequencies are ordered such that each column of values has approximately equal beamwidths.

(2) Acoustic projector transmission frequencies.

(3) Broadside beamwidth multiplier $= \frac{\text{Array Design Frequency } (f_{\lambda/2})}{\text{Analysis Frequency } (f_a)}$

$= \frac{\text{Beamwidth at } f_a}{\text{Beamwidth at } f_{\lambda/2}}$

3.3.2 (U) Calibration

(U) The LAMBDA shipboard electronic equipment was calibrated to yield absolute sound pressure spectrum levels (SPSLs) relative to 1 μPa. The TAP gain was measured as the first step in the calibration sequence. This was accomplished by injecting a constant-amplitude signal into all TAP input channels and recording the output level while varying the frequency. The measured gain of the TAP was then combined with hydrophone sensitivities, array gains, and bandwidth correction factors to establish the overall gain of the measurement apparatus and, thereby, permit the computation of SPSLs at the hydrophone input terminals. The TAP gain measurement was performed at the beginning of the exercise and was not repeated.

(U) The second part of the TAP calibration process was performed before data collection activities commenced at each site. This step calibrated the TAP's beamformer by equalizing the gain and phase in every one of 64 input channels for each of the three LAMBDA arrays. For this calibration, a sine wave was injected into the signal conditioning units (SCUs) at selected analysis frequencies. The TAP's internal calibration routine then obtained the amplitude and phase differences relative to a reference channel and calculated correction factors (complex numbers) to equalize the amplitude and phase in each channel.

(U) Only three calibration tables were provided in the TAP for each LAMBDA array and, thus, a separate calibration table was not available for every one of the five analysis frequencies. However, the TAP was calibrated for each array at the five frequencies shown

in Table 2; results of the calibration routine were then compared to determine the best compromise for the beamformer calibration tables. For example, the header information in Fig. 2 indicates that MF array calibration table 3 was used to equalize measurements at 57, 50 and 36 Hz. Similarly, MF array calibration tables 2 and 1 were used to equalize measurements at 19 and 11 Hz, respectively.

3.3.3 (U) Data Collection

(C) LAMBDA ambient noise measurements were collected automatically by the TAP. The system operator on watch had to initialize each 15-min run and exercise supervisory control but was not required to log much information manually. The basic sequence of operator actions which occurred during any 15-min data-sampling period is outlined below:

a. Select the LAMBDA array (HF, MF or LF) to be used and configure the analog signal conditioning equipment accordingly.

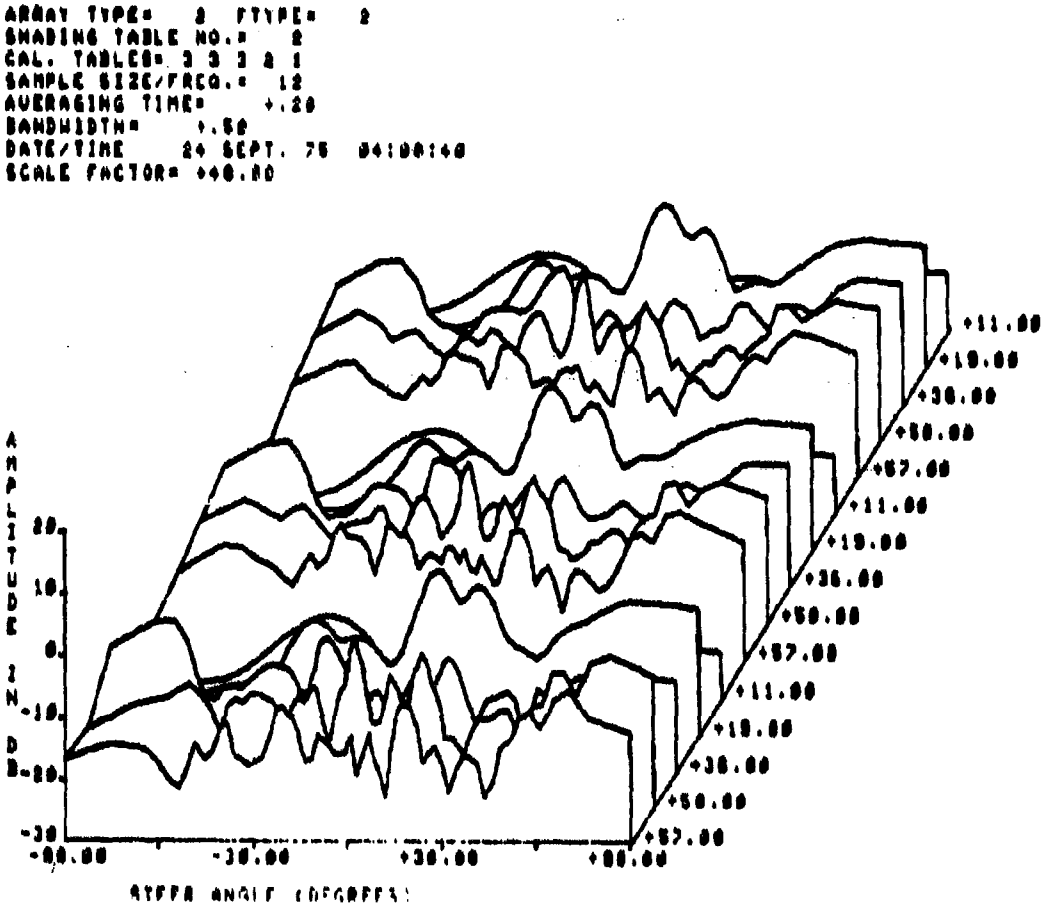

Figure 2. (S) Three array processor display format for beam noise measurements. (U)

b. Initialize the TAP for the run by selecting:

- Hann window for amplitude-weighting of the DFT input data in the time domain;
- Applicable table of spatial shading coefficients; Note: Hann shading function always used.
- DFT bin width (0.5 Hz or 1.0 Hz from Table 2);
- The set of analysis frequencies (from Table 2);
- One calibration table for each analysis frequency;
- Number of DFTs to be taken at each frequency (NS);
- Number of iterations through the set of analysis frequencies (NG); and
- Start time and date for the particular run.

c. Obtain hard copy plots and tabular listings of the acquired data in the formats shown in Figs. 2 and 3.

PLOT DATA TABLE 24 SEPT. 78 04:00:40
NUMBER OF UPDATES= 0 SCALE FACTOR +40.00 PTYPE= 2
ARRAY = 3 SHADING TABLE NO.= 2 CAL. TABLE= 3 3 3 3 1
SAMPLE SIZE= 512 AVERAGING TIME= +.00 BANDWIDTH= +.50

STR. ANGLE (DEG)	FREQ./	AMPLITUDE (DB)				
	+37.00	+30.00	+36.00	+10.00	+11.00	
-90.00		-15.64	-13.42	-11.40	-20.36	-27.00
-78.52		-12.28	-9.00	-7.41	-25.30	-27.55
-69.47		-11.76	-11.32	-7.21	-24.62	-20.73
-64.78		-14.76	-14.11	-10.33	-24.24	-25.63
-60.01		-15.07	-13.07	-15.63	-24.13	-24.30
-57.27		-17.21	-12.70	-17.05	-23.05	-23.00
-54.04		-17.00	-14.60	-17.03	-23.61	-21.07
-51.05		-16.05	-15.00	-10.03	-22.00	-20.70
-48.24		-14.25	-17.01	-10.14	-22.02	-10.07
-45.50		-16.40	-16.00	-17.00	-21.30	-10.14
-43.04		-14.00	-13.04	-15.05	-20.01	-10.52
-40.00		-10.00	-13.56	-10.17	-10.07	-10.20
-30.24		-10.22	-14.70	-15.03	-10.04	-10.15
-35.05		-10.00	-14.30	-15.04	-14.44	-10.10
-33.74		-11.20	-12.05	-15.10	-13.03	-10.30
-31.00		-11.05	-12.02	-15.00	-13.40	-10.74
-20.47		-12.40	-14.22	-15.17	-14.00	-10.23
-27.40		-15.04	-10.05	-14.04	-15.00	-10.00
-25.37		-13.20	-15.01	-12.05	-10.04	-20.03
-23.37		-0.53	-12.10	-10.33	-10.23	-21.51
-21.41		-0.00	-10.01	-0.02	-15.03	-22.46
-10.47		-0.03	-0.01	-0.40	-15.44	-23.30
-17.05		-10.01	-0.02	-0.41	-15.30	-24.13
-15.05		-12.09	-12.00	-10.01	-15.07	-24.00
-13.77		-15.54	-15.13	-15.00	-16.07	-24.70
-11.00		-15.30	-10.00	-17.01	-10.03	-24.04
-10.05		-14.70	-15.11	-10.41	-17.70	-24.40
-0.01		-14.74	-12.05	-10.01	-10.20	-24.33
-0.37		-15.31	-5.03	-17.00	-10.12	-24.20
-4.05		-13.46	-3.20	-15.72	-17.01	-24.00
-2.72		-12.01	-0.20	-15.55	-14.04	-23.04
-.00		-13.10	-13.03	-15.00	-12.10	-23.74
+.00		-12.00	-15.04	-17.07	-10.00	-23.01

Figure 3. (S) Three-array processor listing format for beam noise measurements. (U)

PLOT DATA TABLE 04 SEPT, 78 04:00:48
NUMBER OF UPDATES= 8 SCALE FACTOR +40.00 PTYPE= 2
ARRAY = 2 SHADING TABLE NO.= 2 CAL. TABLE= 3 3 3 2 1
SAMPLE SIZE= 512 AVERAGING TIME= +.25 BANDWIDTH= +.50

STR. ANGLE (DEG)	FREQ./	AMPLITUDE (DB)				
		+57.00	+50.00	+38.00	+10.00	+11.00
+.00		-12.03	-15.43	-10.15	-0.27	-23.47
+2.72		-15.00	-13.15	-17.00	-8.01	-23.15
+4.55		-18.31	-11.75	-18.05	-5.00	-22.00
+8.37		-14.00	-11.33	-15.63	-4.10	-22.01
+8.21		-18.54	-13.00	-15.00	-4.20	-22.45
+10.05		-18.24	-15.12	-18.00	-5.15	-22.30
+11.00		-18.54	-13.00	-10.23	-0.04	-22.40
+13.72		-14.07	-0.72	-10.10	-0.04	-22.44
+15.05		-10.44	-0.02	-13.02	-0.20	-22.45
+17.05		-0.30	-10.14	-13.07	-0.50	-22.30
+10.47		-10.27	-11.00	-14.44	-0.02	-22.21
+21.41		-12.00	-14.20	-15.00	-0.01	-22.01
+23.37		-17.01	-10.01	-17.01	-10.10	-21.03
+25.37		-15.50	-17.40	-10.72	-12.75	-21.70
+27.40		-10.10	-10.71	-10.24	-15.03	-21.00
+20.47		-10.40	-20.11	-10.43	-17.70	-20.04
+31.50		-20.20	-10.05	-10.30	-17.45	-20.42
+33.74		-17.22	-17.74	-17.30	-10.75	-20.04
+35.00		-14.02	-17.07	-15.20	-10.03	-23.03
+30.24		-14.25	-15.50	-13.00	-10.07	-24.12
+40.00		-15.21	-15.25	-14.15	-10.00	-24.04
+41.04		-17.17	-15.14	-15.77	-10.50	-24.00
+45.50		-17.00	-17.00	-17.04	-15.00	-24.30
+40.24		-10.44	-15.01	-10.07	-14.01	-23.01
+01.00		-14.45	-14.40	-10.03	-13.52	-23.07
+04.04		-11.71	-12.00	-14.00	-12.02	-22.32
+07.27		-10.50	-0.50	-14.02	-11.55	-21.00
+00.01		-11.42	-0.30	-15.00	-10.05	-21.14
+04.70		-0.50	-10.00	-14.20	-0.00	-20.70
+00.42		-0.70	-0.45	-11.34	-0.03	-20.02
+75.02		-7.30	-7.00	-0.00	-0.01	-20.02
+00.07		-10.13	-0.07	-10.71	-10.01	-20.70

Figure 3. (S) Continued. (U)

As discussed in Appendix A, the TAP's basic beamforming computation sequence consisted of a DFT for a single combination of spectral analysis frequency and bandwidth parameters, followed by beamforming and beam power averaging operations. This basic computation cycle was executed NS times for the first analysis frequency, and then repeated NS times for each successive analysis frequency. Thus, the beamforming and beam power averaging operations for any one analysis frequency were completed prior to data collection at the next analysis frequency. At the conclusion of one iteration through the entire set of analysis frequencies, the entire sequence was repeated for a total of NG iterations. The number of points used in the DFT was not fixed at any particular value. Rather, it was a variable that was determined by the DFT bin width and the upper frequency of the LAMBDA array being analyzed.

(C) As a result of the TAP mechanization, the beam power levels plotted on one line in the display format shown in Fig. 2 do not represent average beam power levels over the full 15-min data sampling interval. Instead, they should be considered as the average beam power levels over much shorter intervals (typically on the order of 3-min averages). The longest term average beam power levels available in the TAP mechanization are contained

in the so-called master accumulator tables. Beam power levels contained in the master accumulator tables (organized by frequency and steering angle) were averaged over the number of iterations (NG) through the set of analysis frequencies, and it is these values that were used in subsequent data processing activities.

3.3.4 (U) Anomalies in High-Frequency Array Measurements

(S) Beam noise measurements acquired with the HF array exhibited some unusual features that were not immediately explainable from the array's acoustic characteristics or from a consideration of acoustic and/or bulge wave propagation. A typical set of 320-Hz beam noise measurements is shown in Fig. 4. These measurements were obtained during four legs of the third polygon at Site λ_B. The most prominent anomaly is the unusually large beam noise level at approximately 20 deg from the forward and aft endfire directions. These large levels could be caused by a standing wave in the steel strength members of the array; however, calculations indicated this to be unlikely. Unusually large peaks are also present at several other angles (i.e., approximately 32, 42, 72 and 150 deg from forward endfire) but are not readily explainable by any other phenomena.

(C) The cause of the observed anomalies was not discovered until some time after the exercise. As described in Appendix A (see Table A-1) the HF array construction is unique. The HF array is constructed from four "C" sections, each of which contains 16 hydrophone groups. However, the length of each "C" section is 17 times the hydrophone group center-to-center spacing. Thus, when two "C" sections are joined, the resulting array is physically the same length as 33 uniformly spaced elements but only contains 32 active elements (i.e., the hydrophone group that should be located at the connection point between the two "C" sections has been omitted). When the four "C" sections are assembled to form the HF array, the resulting array is physically the same length as 67 uniformly spaced elements but only has 64 elements (i.e., hydrophone groups are missing at element numbers 17, 34, and 51). Unfortunately, the details of the HF array's construction were not known by either the designers of the TAP beamformer or the researchers aboard M/V SEISMIC EXPLORER during the CHURCH OPAL Exercise. As a result, the TAP beamformer processed the 64 HF hydrophone group outputs as if the array were a set of 64 uniformly spaced elements.

(S) The 320-Hz beam patterns presented in Fig. 5 illustrate the effects of the improper beamforming procedures. The beam patterns on the left-hand side of Fig. 5 were prepared for a uniformly spaced array of 64 elements consisting of 61 hydrophone groups and three "dead" hydrophone groups at the module connection points. Spatial shading was accomplished with a Hann weighting function and, thus, the side lobes were uniformly suppressed by about 24 dB regardless of the steering angle. The beam patterns on the right-hand side of Fig. 5 depict the beamforming process actually used during the CHURCH OPAL Exercise and exhibit three adverse effects. The first adverse effect is the nonuniform suppression of the side lobes (i.e., many of the side lobes shown in Fig. 5 have only been suppressed by 10 to 15 dB while others are 30 to 40 dB down from the main lobe response). The second adverse effect is the suppression of the main lobe response. At ±90 deg, the main lobe response was 3.3 dB lower than it should have been.

(U) The third effect is believed to be the one responsible for the unusually large beam noise levels evident in Fig. 4. As a result of the incorrect beamforming, the beam

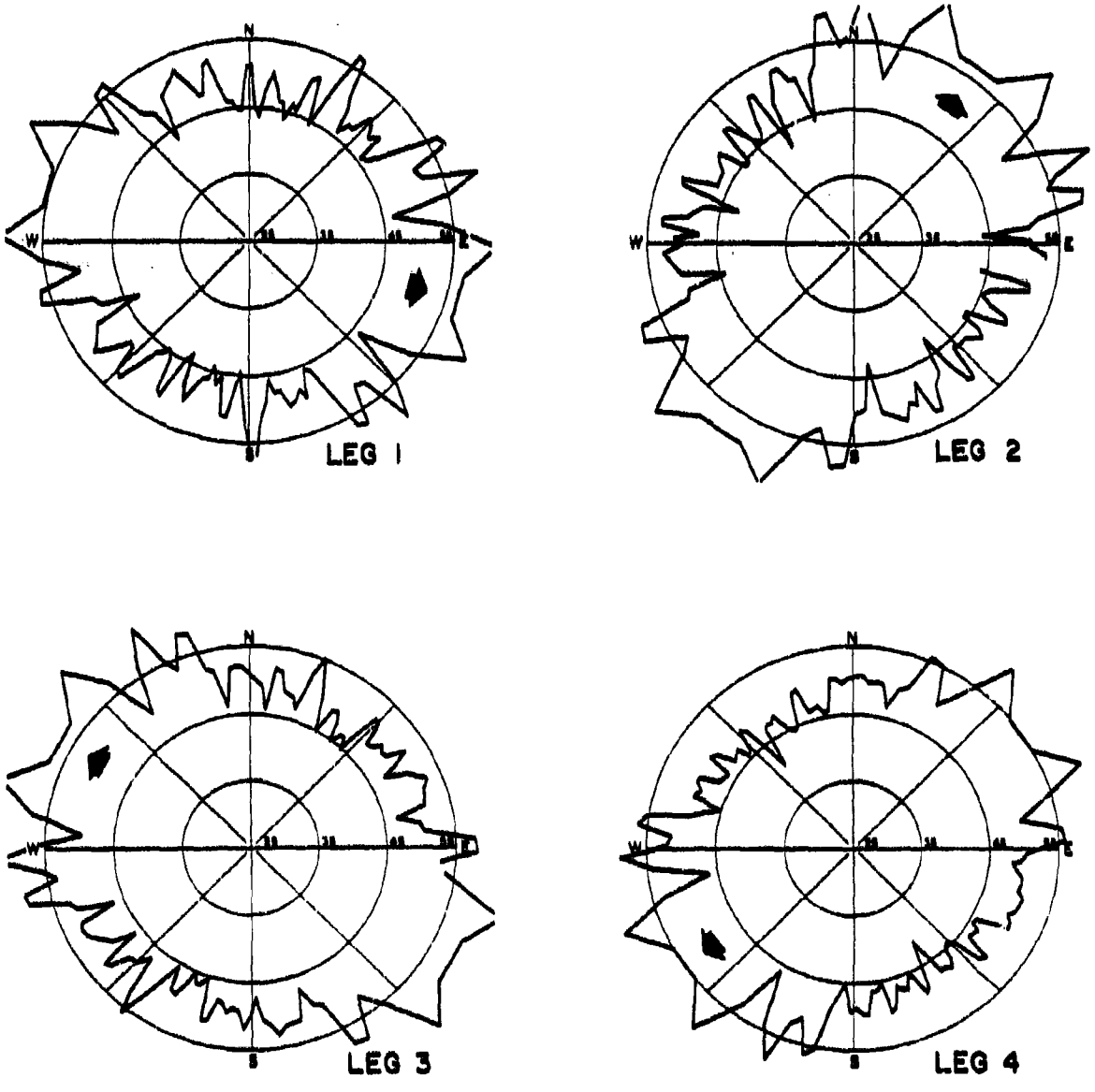

Figure 4. (C) Typical 320-Hz artifacts near endfire directions from LAMBDA HF array measurements during several noise polygon legs. (C)

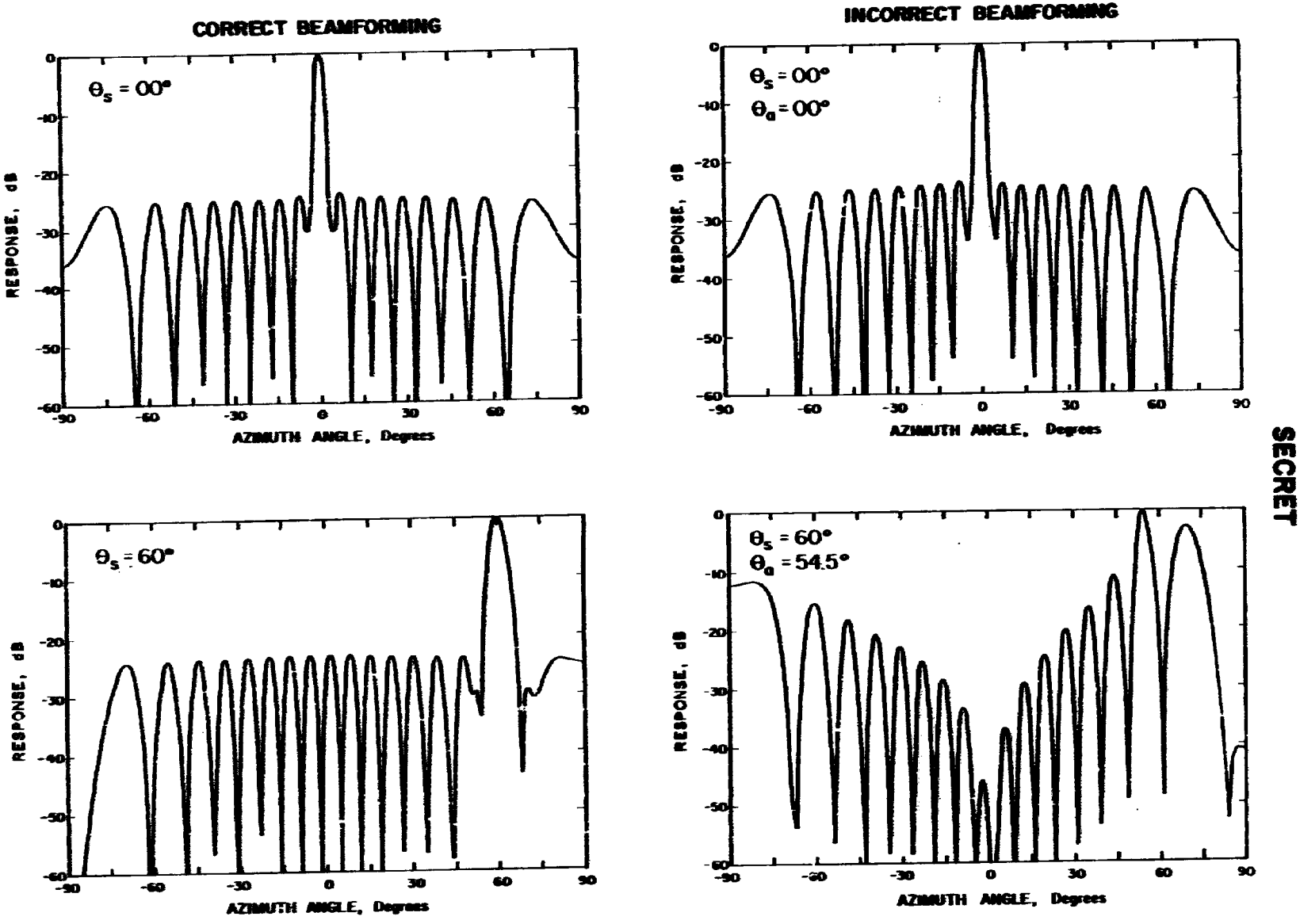

Figure 5. (C) LAMBDA HF array beam patterns at 320 Hz for various intended and actual steering angles (θ_s and θ_a, respectively). (C)

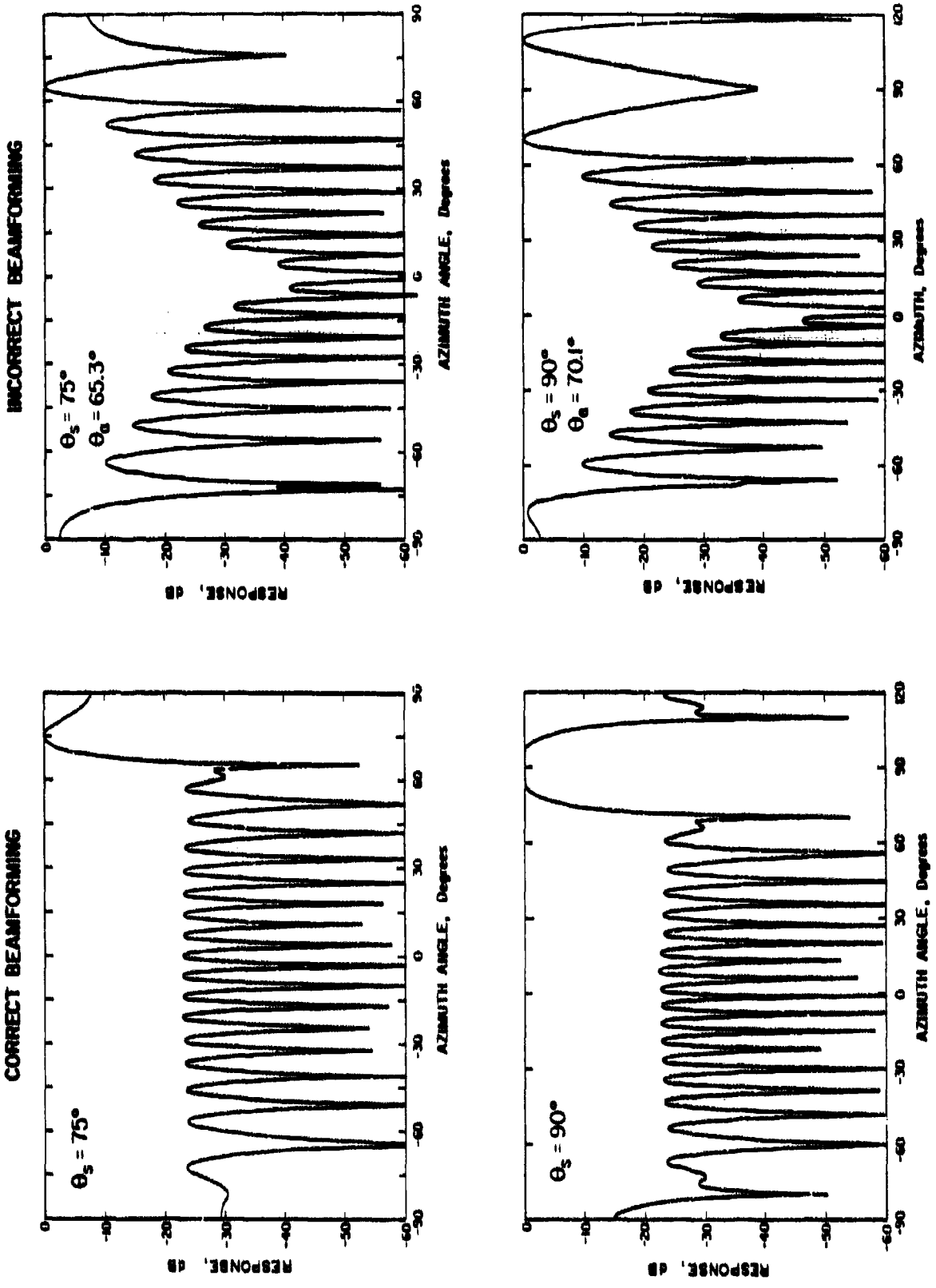

Figure 5. (C) Continued. (U)

steering angle can be in error by as much as 20 deg. The beam steering error was independent of frequency and increases as the steering angle departs from broadside. For spatial shading with a Hann weighting function, the relationship between the intended steering angle (θ_s) and the steering angle actually achieved (θ_a) is:

$$\theta_a = \sin^{-1} (0.94 \sin \theta_s).$$

Thus, the endfire beam is steered approximately 20 deg away from the endfire direction, while the beams near broadside are steered properly. A more complete discussion of these effects is given in Ref. 7.

(U) It should be noted that the results presented in the body of this report do not include any significant errors introduced by incorrect beamforming of the HF array. For the most part, measurements taken with the HF array beams near endfire were excluded from the data set prior to the analysis.

3.4 (U) DATA PROCESSING AND ANALYSIS

(C) The TAP calculated only the average (mean) value of each time-series of beam noise measurements. Consequently, relatively little processing of the data was feasible. For instance, none of the statistical data quality tests that were planned (e.g., see Ref. 4, Appendix G) could be performed since the entire time-series of noise measurements was not available for any of the beams. Therefore, the data processing and analysis tasks aboard ship were limited to estimating the noise field's directional properties. To accomplish this, the 64 average (mean) beam power levels for each polygon leg and analysis frequency were entered by hand into the computer together with the corresponding array headings and beam steering angles. The ambiguity resolution algorithm used these data to estimate the noise field's directional properties for the time period spanned by the input data. All the directionality patterns reported in this document were developed using the ambiguity-resolution technique documented in Ref. 6.

(U) Two additional forms of analysis were conducted during the post-exercise data analysis period. The first of these dealt with the directional noise characteristics estimated from measurements obtained with the unambiguous endfire beams. Results are discussed in Section 4.2.3. The second form of data analysis performed ashore after the exercise was the generation of azimuthal anisotropy and noise gain improvement (NGI) cumulative distribution functions. Results from this analytical approach are presented in Section 4.6 and Appendix C.

SECTION 4. (U) RESULTS AND DISCUSSION

4.1 (U) INTRODUCTION

(C) Characteristics of the ambient noise field in the Northeast Pacific Ocean basin are summarized in this section. The analytical results presented herein were obtained from data acquired with LAMBDA and, hence, address only those properties of the noise field that can be inferred with this particular measurement device (i.e., omnidirectional levels, horizontal directionality, beam noise levels, and the temporal variation in these quantities).

(C) Although ambient noise measurements are always influenced to some extent by the accuracy and fidelity of the measurement device, the use of a long towed array such as LAMBDA imposes many other important considerations besides the calibration of the hydrophones themselves. The steady-state orientation of the array (e.g., its vertical tilt angle); the dynamics of the array as it moves through the water; self-noise contributions from flow noise, mechanical vibrations, and tow ship sources; as well as the accuracy, stability and noise contributions of the associated signal conditioning and processing equipment will influence the data actually obtained -- often in ways that are not at all obvious or expected. Thus, the analyses of such ambient noise measurements almost always include considerable cross checking and verification of results as well as quality control tests of the measurements themselves. The analytical results presented herein are no exception, and a considerable amount of effort has been expended in verifying the reasonableness of the results.

4.2 (U) HORIZONTAL DIRECTIONALITY

4.2.1 (U) Summary of CHURCH OPAL Results

(C) Horizontal directionality characteristics of the ambient noise field were calculated from the data base acquired at Site λ_B (see Fig. 1). Beam noise data were collected at this site on 17 different headings with an array depth of 500 m and on 9 different headings with an array depth of approximately 180 m (see Table 1). Thus, the directionality assessments represent the time-averaged noise field observed at the test site over the 12-day data acquisition period (13-25 September 1975).

(S) Horizontal directionality characteristics of the ambient noise field at depths of 500 and 180 m are presented in Figs. 6 and 7, respectively, for most of the standard analysis frequencies and processing bandwidths listed in Table 2. Beam noise data for these analyses were obtained as follows:

- 9.5-, 11-, and 12-Hz results are from LF array measurements;
- 19- and 36-Hz results are from MF array measurements; and
- 50-, 100-, 156-, 192-, and 320-Hz results are from HF array measurements.

LF array measurements were used at 11 Hz rather than MF array measurements so that the directionality results at adjacent frequencies would be more readily comparable. At the other two frequencies (19 and 50 Hz) which yielded redundant data samples, measurements were selected from the LAMBDA array having the widest beamwidth. The rationale for this choice is discussed in Section 4.2.4.

Note: All sound pressure levels are given in absolute terms per 1° sector (dB re 1 μPa^2/Hz degree).

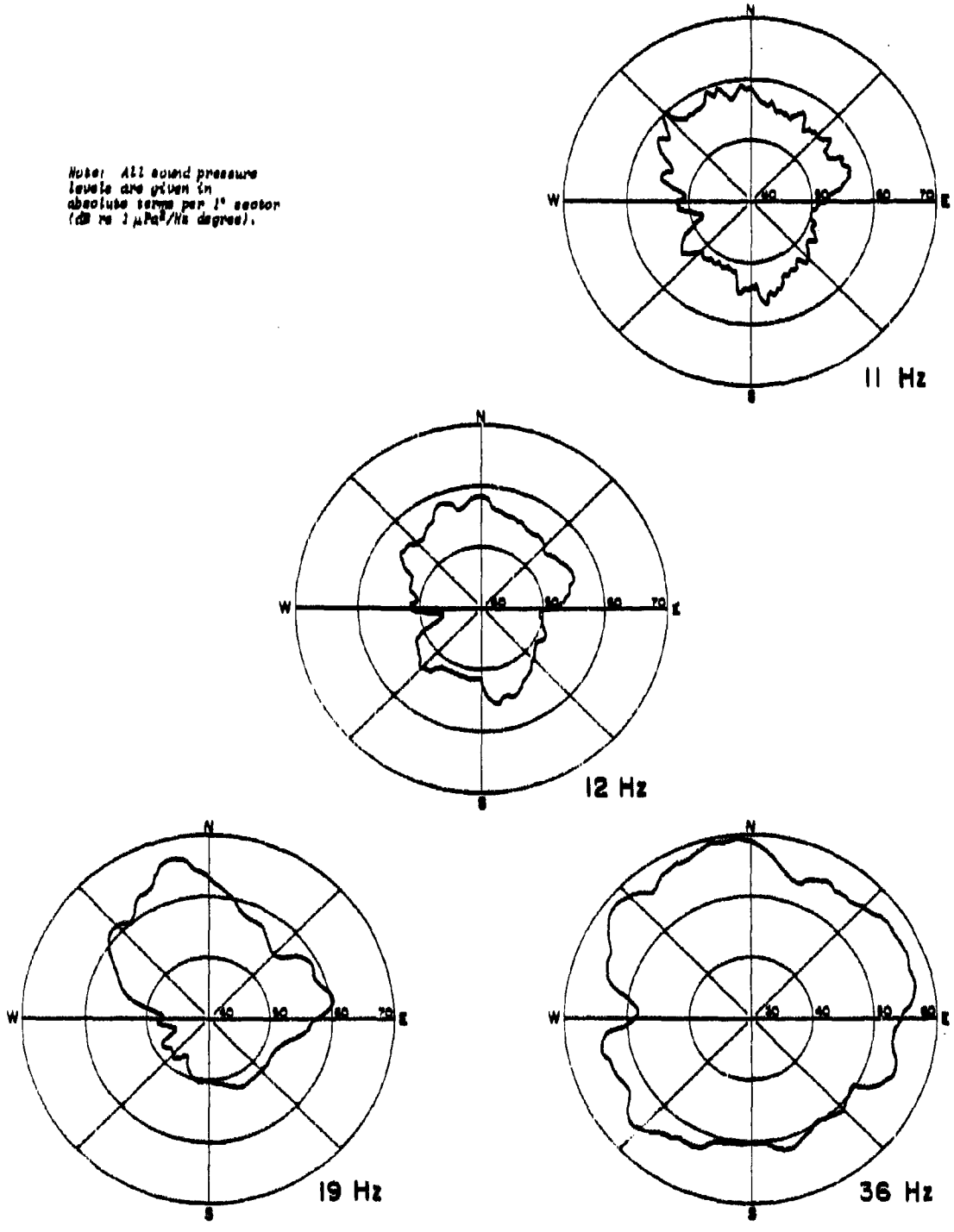

Figure 6. (C) Horizontal directionality of the ambient noise field at CHURCH OPAL Site λ_B for a depth of 500 m. (U)

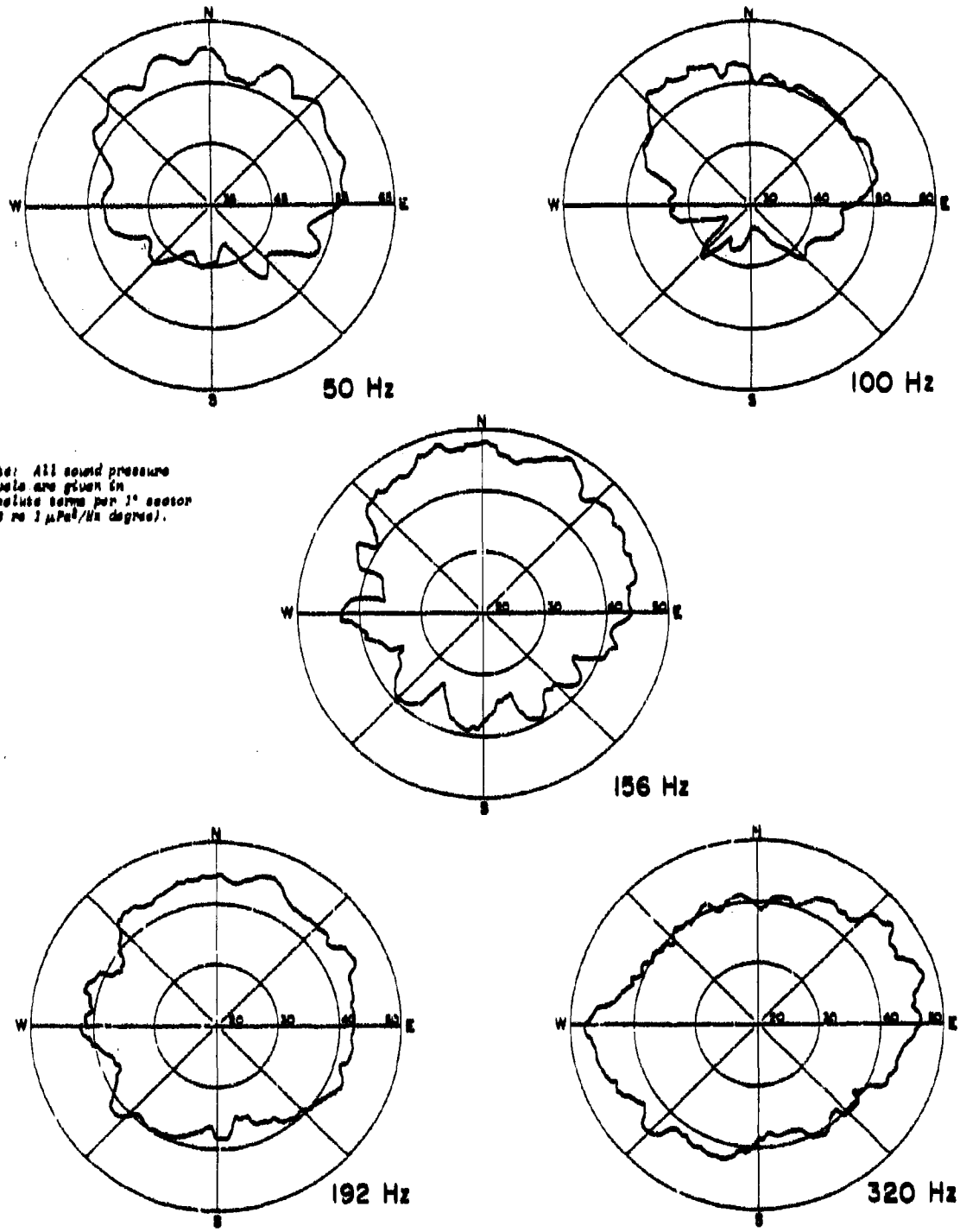

Note: All sound pressure levels are given in absolute terms per 1° sector (dB re 1 μPa²/Hz degree).

Figure 6. (C) Continued. (U)

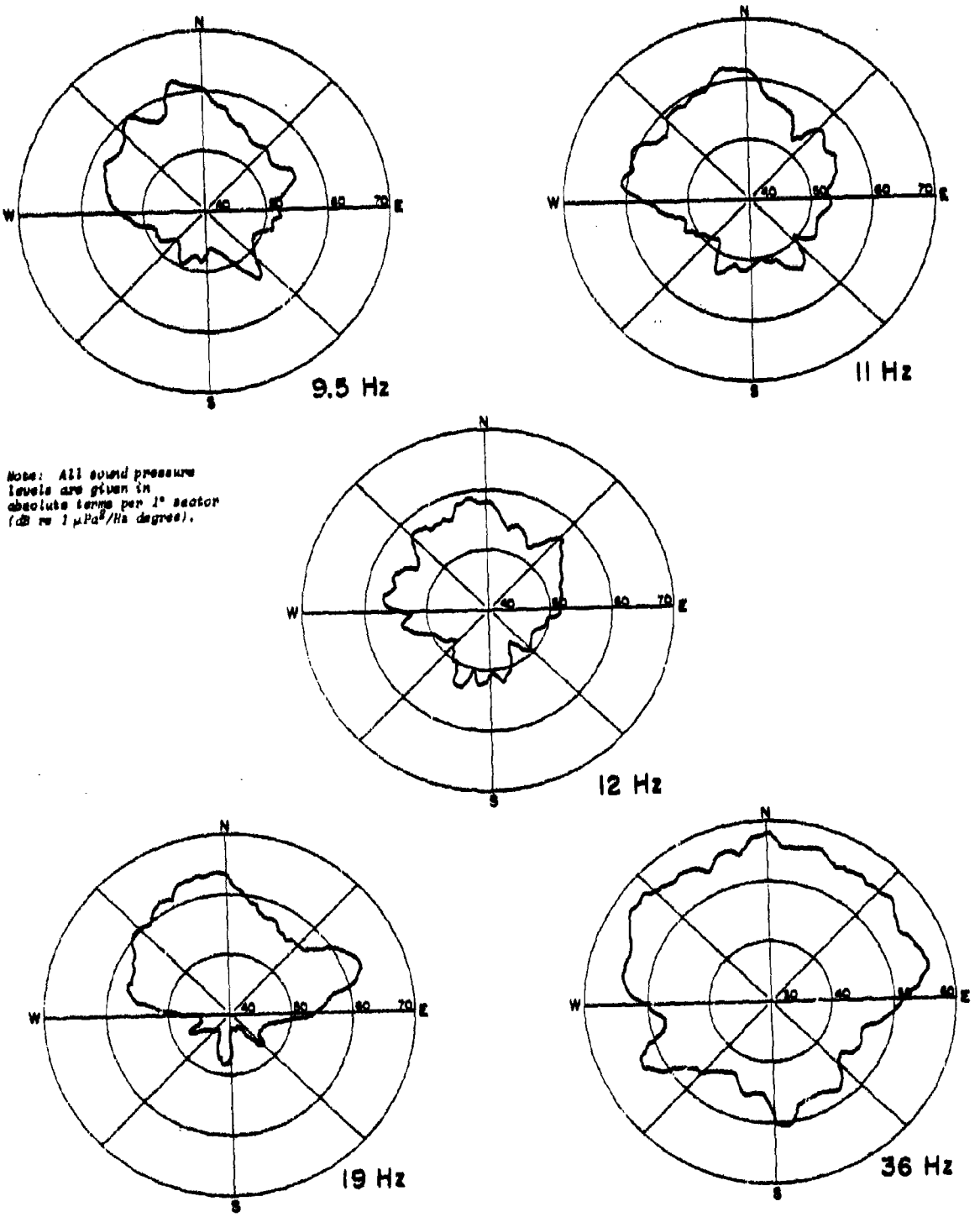

Figure 7. (C) Horizontal directionality of the ambient noise field at CHURCH OPAL Site λB for a depth of 180 m. (U)

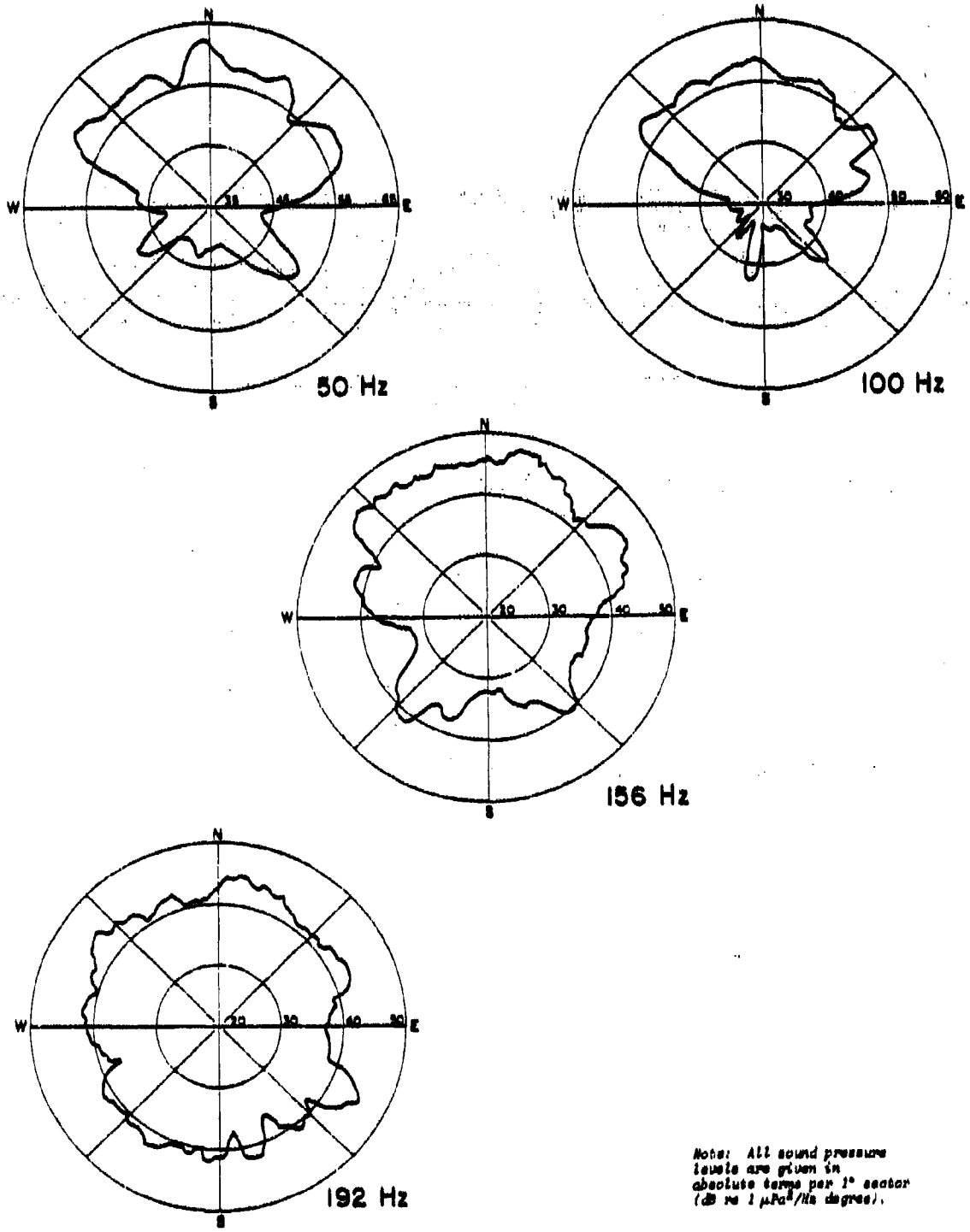

Figure 7. (C) Continued. (U)

(C) Outputs from the ambiguity resolution algorithm have been spatially smoothed in order to eliminate some of the irregular structure caused by the highly nonstationary character of the beam noise measurements. With one exception, the spatial smoothing (averaging) process for all the results given in Figs. 6 and 7 used uniform weighting across an 11-deg azimuthal sector. The exception is the use of a 3-deg azimuthal sector for the 11-Hz data in Fig. 6. Directional noise levels are plotted in terms of absolute sound pressure spectrum levels, relative to 1 μPa, in a 1-deg azimuthal sector. For comparable measurement intervals, an ideal unambiguous beam (i.e., beamwidth = 1 deg and infinitely suppressed side lobes) would have a median noise level equal to the value plotted for the corresponding bearing angle. For wider beams, ambiguous beam pairs, or any other horizontal beam pattern, the estimated noise level is obtained by convolving the noise directionality plot with the beam pattern of interest. For convenience, the main lobe response is usually separated from the sidelobe structure.

(S) Contaminated beam noise measurements were eliminated from the data prior to the ambiguity resolution processing sequence. HF array measurements acquired on beams that were within 40 deg of forward endfire were not used due to radiated noise from M/V SEISMIC EXPLORER, the tow ship. Contamination of the ambient noise measurements at 320 Hz was much more extensive than that observed at lower frequencies due to the beamforming problems discussed in Section 3.3. As a result, only those noise measurements acquired on HF array beams within 30 deg of broadside were used in the 320-Hz directionality assessment at the 500-m array depth. An assessment of the horizontal directionality at 320 Hz was not attempted for the shallow array depth since there were only nine different array orientations to begin with, and two-thirds of the azimuthal coverage (beam measurements) were subsequently excluded.

(C) With the exception of 320 Hz, the directional patterns in Figs. 6 and 7 show ambient noise levels to be higher to the north and northwest of the measurement site than to the south and southwest. At 9.5, 11 and 12 Hz the differences between noise levels over broad azimuthal sectors are generally on the order of 6 to 10 dB. At 19, 50 and 100 Hz the noise in the southern half-space is generally 12 to 18 dB quieter than that in the northern half-space. At 156 Hz, differences between noise levels for the northern and southern directions are generally within the 6- to 8-dB range, while at 192 Hz they are more likely to be in the range from 3 to 6 dB. At 320 Hz, the noise levels appear to be about 6 dB greater in the northeast-southwest directions than in the northwest-southeast directions. With the exception of the 320-Hz results, the confidence levels for all directionality assessments are considered to be rather high. Because of the data contamination problems, much lower confidence levels are placed on the 320-Hz results.

(C) The anisotropic character of the persistent ambient noise field is evident for frequencies in the band from 11 to about 100 Hz. Differences between the highest and lowest noise levels shown in Figs. 6 and 7 are consistently in the range from 15 to 20 dB. Although the directional noise values having relatively large magnitudes are usually estimated quite accurately (and thus, tend to have small variances), this is not normally the case with the low-magnitude noise estimates. Special considerations regarding the lowest observed noise levels are warranted since these levels can be strongly influenced by the measurement array's side-lobe structure. Thus, the noise levels generally prevailing in the southern half-space (i.e., the quietest directions) are not likely to be larger than the magnitudes indicated in Figs. 6 and 7, but they could be significantly lower (see Section 4.2.4 for additional detail).

(S) The 36-Hz directionality results presented in Figs. 6 and 7 appear anomalous since they are much more uniform than the directionality assessments at adjacent frequencies (19 and 50 Hz). This apparent anomaly is believed to be caused by the combined effects of the spatial smoothing and the MF array's characteristics (i.e., beamwidths and side-lobe suppression levels). The analytical results presented in Section 4.2.4 suggest that the 36-Hz noise field could well be just as directional as the noise field at any other frequency below 100 Hz. However, in the frequency range from 100 to 320 Hz, the ambient noise field would be expected to be more uniform since wind effects, which are more uniformly distributed than shipping sources, provide a much larger share of the total radiated noise in this frequency regime.

4.2.2 (U) Comparison with CHURCH ANCHOR Results

(S) During the CHURCH ANCHOR Exercise (September 1973), ambient noise measurements were obtained with the AN/SQR-15(XN-1) TASS array at essentially the same location (Site $\lambda\beta$ in Fig. 1) and depth used 2 years later during the CHURCH OPAL Exercise. A comparison of the horizontal directionality characteristics derived from data taken during the two exercises is presented in Fig. 8. Directionality plots drawn with solid lines are CHURCH OPAL results (from Fig. 6) while the plots drawn with dashed lines depict CHURCH ANCHOR results reported in Ref. 4. Analysis parameters and other information concerning the two data sets are summarized below.

	CHURCH ANCHOR	CHURCH OPAL
Array	AN/SQR-15(XN-1) TASS	LAMBDA HF
No. of Headings	5	17
Depth	≃ 500 m	≃ 500 m
Analysis Bandwidth	1/3 octave	0.5 Hz
Ambiguity Resolution Technique	Modified All Bearings (MAB)	Wagstaff Iterative Technique (WIT)

(C) CHURCH OPAL and CHURCH ANCHOR noise directionality results shown in Fig. 8 agree to a remarkable extent, considering the variations in the data acquisition and processing parameters. Differences between the directionality estimates are generally small in the high-level sectors (i.e., the northerly directions) but are somewhat larger in the low-level noise sectors to the south. At these two frequencies, the differences in the horizontal directionality estimates are attributed to:

- Nonstationary properties of the ambient noise field;
- Spectral analysis bandwidths;
- The different acoustic characteristics of the arrays (i.e., beamwidths and side-lobe suppression levels); and
- The ambiguity resolution methods utilized to obtain the directionality patterns.

For example, a directionality assessment obtained from data collected on 5 headings within a 1-day period (CHURCH ANCHOR) would be influenced more by noise field nonstationarities than one derived from data collected on 17 headings within a 2-week period (CHURCH

Note: All sound pressure levels are given in absolute terms per 1° sector (dB re 1 μPa^2/Hz degree).

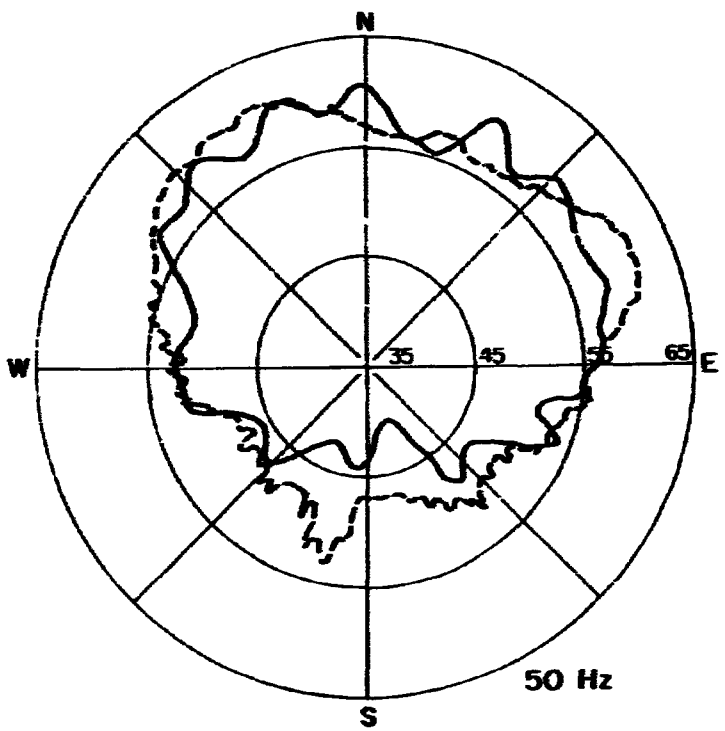

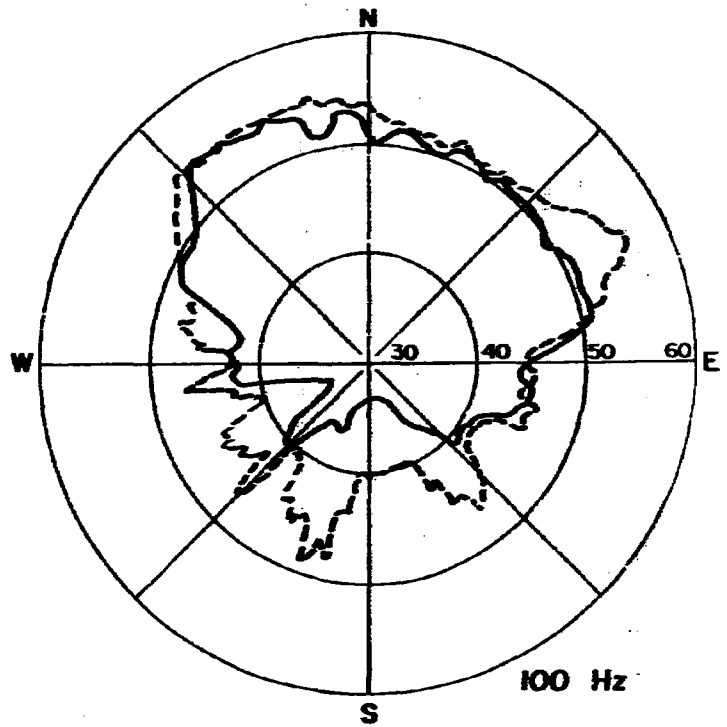

Figure 8. (C) Comparison of horizontal directionality properties measured at CHURCH OPAL Site λg (——) for a depth of 500 m with similar data obtained during the CHURCH ANCHOR Exercise (- - - -). (U)

OPAL). Also, the MAB ambiguity resolution method is limited in its ability to discriminate against high-level noise sources along ambiguous azimuths and, hence, does not faithfully reproduce the noise along low-noise-level azimuths. The MAB method, however, does adequately reproduce the noise field in the high-level-noise sectors.

(C) The results shown in Fig. 8 are representative of comparisons between CHURCH OPAL horizontal directionality results and other CHURCH ANCHOR results given in Ref. 4 for different times and frequencies. The excellent agreement between these noise directionality results supports the hypothesis that a relatively stable, time-averaged and spatially smoothed noise field exists in the Northeast Pacific Ocean. The noise field is most likely repeatable on a yearly cycle provided that the surface shipping patterns do not change drastically. Hence, the mean horizontal directionality, the mean vertical directionality and omnidirectional levels of the ambient noise in the Northeast Pacific Ocean appear to be predictable with a reasonable degree of confidence.

4.2.3 (U) Horizontal Directionality Assessments from Endfire Beam Data

(U) Since the endfire beams of a horizontal line array are unambiguous, noise levels measured with those beams can be used directly to determine the ambient noise field's horizontal directionality characteristics. While this approach eliminates the need for ambiguity-resolution algorithms and associated data processing actions, several operational disadvantages limit the general usefulness of this directionality measurement technique.

(C) Two disadvantages arise from the magnitude of the endfire beam widths since these range from 5 to 10 times the width of the broadside beams, depending on the relationship of the measurement frequency to the array design frequency. When the measurement array's beamwidth is considerably broader than the widths of the high- or low-level-noise sectors, the array smooths out the spatial variation in the noise field "clipping" the high levels and "filling-in" the low levels. Consequently, horizontal directionality assessments obtained from endfire beam data alone will usually result in estimates of the directional properties that are spatially smoothed to a much larger extent than those obtained using all the beam noise measurements together with a suitable ambiguity resolution technique. This is particularly true for measurement frequencies that are less than 50% of the array design frequency since the endfire beamwidths become quite large at these frequencies. The second major disadvantage arises from the limited azimuthal coverage of the endfire beams. Although the endfire beamwidths are usually quite broad relative to the broadside beamwidths, they are still rather narrow when compared to the 360 deg field-of-view to be investigated. Consequently, endfire beam noise data must be accumulated on many different array headings in order to completely define the horizontal directionality properties at one combination of site and depth parameters. For example, a 64-element array with uniform amplitude shading has a theoretical endfire beamwidth of about 18 deg at the array design frequency. Assuming both the forward and aft endfire beams yield valid data, at least 10 separate array headings would be necessary to characterize the ambient noise field at one depth for the array's design frequency.

(U) Another disadvantage arises from the temporal variability of the ambient noise field. Since the noise arriving along any given azimuth tends to be highly variable, a long averaging time (on the order of several hours) must be used to achieve a reasonable degree of confidence in the measured median beam noise level for that particular look direction.

The sample length can be achieved by one continuous run or by several (shorter) data samples in the same direction. The important point is that the data collection period on any given azimuth must be of sufficient duration to yield a reasonable estimate of the median noise level in that particular direction.

(U) The last disadvantage, but by no means the least important, is the potential for data contamination from strong sources of radiated noise in the immediate vicinity of the measurement array. The tow ship itself often radiates sufficiently high noise levels to render the forward endfire beam completely useless for data acquisition purposes.

(U) Because of these inherent limitations, the analysis of LAMBDA endfire beam noise measurements was intended as a check on the reasonableness of the results from the primary directionality assessment technique and not as a completely independent estimate of the horizontal directionality properties. Directional noise levels were calculated from the endfire beam noise measurements by the following equation:

$$\begin{array}{l}\text{Directional Noise Level} \\ (\text{dB re } 1\ \mu\text{Pa}^2/\text{Hz deg})\end{array} = \begin{array}{l}\text{Mean Value of} \\ \text{Endfire Beam Noise} - 10\log[\text{Beamwidth}] \\ \text{Time-Series} \\ (\text{dB re } 1\ \mu\text{Pa}^2/\text{Hz})\end{array} \qquad (1)$$

The result is an estimate of the directional noise level that is assumed to be uniformly distributed across the width of the main lobe. Ambient noise levels derived in this manner are plotted as circular arcs, where the angle subtended by each arc corresponds to the beamwidth of the measurement array at that frequency.

(S) Typical results given in Fig. 9 were derived from the LAMBDA endfire beam noise measurements accumulated at CHURCH OPAL Site λ_B with an array depth of 500 m. Endfire-derived directional noise levels plotted in Fig. 9 are superimposed on the corresponding directionality patterns (from Fig. 6) for four of the analysis frequencies (11, 19, 50, and 100 Hz). Noise measurements used in the 50-Hz and 100-Hz analyses were limited to the aft endfire beams since the forward endfire beams were contaminated by radiated noise from the tow ship at frequencies above 50 Hz. However, such contamination was not evident at frequencies below 36 Hz and, hence, noise measurements from both forward and aft endfire beams were used in the 11-Hz and 19-Hz analyses. Endfire beam noise measurements above 100 Hz were not suitable for this form of analysis due to the beamforming problems discussed earlier (see Section 3.3).

(U) It is evident from the results shown in Fig. 9 that the noise level received by an endfire beam can vary as much as 10 to 15 dB from one measurement time interval to another. This is especially true along the low noise azimuths in the southern half-space, where the noise is generally 10 to 15 dB lower than the noise in the northern half-space, and a nearby ship can produce a significant change in the endfire beam level.

(C) Comparisons of the endfire-derived directionality levels with the resolved directionality results (from Fig. 6) should be made with caution since the averaging times for the two estimates are completely different (15 min vs. several days). The most appropriate technique for such a comparison would be to average (on an intensity basis) the endfire-derived noise levels in narrow (e.g., 1- to 5-deg) sectors and then compare these averaged values with

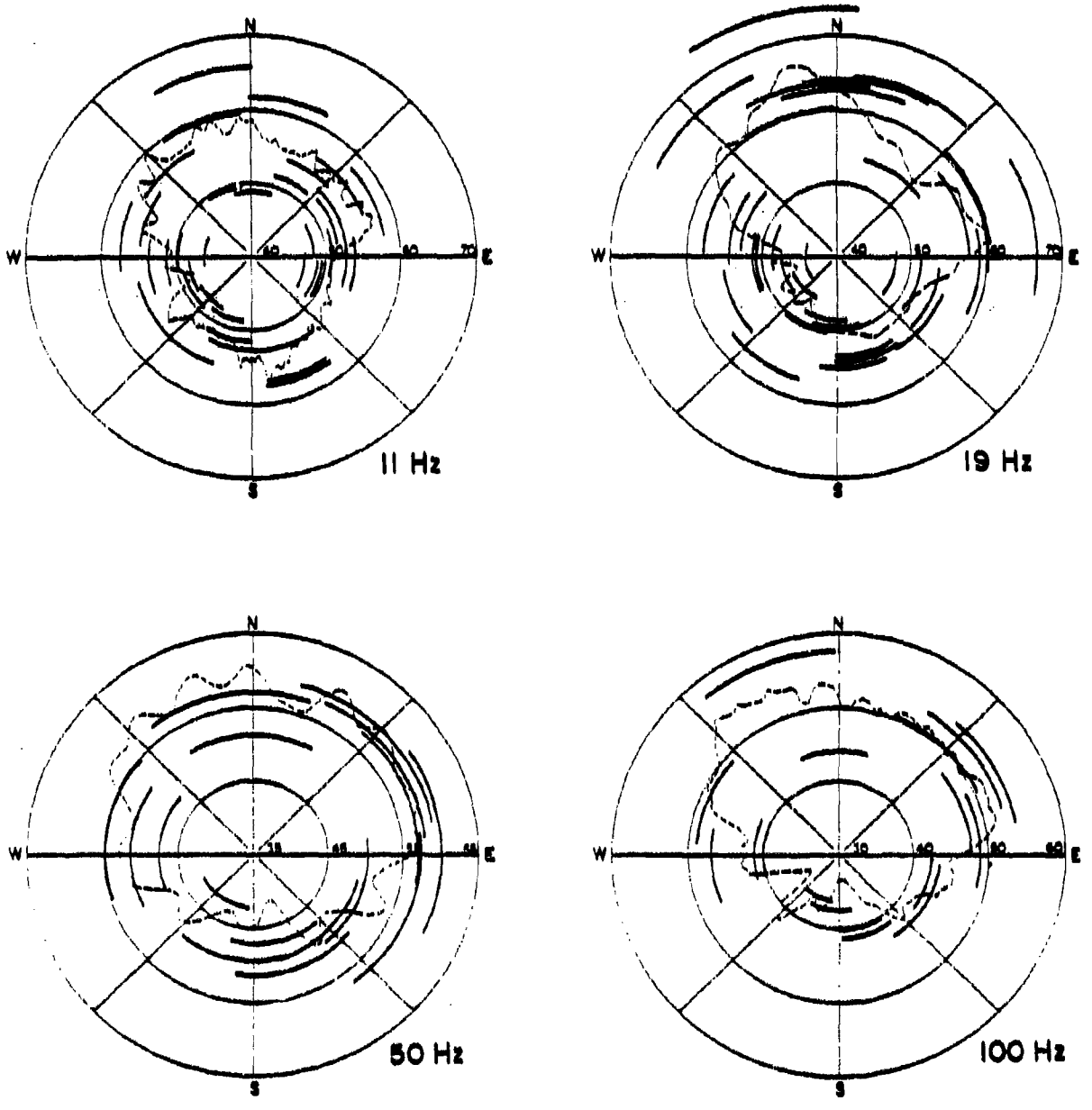

Figure 9. (S) Horizontal directionality properties derived from LAMBDA endfire beam measurements at CHURCH OPAL Site λβ for a depth of 500 m. (U)

corresponding results from Fig. 6. This was accomplished for a number of azimuthal sectors that contain more than one endfire beam measurement. In nearly all the cases considered, the directional results from the two different methods agree reasonably well, and differences between the two results generally were within the range of variability in the data. Directionality patterns estimated from the endfire beam results would necessarily be smoother than those obtained by the iterative technique, but the general shapes of corresponding patterns would be similar.

4.2.4 (U) Measurement Array Influences

(S) As indicated in Table 2, three of the analysis frequencies chosen for the LAMBDA MF array are common to the other two LAMBDA arrays (i.e., 11 and 19 Hz are common to both the LF and MF arrays, while 50 Hz is a common analysis frequency for the MF and HF arrays). This degree of redundancy was chosen deliberately in order to ascertain the impact of the measurement array's characteristics (e.g., beamwidth and side-lobe suppression levels) on the resultant directionality assessments.

(S) Horizontal directionality characteristics at 19 and 50 Hz have been calculated from all LAMBDA array measurements obtained at a depth of 180 m and are presented in Fig. 10. The dashed curves are identical to the characteristics presented earlier in Fig. 7 and result from measurements using the larger of the two beamwidths (MF array at 19 Hz; HF array at 50 Hz). The solid curves in this figure present the results obtained from the narrower beam measurements (LF array at 19 Hz; MF array at 50 Hz). The differences are dramatic and appear to be exactly the opposite of the anticipated relationships. Intuitively, the narrow-beam results (solid curves) are expected to show the most variation since there would be less spatial smoothing of shipping noise sources ("peaks") or the low-level-noise sectors ("valleys"). Furthermore, the array with the narrower beamwidths would be expected to yield lower ambient noise measurements when it is steered in the quiet directions. The apparent contradiction between the actual results and the intuitive conclusions can be resolved by a more thorough examination of the intuitive model and the computation process. In so doing, some of the subtleties of the interaction between the measurement array's characteristics and the deduced noise field properties may become more evident.

(U) To simplify the visualization process, first assume that the measurement device is capable of producing an unambiguous beam pattern (e.g., an endfire beam). Beam noise measurements to be used in the directionality assessments are time-averages of the beamformer outputs as the beams are steered to various look angles. However, it is important to remember that the measured beamformer output contains contributions from the side lobes that cannot be separated from the main lobe response. Assuming that the noise power is uniformly distributed over the main lobe of the unambiguous beam, the directional noise level can be estimated with the following equation:

$$\text{Directional Noise Level (per 1-deg sector)} = 10 \log \left(\frac{\langle \text{Beam Noise Power (main beam + side lobes)} \rangle}{\text{Beamwidth}} \right) \qquad (2)$$

where: $\langle\ \rangle$ denotes the time-averaging operation.

This approach is precisely the same as that followed in the endfire beam analysis technique (see Section 4.2.3). As long as the contribution to the beam noise measurement from the

SECRET

Note: All sound pressure levels are given in absolute terms per 1° sector (dB re 1 μPa^2/Hz degree).

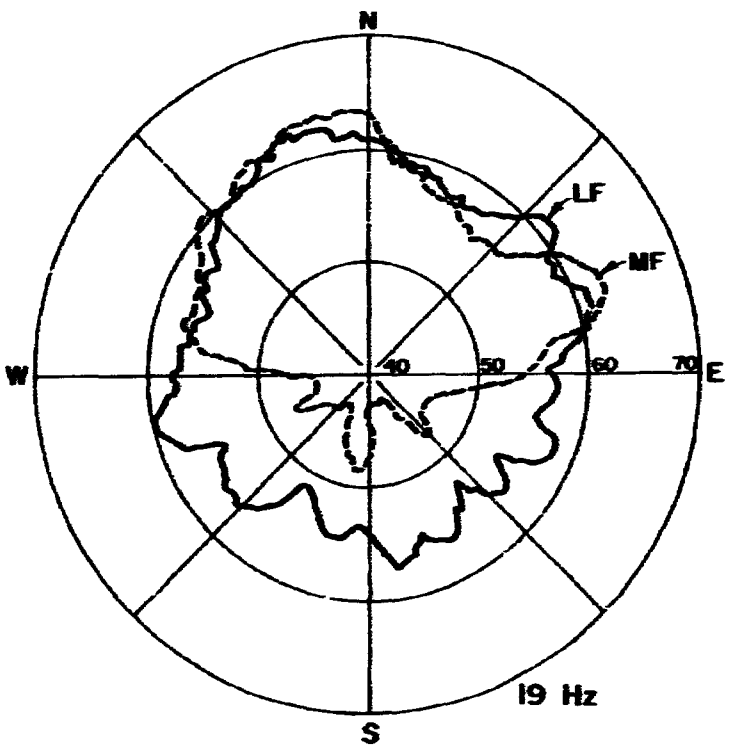

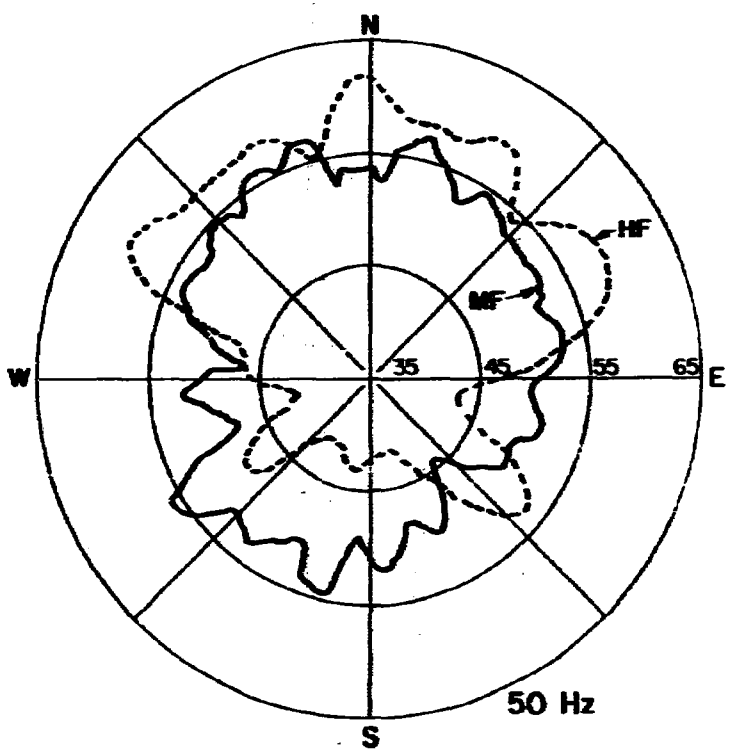

SECRET

Figure 10. (S) Horizontal directionality characteristics derived from different LAMBDA arrays. (U)

side lobes is relatively small, the directional noise level resulting from the above formula produces results that match intuitive reasoning. However, when the side-lobe contribution becomes a significant fraction of the total measured beam noise, then the underlying assumptions are less valid and the estimation technique is more likely to yield erroneous results.

(U) Beam noise measurements in the quietest directions have been dominated by side-lobe contributions in many experiments and, thus, provide a practical and interesting case for further examination. When the beam noise measurement is almost entirely due to side-lobe contributions, the width of the main lobe has very little impact on the noise power level actually measured. However, the beamwidth has a significant impact on the estimated directional noise level for any algorithm comparable to Eq. (2). If the measured beam noise is assumed constant for this side-lobe-dominated case, a decrease in main lobe beamwidth will cause an increase in the estimated directional noise level.

(U) Although the foregoing discussion has been based on the interpretation of unambiguous beam noise measurements, much the same approach is used in the processing of ambiguous beam noise data sets for horizontal directionality assessments. The Wagstaff Iterative Technique (see Ref. 6) attempts to account for side-lobe contributions as each beam noise measurement is processed (deconvolved), but there is a finite limit in its ability to allocate the noise power to the various parts of the beam pattern. Although ambiguous beam measurements complicate the data processing procedures, side-lobe-dominated beam noise measurements almost always produce the same type of error in the estimated directional noise levels as that produced by the simple model discussed above (i.e., the estimated directional noise levels in the quietest directions are larger than they should be).

(S) This line of reasoning provides a framework to examine the divergence between the 19-Hz directionality results shown in Fig. 10. At 19 Hz, MF array beamwidths are approximately three times the magnitude of corresponding LF array beamwidths. For example, broadside beamwidths are about 8 and 2.5 deg for the MF and LF arrays, respectively. Assuming that the 19-Hz beam noise measurements are indeed side-lobe-dominated for most of the southern half-space, then the narrow-beam (LF array) assessment will result in directional noise levels that are about 5 dB (10 log 8 - 10 log 2.5) greater than the equivalent results from the wide-beam (MF array) assessment. Thus, beamwidth considerations alone could account for about half of the divergence between the two estimates of the directional noise levels. In large measure, the remainder of the divergence is attributed to variations in side-lobe suppression levels actually achieved by the two arrays. Thus, the minima in the directionality patterns suggest that the MF array's side lobes (at 19 Hz) were suppressed by about 5 dB more than those of the LF array at the same frequency. This type of behavior is not uncommon in amplitude-shaded linear arrays. As the measurement frequency decreases from the design frequency, the beamwidth increases, but the side lobes are suppressed somewhat better. Furthermore, the LF array is three times as long as the MF array (7900 ft vs. 2650 ft) and, thus, is much more difficult to maintain in an optimum shape. Both of these considerations lend credence to the suggestion that the LF array's side lobes (at 19 Hz) are not suppressed as well as those of the MF array at the same frequency.

(S) The minimum values in any highly variable noise directionality pattern can be tested for reasonableness if the major parameters of the measurement array are known and

the omnidirectional noise level is available for a comparable time interval. Neglecting the main lobe's contribution, side-lobe-dominated beam noise measurements can be expressed as $L_O - S_{sl}$

where:

L_O = Median value of omnidirectional noise measurements over the time period of interest (in dB)

S_{sl} = Minimum suppression level of the measurement array's side-lobe structure during the time period of interest (in dB).

The minimum directional noise level possible under these circumstances can be approximated by the simple noise estimation algorithm given in Eq. (1) and, therefore:

$$L_{DN}(\text{minimum}) = L_O - S_{sl} - 10 \log (\text{Beamwidth}) \quad (3)$$

Realistic side-lobe suppression levels for any one of the 64-element LAMBDA arrays appear to range from about 24 to 30 dB when Hann spatial shading is used. However, the side-lobe suppression value can change significantly over relatively short time periods due to array curvature and vertical displacements.

(S) At 19 Hz, the comparable omnidirectional noise level is 82.4 dB re 1 μPa^2 for the LAMBDA MF array measurements at a depth of 180 m (see Section 4.3). Thus, the minimum directional noise levels attainable from the MF array data would be expected to fall within the 43- to 49-dB range, while the minimum directional noise levels achievable from the LF array data would be anticipated to be in the 48- to 54-dB range. The fact that these calculated levels are in very close agreement with the 19-Hz directionality pattern minima (in Fig. 10) confirms the hypothesis that the 19-Hz beam noise measurements are side-lobe-dominated in much of the southern half-space. Thus, the conclusion that the minima in the 19-Hz ambient noise field's directionality pattern are at least as low as the levels shown in Fig. 10 (dashed curve) but could possibly be even lower. Comparison of the calculated minima with the plotted results suggests side-lobe suppression levels of almost 30 dB for the MF array but probably no more than 25 dB for the LF array. Consequently, side-lobe suppression levels on the order of 35–40 dB would be required to determine if the actual ambient noise levels are significantly less than those plotted.

(S) Interpretation of the 50-Hz directionality results presented in Fig. 10 is more difficult. The divergence between the two directionality patterns along the azimuths of maximum noise is particularly difficult to reconcile and suggests that at least one set of measurements may not be adequate for horizontal directionality analysis purposes. As with the 19-Hz data, the wide-beam (HF array) directionality assessment spans a much larger range of magnitudes (41 dB to 62 dB) than the narrow-beam (MF array) results (44 dB to 57 dB). Beamwidth differences are clearly evident since the HF results are spatially smoothed to a much larger extent than the MF results. Indeed, HF beams are up to six times the width of comparable MF beams. For example, broadside beamwidths are about 2.6 and 16 deg for the MF and HF arrays, respectively. At 50 Hz the comparable omnidirectional level is 80 dB. On the basis of the same representative side-lobe suppression levels (24 dB to 30 dB), the expected minimum directional levels for the HF data are in the 38-dB to 44-dB range. Expected minimum levels for the MF data would be in the 46-dB to 52-dB range. These values compare favorably with the minimum levels shown in Fig. 10 for each

particular directionality pattern taken individually, but the observed minima are not consistent as a function of azimuth. Statistical analysis of the beam noise time-series would normally be accomplished to resolve these types of difficulties, but the time-series data were not available for post-exercise analysis. Based on the directionality patterns shown in Figs. 6 and 7, the HF array results are the more plausible of the two and are believed to be a reasonable representation of the ambient noise field.

(S) The analysis procedures described above for the 19-Hz data were also used to investigate the 36-Hz directionality results since these patterns were unusually isotropic relative to the results at the adjacent analysis frequencies of 19 and 50 Hz (see Section 4.2.1). Minimum directional noise levels were computed for the side-lobe-dominated case using the MF array's broadside beamwidth of 4 deg and side-lobe suppression levels of 24–30 dB. Side-lobe-dominated minima are compared below with the actual minima depicted in Figs. 6 and 7:

Array Depth (m)	Omnidirectional Levels (dB re 1 μPa^2/Hz)	Side-Lobe-Dominated Minima (dB per 1 deg)	Actual Minima (dB per 1 deg)
500	80.4	44–50	48–50
180	78.5	42–48	44–46

The favorable agreement between the predicted minima and the actual minima suggests that the 36-Hz ambient noise field in the SE to SW quadrant could be significantly quieter than the levels shown in Figs. 6 and 7. Considering these results and the highly directional properties of the ambient noise field at adjacent frequencies, it appears that the MF array was not the most appropriate measurement device for the particular 36-Hz noise field encountered at CHURCH OPAL Site λ_B. A measurement array with broader beamwidths or more highly suppressed side lobes might have produced 36-Hz directionality patterns that were similar to those obtained at 19 Hz and 50 Hz.

4.2.5 (U) Computation Algorithm and Error Sources

(U) The Wagstaff Iterative Technique (WIT) was used to estimate the horizontal directionality of the ambient noise field from sets of ambiguous beam noise measurements obtained during CHURCH OPAL (see Ref. 6 for a complete description of the process). As the name implies, the mathematical technique is an iterative one that uses known properties of the measurement array (i.e., the array's beam patterns) together with the beam noise measurements to resolve ambiguities in the beam noise data and calculate the directional noise field as a function of true bearing angle. Unlike most previous ambiguity resolution techniques, WIT is not predicated on the assumption that the side-lobe contributions to the beam noise measurements are negligible. Rather, the technique allocates the noise power between the main lobe and the side lobes but is limited in its ability to consider the side lobes in detail.

(U) The process begins with an initial estimate of the noise field's directionality pattern; lacking *a priori* information concerning the noise field, the initial estimate may be an isotropic field having some representative omnidirectional level. The initial estimate of the

noise field is convolved with the array beam patterns (as a function of true bearing) corresponding to the first set of beam noise measurements. The differences between the calculated and measured levels are used to modify the original noise field estimate. The array beam patterns on the second heading are then convolved with the modified noise field estimate. Differences between the measured and calculated beam noise levels are used to guide the further modification of the noise field estimate. This process is continued for all the beam noise measurements in the data set (and repeated if necessary) until the pooled standard deviation between the measured beam levels and the calculated beam levels either reaches a minimum or improves by some arbitrarily chosen small value (about 0.005 dB). As the iterations converge, the array loses its ability to distinguish between the averaged noise field and the noise field estimate. In the limit, the array cannot distinguish between them. This does not guarantee the two are the same, but only that the array cannot differentiate between them. For a nonstationary noise field, such as the Northeast Pacific, pooled standard deviations typically range from 1 to 3 dB when data from 3 to 18 different array headings are used in the estimation process. The magnitude of the pooled standard deviation provides a crude indication of the temporal variability in the data, since it has been demonstrated in computer simulations (unpublished results) that pooled standard deviations for stationary noise fields are generally less than 0.5 dB.

(U) Accurate measurements of array heading are mandatory for any of the ambiguity resolution techniques, including WIT. The effects of array heading errors on the ambiguity resolution process will be azimuthal smoothing of the stationary (or persistent) noise sources over an angle equal to the magnitude of the heading error. The lowest levels in the directionality patterns will be most readily affected; they will occur less often, occupy narrower azimuthal regions, and be higher in level than they would be otherwise. Regions of high-level noise will occupy broader azimuthal regions and will have lower magnitudes than would be estimated from identical data not containing heading errors.

(U) The LAMBDA wet-end configuration used during CHURCH OPAL did not include a heading sensor. Consequently, other means were necessary to determine the actual array heading. The VIBROSEIS projector transmitted tonals during most of the CHURCH OPAL polygon tows and provided a beacon whose bearing (relative to the array's fore-aft axis) could be determined both accurately and continuously. Geographic locations of the VIBROSEIS projector and the LAMBDA array were obtained from AMERICAN DELTA II and SEISMIC EXPLORER track charts and, in turn, these data were processed to yield the true bearing from the array to the projector as a function of time. Unfortunately, the projector did not perform according to expectations and was detectable only about half the time. When the beacon frequency was detectable, the array heading was obtained by comparing the true (reconstructed) bearing to the projector with the measured relative bearing. At all other times the array heading was assumed to be equal to the ship's heading. Since ocean current speeds are often the same order of magnitude as the array tow speeds, the differences between ship's heading and array heading can be significant. For these reasons, ship's heading is only used as a last resort in directionality assessments.

4.3 (U) OMNIDIRECTIONAL NOISE

4.3.1 (U) Summary of CHURCH OPAL Results

(U) Omnidirectional noise levels measured at CHURCH OPAL Site λ_B are shown in Fig. 11. The numerical values presented in this figure were derived from the horizontal directionality patterns presented earlier in Figs. 6 and 7. Power levels indicated in the directionality patterns were converted from decibels to intensities, integrated over all azimuths (0 to 360 deg) and then converted back to decibel levels. An equivalent omnidirectional level calculated in this manner uses all of the information available and, thus, has been effectively averaged over all the longest possible duration in the time domain. Since the averaging periods in the time domain are identical, omnidirectional levels calculated in this manner can be compared directly with the directionality assessments, and there is no need to consider the effects of different averaging times in such comparisons.

4.3.2 (U) Comparison with CHURCH ANCHOR Results

(C) Representative ambient noise levels obtained during the CHURCH ANCHOR Exercise (September 1973) have been extracted from Ref. 8 and are presented in Fig. 12. These data were acquired with acoustic data capsule (ACODAC) hardware at a hydrophone depth of 4300 m. A 10-min integration time was used in the ACODAC data recordings.

(C) CHURCH OPAL ambient noise levels obtained 2 years later at approximately the same geographic location are overplotted in Fig. 12. It should be noted that the CHURCH OPAL measurement depths (180 and 500 m) are considerably different than the CHURCH ANCHOR measurement depth (4300 m). At frequencies below 100 Hz, the differences between the CHURCH OPAL and the CHURCH ANCHOR results are small enough to attribute to depth dependence. At and above 100 Hz, the differences are attributed to the prevailing 30-knot wind during CHURCH ANCHOR versus the 5-knot wind speed encountered during CHURCH OPAL. These data illustrate that the LAMBDA measurements are reasonable and suggest that whales may account for the high noise levels observed at 19 Hz. This particular aspect of the ambient noise spectra will be discussed in more detail in Section 4.5.

4.4 (U) DEPTH DEPENDENCE

(C) From Fig. 11, it is apparent that the omnidirectional levels at a depth of 500 m are about 1 dB greater than corresponding noise levels at a depth of 180 m throughout the entire frequency range from 19 to 192 Hz. However, when the individual noise directionality patterns in Figs. 6 and 7 are compared on the basis of depth, some significant differences are observed. To facilitate the discussion of these differences as a function of azimuth, lines of bearing have been established from the λ_B measurement site to various locations throughout the North Pacific Basin (see Fig. 13).

(S) In the frequency range from 11 to 100 Hz, noise contributions resulting from the relatively low wind speeds and sea states prevailing during CHURCH OPAL should be sufficiently low to be unobservable in the LAMBDA data. With the exception of whale noise at 19 Hz, noise in the 11- to 100-Hz regime is attributed to surface shipping which, in some cases, can be more than 1000 miles away from the measurement site. At 50 and

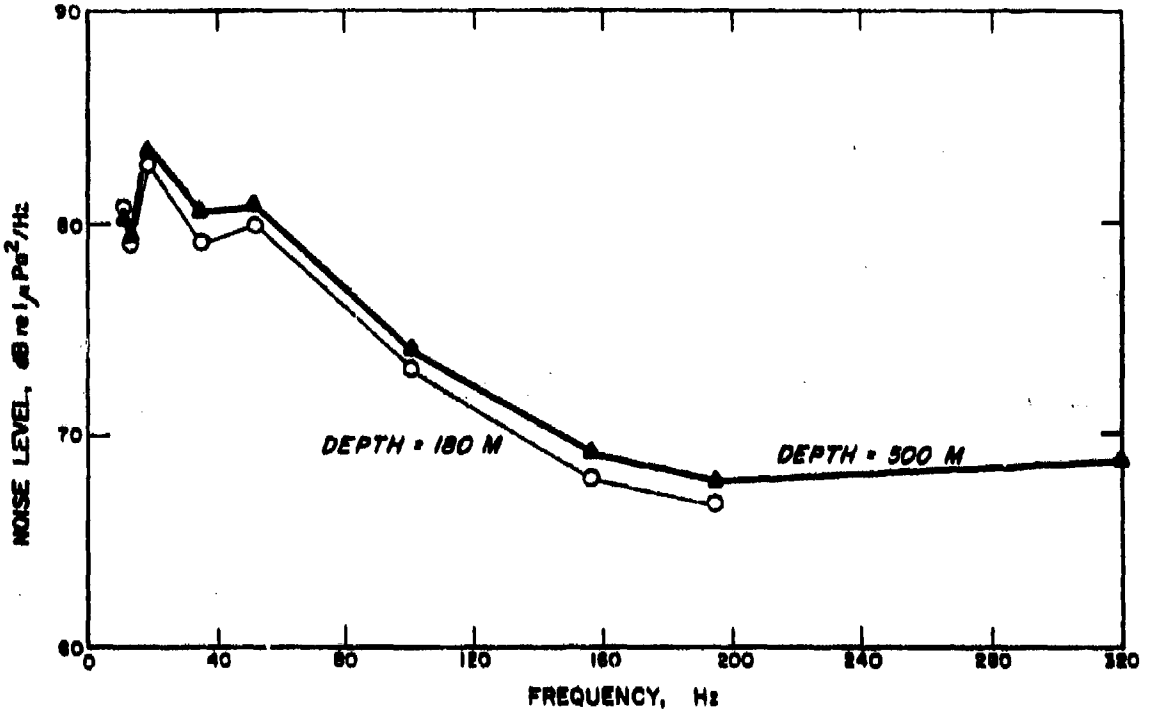

Figure 11. (C) Omnidirectional noise levels at CHURCH OPAL Site λβ. (U)

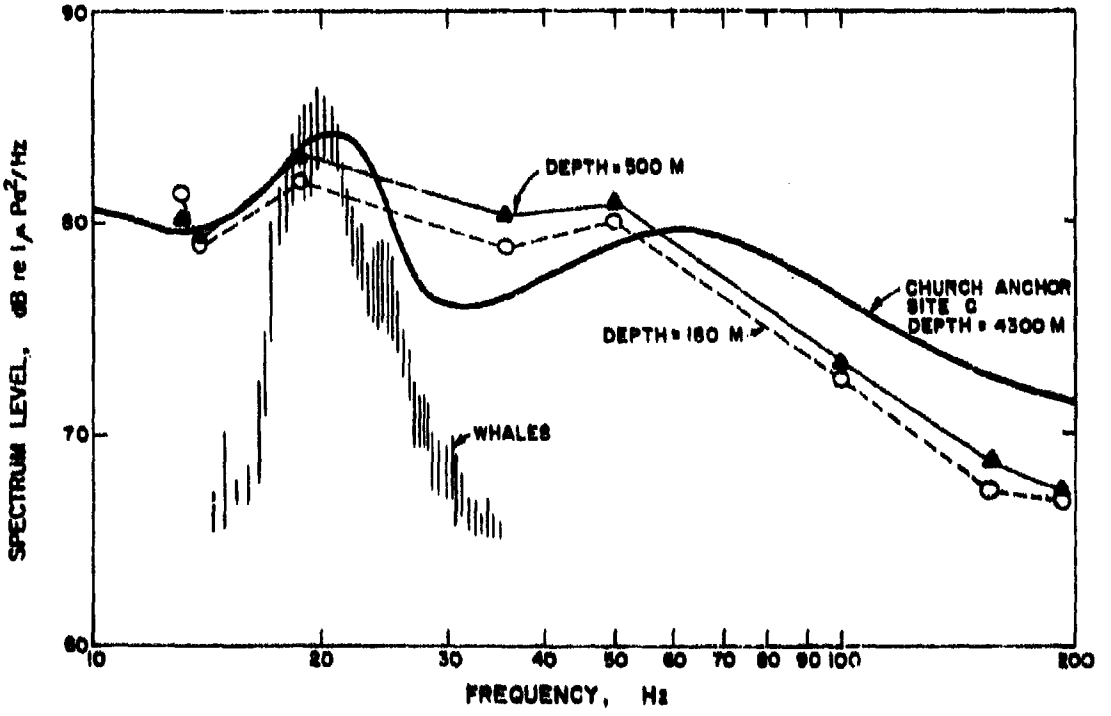

Figure 12. (C) Comparison of omnidirectional noise levels measured during the CHURCH ANCHOR and CHURCH OPAL exercises. (U)

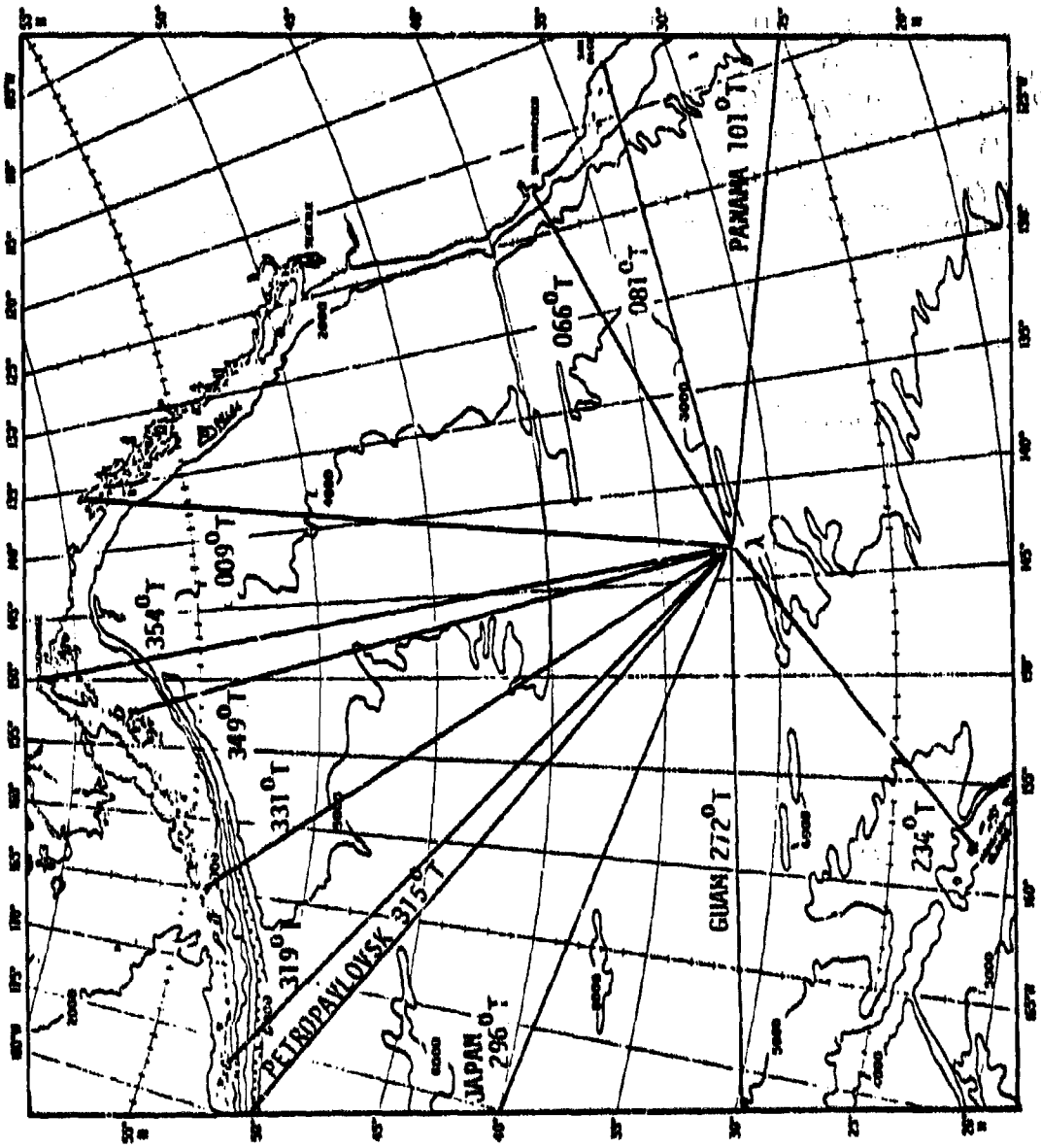

Figure 13. (C) Bearings from CHURCH OPAL Site 4g to various locations in the North Pacific Ocean Basin. (U)

100 Hz, for example, the noise levels along westerly azimuths toward Guam are about 6 to 8 dB greater at depths near the Sofar channel axis (500 m) than corresponding levels at near-surface depths (180 m). Shipping concentrations responsible for the high levels observed in this direction (at Site λ_B) could be located near or even west of the Emperor Seamount chain. At 500-m depths, acoustic energy can travel throughout the Northeast Pacific Ocean by relatively low-loss (continuously refracted) acoustic propagation paths. The most plausible mechanisms that can couple the surface-generated noise into the Sofar channel are:

- Reflections from seamounts, islands, and uneven bottom topography throughout the ocean basin.
- The down-slope conversion process which funnels acoustic energy from noise sources along the Pacific basin's boundary into the Sofar channel.
- Shoaling of the Sofar channel axis to the north of the site.

The first two mechanisms are discussed more fully in Refs. 5, 6, and 10.

(S) Directional noise levels at 50 and 100 Hz toward San Diego (81 deg) and Panama (101 deg) are also 2 to 3 dB greater at the 500-m depth than at the near-surface depth. Surface shipping noise generated in the vicinity of these coastal areas coupled to the Sofar channel by the down-slope conversion process could be responsible for the observed differences.

(S) At 36 Hz, the directional noise levels in the southern half-space are 2 to 3 dB greater at the deeper depth, but this difference may not be significant. Directional noise levels at 19 Hz are more complex. Noise levels throughout the southern half-space are consistently larger at the greater depth. However, along azimuths toward San Francisco and to the west, the directional levels at the 500-m depth are several dB lower than comparable values at the shallower depth. Surface shipping and whales are jointly responsible for the noise at this frequency, but the distribution of each type of noise source (as a function of azimuth) is not known.

(S) The 11-Hz and 12-Hz directionality patterns are similar to one another and are characterized by the large differences in the directional noise levels toward the west. Noise levels toward Guam near the Sofar axis are on the order of 5 dB lower than those observed at the shallower depth. This behavior is completely opposite the difference observed at 50 and 100 Hz. The unusual behavior of the directional noise levels to the west of the measurement site cannot be explained with the present data base.

(S) At frequencies above 100 Hz much less variation in the directional noise levels is evident as a function of depth. At 156 Hz the levels in the southern half-space are perhaps a few decibels greater at the deeper depth. This difference, however, is not considered particularly significant. At 192 Hz, the directional noise levels are essentially independent of depth. Wind noise begins to have a measurable contribution above 150 Hz, but the levels do not vary appreciably as a function of depth. Hence, no significant differences in the directionality patterns would be expected along low-level noise azimuths. Differences along high-level noise azimuths are attributed to range-dependent propagation losses from ships within, perhaps, 400 to 500 nautical miles. Frequency dependent attenuation would severely reduce the noise from ships at ranges greater than 500 nautical miles.

4.5 (U) WHALE NOISE

(U) The omnidirectional ambient noise levels illustrated in Fig. 12 suggest that the large noise levels observed near 19 Hz are of biological origin. Although various species of whale such as grey whales, *Eschrichtius glaucus* (Ref. 11), blue whales, *Balaenoptera musculus* (Ref. 12), and fin whales, *Balaenoptera physalus* (Ref. 13) produce sound at this frequency and are known to inhabit the Pacific waters, the dominant source of biological noise at 19 Hz is probably the fin whale (Refs. 14, 15, and 16). The noise outside the band from about 14 Hz to approximately 25 Hz is attributed to shipping. This being the case, the noise due to biological sources and the noise due to shipping should exhibit different directional properties if the spatial distributions of the two types of noise sources are different.

(U) Figure 14 illustrates the relative distribution of fin whales as estimated from Japanese catch records (from Ref. 17). The various shaded regions indicate the concentrations of fin whales per 10-deg square. Judging from some of the results in Ref. 17, the distribution of fin whales illustrated in Fig. 14 is applicable to late summer. As fall approaches, the whale population along the Aleutian Islands and in the Gulf of Alaska decreases, with the greatest proportional reduction occurring in the Gulf of Alaska. The concentration of fin whales thus shifts from the vicinity of Anchorage (61°N, 150°W), which has a bearing of about 354 deg from the measurement site toward Adak (52°N, 172°W), which bears 319 deg

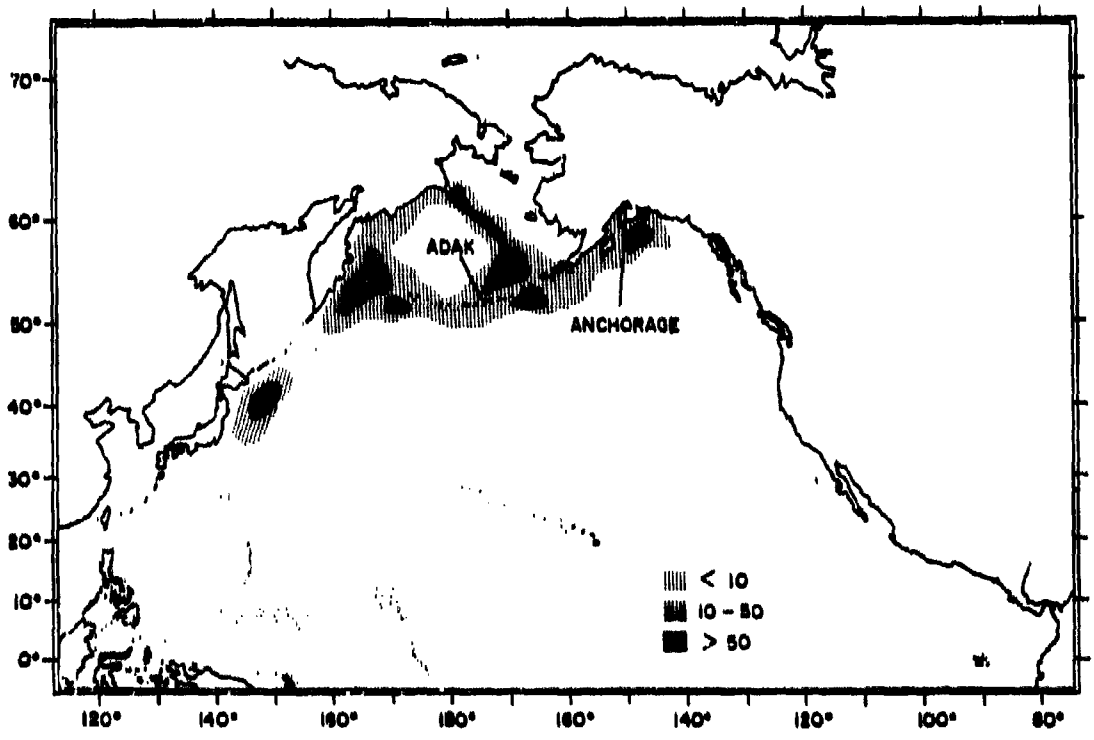

NOTE: THIS FIGURE WAS REPRODUCED FROM REFERENCE 17.

Figure 14. (U) Distribution of fin whales from Japanese historical catch records 1945-1962. (U)

from CHURCH OPAL Site λ_B. Unfortunately, historical shipping distributions such as Ref. 18 indicate that the shipping density along azimuths toward Alaska and the Aleutian Islands would also be high and, therefore, somewhat similar to the relative distribution of the fin whale. For bearings in these directions from CHURCH OPAL Site λ_B, relatively high noise levels would be expected in both the frequency regime dominated by whale noise (19-25 Hz) and the regime dominated by shipping noise (10-19 Hz and 25-100 Hz). The directionality patterns presented in Figs. 6 and 7 confirm these expectations. Hence, from considerations of noise directionality alone, the 19-Hz noise data cannot be attributed to noise sources other than those responsible for the levels observed at 50 or 100 Hz. Since the noise in the frequency regime near 19 Hz is due to both shipping and whales, extrapolation (in time) and interpolation (in frequency) are more complicated than at 50 Hz, for example, where shipping is the only major source of noise. This also adds another dimension of complexity to noise prediction or modeling efforts for the Northeast Pacific basin, since the geographic distribution of fin whales must be considered in any realistic model of ambient noise for frequencies near 19 Hz.

4.6 (U) AZIMUTHAL ANISOTROPY AND NOISE GAIN IMPROVEMENT

4.6.1 (U) Introduction

(U) The ambient noise field at any particular location in the ocean's water column is a function of three variables: horizontal arrival angle, vertical arrival angle and time. The horizontal directionality characteristics presented earlier describe the variability of the mean ambient noise levels in terms of the horizontal arrival angle only. Consequently, the horizontal directionality patterns given earlier (e.g., Figs. 6 and 7) do not provide any insight into the vertical structure of the ambient noise field or its temporal variability. The structure of the ambient noise field as a function of vertical arrival angle is usually represented by a vertical directionality pattern. Such patterns can be developed to portray the distribution of the total energy at the measurement site (i.e., all horizontal arrival angles included) or to depict the vertical structure of the ambient noise field within some horizontal sector.

(U) The horizontal directionality characteristics plotted in Figs. 6 and 7 indicate the level of persistent background noise measured in one part of the Northeast Pacific during a 2-week period. Average (mean) beam noise levels for any horizontal array at CHURCH OPAL Site λ_B during the same season (i.e., September) can be predicted by convolving the array's beam patterns with the resolved directionality characteristics. However, since the horizontal directionality plots represent long-term averaged data, the estimated beam noise levels are the mean values over a long time interval. Information regarding the beam-to-beam variability of the noise field has been lost in the averaging process.

(U) On the other hand, temporal variations of the ambient noise field are most often described in statistical terms, using the form of the distribution (normal, binomial, etc.) and its properties (i.e., moments, probability density functions and/or cumulative distribution functions) to represent the salient features of the ambient noise field in the time domain. Statistical techniques can also be used to describe the variability of beam noise levels. The term azimuthal anisotropy denotes one particular method of describing the variability in beam noise levels. Azimuthal anisotropy characteristics describe the beam noise levels resulting from the combined effects of spatial and temporal variations in the ambient noise field at any geographic location and depth. Azimuthal anisotropy characteristics are presented as

cumulative distributions of expected beam noise levels as a function of beamwidth. Since azimuthal anisotropy results deal only with ambient noise levels at the beamformer outputs, they are not sufficient to indicate the array gain which could be obtained at a particular geographic location and depth. Array gain investigations require that the relationship between beam noise levels and the omnidirectional noise level be known. The term noise gain improvement (NGI) identifies one method of presenting the latter relationship in a statistical manner. By definition, the parameter NGI is closely related to the term "array noise gain" (ANG) used throughout the literature. The remainder of this section presents several examples of azimuthal anisotropy and NGI results, outlines the data processing sequence used for the computations, and indicates some of the limitations inherent in the results.

4.6.2 (U) Typical Azimuthal Anisotropy Characteristics from CHURCH OPAL Beam Noise Measurements

(S) The form and content of the azimuthal anisotropy analysis results are illustrated in Fig. 15. These results were derived from the 50-Hz beam noise measurements accumulated at CHURCH OPAL Site λ_B at a depth of 500 m. For azimuthal anisotropy investigations,

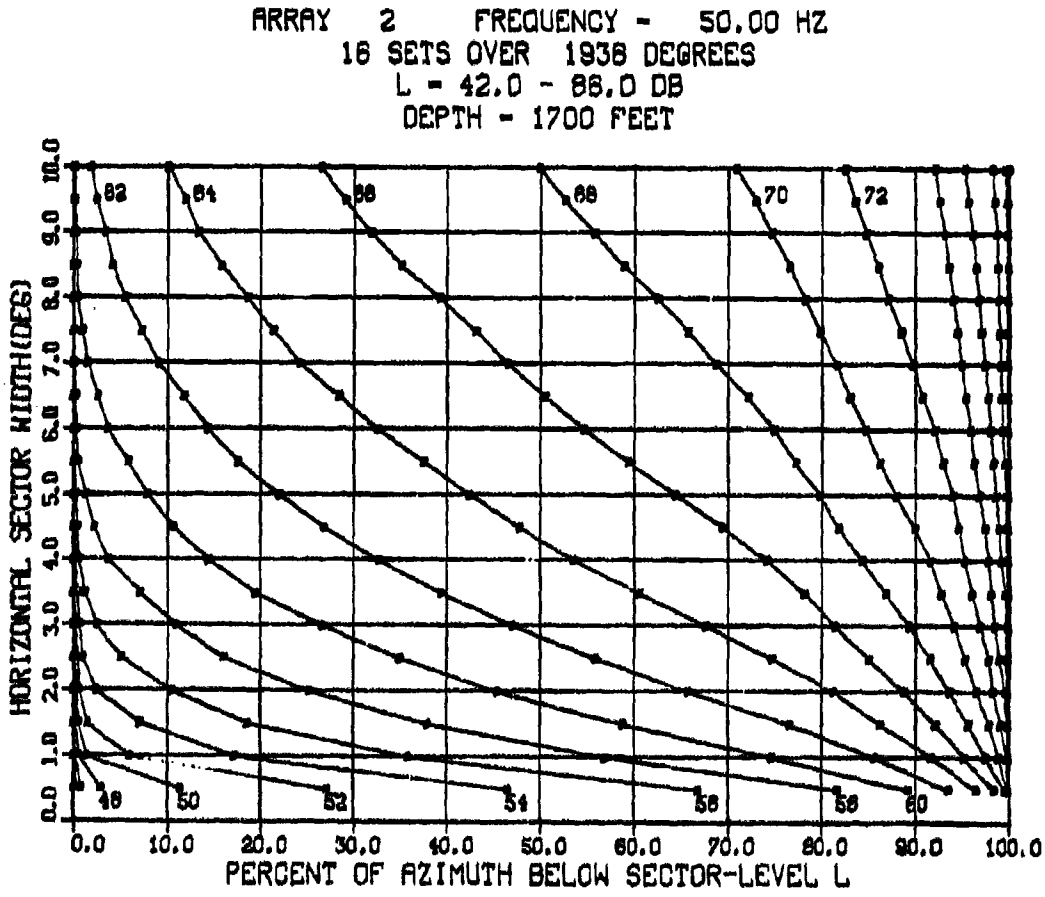

Figure 15. (C) Azimuthal anisotropy characteristics from 50-Hz beam noise measurements at CHURCH OPAL Site λ_B and a depth of 500 m. (C)

the preferred measurements are those obtained with the narrowest beamwidth. Thus, the data set analyzed for Fig. 15 was obtained with the LAMBDA MF array, therefore, 3-dB beamwidths during data collection ranged from approximately 3 deg for the broadside beam to about 6 deg for steering angles of ± 60 deg. It should be emphasized that the beam noise measurements used in this analysis are the average (mean) values for the 15-min data sampling periods. Thus, integration times on the order of 15 min are associated with the azimuthal anisotropy characteristics presented herein, as opposed to the much longer averaging period associated with the horizontal directionality and omnidirectional levels described earlier.

(C) Since the beam noise measurements were obtained on many headings, the azimuthal anisotropy characteristics presented in Fig. 15 are not biased toward any particular azimuthal sector or look direction. The results in Fig. 15 indicate that a horizontal line array with an ideal beamwidth of 3 deg would have the following distribution of 50-Hz beam noise levels as a function of azimuthal orientation.

a) 90% of azimuths ≤ 68 dB

b) 50% of azimuths ≤ 62.3 dB

c) 10% of azimuths ≤ 58 dB

However, for any practical array geometry the actual distribution of beam noise levels would be altered somewhat by the side-lobe contributions. For instance, if the array's side lobes are only suppressed by 20 dB, then the beam noise levels would generally not be less than approximately 61 dB (assuming the omnidirectional level is about 81 dB as reported in Section 4.3).

(C) Azimuthal anisotropy characteristics are useful for performance prediction or system design purposes. When used for system design investigations, the azimuthal anisotropy characteristics indicate the minimum beamwidth and, hence, the length of the array necessary to attain any particular noise level at the beamformer output. For example, a horizontal line array having a 50-Hz beamwidth of 1 deg would be expected to have beam noise levels (15-min average) of less than 56 dB for approximately 35% of all azimuths. Extrapolation of the data to narrower beamwidths assumes that the coherence remains constant as the aperture increases. Since this may not be the case, less confidence should be placed in the results presented for sector widths which are significantly less than the measurement array's beamwidths. Azimuthal anisotropy characteristics of the ambient noise field for frequencies of 11, 19, 50 and 100 Hz and depths of 180 and 500 m at CHURCH OPAL Site λ_B are presented in Appendix C.

4.6.3 (U) Noise Gain Improvement

(U) Azimuthal anisotropy characteristics present the statistical distribution of beam levels as a function of the ideal beamwidth. However, additional information can be extracted from the data. The parameter *Noise Gain Improvement* (NGI) indicates the relationship between beam noise levels and the omnidirectional noise level. Mathematically, NGI is defined as:

$$NGI = [L(omni) - L(beam)] + 20 \log \frac{Wu}{Wa} \qquad (4)$$

where:

L(omni) = omnidirectional noise level, in dB
L(beam) = ideal beam noise level, in dB
Wu = sum of uniform spatial shading (weighting) coefficients
Wa = sum of actual spatial shading (weighting) coefficients, max Wa = max Wu

A Hann weighting function was used to spatially shade the LAMBDA arrays (Wu/Wa = 0.5) and, consequently, the definition of NGI reduces to:

$$NGI = [L(omni) - L(beam)] - 6\ dB$$

The omnidirectional noise level (15-min average) for each leg of the noise polygon was calculated using Eq. (5) below:

$$L(omni) = 10 \log_{10} \sum_{i=1}^{i=64} 10^{[L_i/10]} - 10 \log_{10} \sum_{i=1}^{i=64} \frac{BW_i}{180} \qquad (5)$$

where:

L_i = noise level for the i^{th} beam, in dB; and
BW_i = beamwidth (-3 dB) of the i^{th} beam

(S) NGI results derived from the 50-Hz beam noise measurements acquired with the LAMBDA MF array are presented in Fig. 16. Since the same data set was used to generate the results presented in Figs. 15 and 16, both sets of characteristics are valid for an arbitrary azimuthal orientation of the array (i.e., all angles equally probably). By definition, noise gain improvement characteristics incorporate the effects of omnidirectional noise levels and are more directly related to system performance. However, care should be exercised in using the results presented in Fig. 16 and Appendix C since the measurements used in their preparation apply to only one time of year (September) and one geographic location (CHURCH OPAL Site λ_B).

(C) The effects of sidelobe suppression levels must also be considered in order to apply NGI results to any real array. Since side-lobe suppression levels establish the minimum beam noise level attainable with any real array, they also establish the maximum NGI attainable for the same array. From Eq. (4) it is apparent that the maximum value of NGI equals the side-lobe suppression level together with a correction term for the amplitude-shading function employed and, therefore, the NGI curves for real arrays either intersect this upper limit or approach it asymptotically.

4.6.4 (U) Data Processing Methods and Limitations

(U) Beam noise data acquired during noise polygon maneuvers provide the raw material for azimuthal anisotropy and noise gain improvement computations. The initial step in the processing sequence is to associate each average (mean) beam noise level with the corresponding look direction (i.e., true bearing or azimuthal angle) for that beam. Implicit

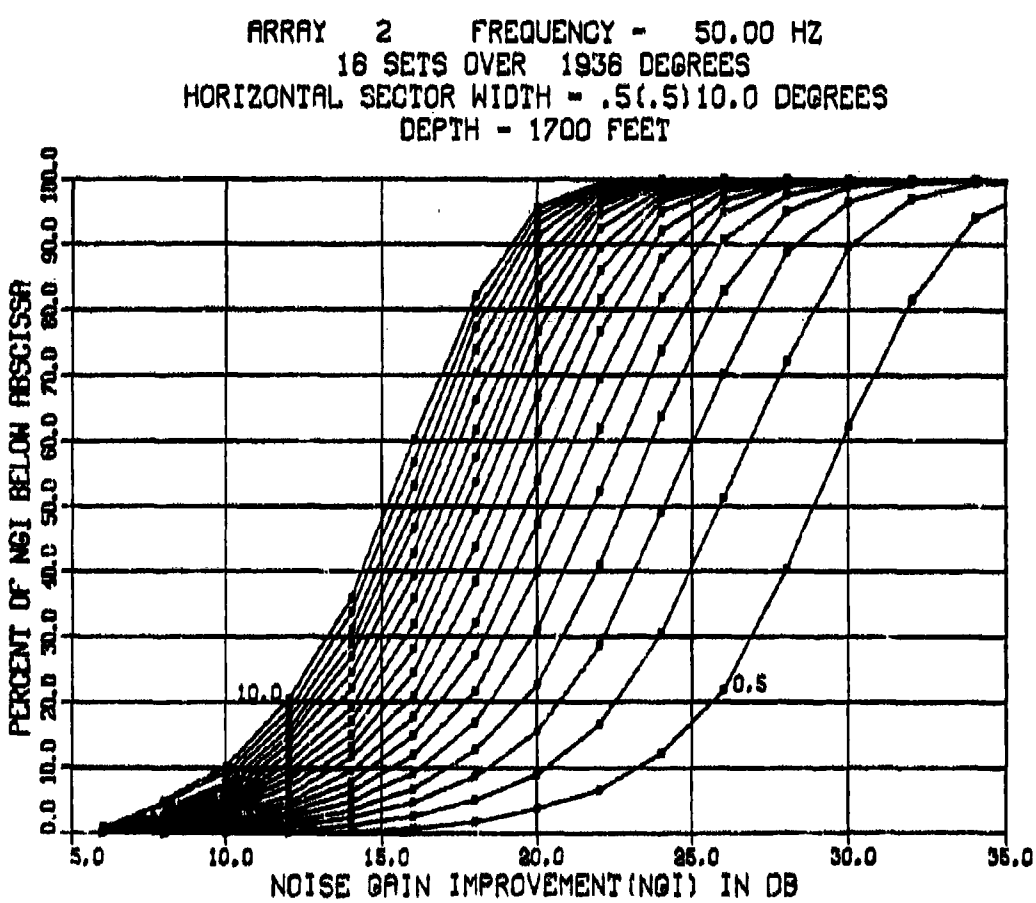

Figure 16. (C) Noise gain improvement characteristics from 50-Hz noise measurements at CHURCH OPAL Site λ_B and a depth of 500 m. (C)

in this step is the need for an accurate estimate of the array heading during each leg of the polygon and a complete set of beam patterns for the frequencies of interest. Measured beam noise levels are then organized (sorted) by look direction in order to determine the directions that generally have the highest or lowest levels and to depict the distribution of beam measurements as a function of azimuth.

(U) The next step is an attempt to remove the spatial smoothing effects of the array without resolving the left-right ambiguities in the data caused by the symmetrical beam pattern. This step is accomplished by deconvolving the array's beam patterns with each set of beam noise measurements acquired during every leg of the noise polygon. The deconvolution algorithm is the same as that employed during the horizontal directionality computations (see Section 4.2 of Ref. 6) but, in this case, it is applied to the beam noise measurements obtained on each leg of the polygon. The computation yields an estimate of the ambiguous noise field for each leg of the noise polygon and, thus, the azimuthal variation in the measured data is retained.

(U) Beam patterns for an ideal horizontal line array (i.e., uniform response across the main lobe and infinitely suppressed side lobes) are then convolved with the estimated noise field for each leg of the polygon. However, the ideal beam patterns are seldom convolved over the entire range of possible azimuthal angles. Instead, the convolution process is usually restricted to some range of angles about the broadside beam (typically, 90 ± 60 deg) that corresponds to a reasonable range of beamwidths. The convolution process yields ideal beam noise levels for each leg of the noise polygon, as functions of azimuth and sector width (or ideal beamwidth), that are accumulated and plotted as a cumulative distribution function. By eliminating the influence of the endfire beam measurements, the number of dependent samples in the cumulative distribution function is minimized.

(U) Noise gain improvement (NGI) functions are developed from the results of the azimuthal anisotropy processing sequence (i.e., the ideal beam levels) and the omnidirectional noise levels calculated for each leg of the noise polygon. Differences between the beam levels and the corresponding omnidirectional level are formed, sorted according to the magnitude of the difference and then accumulated for plotting as a cumulative distribution function.

(U) In the work reported herein, all the valid ideal beam noise levels have been used in the azimuthal anisotropy and noise gain improvement computations. With a large number of array headings the results calculated in this manner are not biased toward any particular look direction or azimuthal sector. However, azimuthal anisotropy and noise gain improvement characteristics can be generated for any true bearing sector by cumulating only those ideal beam levels or NGI values that correspond to look directions within the true bearing sector of interest.

(U) It should be noted that the azimuthal anisotropy and NGI characteristics resulting from these computations are only applicable to horizontal line towed arrays. No attempt was made to remove ambiguities introduced into the data by the inherent left-right ambiguity in the measurement array's beam patterns. Furthermore, since an independent estimate of the vertical arrival structure is not available, effects of the conically shaped beams cannot be removed from the measurements. The measurement array's finite side-lobe structure also affects azimuthal anisotropy and NGI results -- especially at the lowest beam levels. Although the deconvolution technique attempts to account for the noise contributions obtained from the side lobes, this is not entirely possible. Some residual contamination of the lowest measured beam levels will always be present.

(U) In addition, it should be noted that the convolution process obtains noise levels in ideal beamwidths or azimuthal sectors. Side-lobe structures are not included in the convolution process since these are characteristics of the measurement array and not properties of the noise field. Thus, in order to obtain realistic beam noise or NGI levels for any practical towed array geometry, side-lobe contributions must be considered. However, for any reasonably configured array the effect is significant only at the lower beam noise levels. Also, the extrapolation of the measured data to narrow beamwidths assumes that the same coherence would exist across a proportionately larger aperture. This may not be the case. Therefore, caution should be exercised when using the azimuthal anisotropy or noise gain improvement results for beamwidths or sector widths that are substantially narrower than those of the measurement array. These considerations should not impair the usefulness of the derived noise field properties, provided that their application is restricted to horizontal line arrays and that the limitations are recognized.

SECTION 5. (U) REFERENCES

1. Xonics, Inc. "CHURCH OPAL Exercise Plan (U)." Xonics Document Control No. 1011. Office of Naval Research. Arlington, Virginia. August 1975. SECRET.

2. Xonics, Inc. "CHURCH OPAL Exercise Summary (U)." Xonics Document Control No. 1030. Office of Naval Research. Arlington, Virginia. September 1975. SECRET.

3. Long Range Acoustic Propagation Project. "CHURCH OPAL Environmental Acoustic Summary (U)." LRAPP Report S77-002. Naval Ocean Research and Development Activity. NSTL Station, Mississippi. April 1977. SECRET.

4. R. A. Wagstaff, J. D. Pugh, and J. W. Aitkenhead. "Horizontal Directionality of Ambient Sea Noise in the North Pacific Ocean (U)." NUC TP 419. Naval Undersea Center. San Diego, California. May 1976. SECRET.

5. R. A. Wagstaff and J. W. Aitkenhead. "Horizontal Directionality of Ambient Noise in the Sofar Channel of the Northeast Pacific Ocean (U)." JUA. Vol. 26, No. 2. April 1976. CONFIDENTIAL.

6. R. A. Wagstaff. "Iterative Technique for Ambient Noise Horizontal Directionality Estimation From Towed Line Array Data." J. Acoust. Soc. Am. Vol. 63, No. 3. March 1978. pp 863-869.

7. G. E. Martin. "Beamforming for CHURCH STROKE and CHURCH OPAL (U)." NOSC TN . Naval Ocean Systems Center. San Diego, California. (To be published.)

8. A. F. Wittenborn. "Ambient Noise and Associated Propagation Factors as a Function of Depth and Wind Speed in the Deep Ocean (U)." (Preliminary Report) Report No. T76 RV 5060C. Tracor, Inc. Arlington, Virginia. April 1976. CONFIDENTIAL.

9. Long Range Acoustic Propagation Project. "Exercise Plan for CHURCH STROKE ONE (U)." LRAPP Report S77-001. Naval Ocean Research and Development Activity. Bay St. Louis, Mississippi. April 1977. SECRET.

10. R. A. Wagstaff. "Ambient Noise Depth Dependence (U)." JUA. Vol. 23, No. 4, pp 543-549. CONFIDENTIAL.

11. W. C. Cummings, P. O. Thompson, and R. Cook. "Underwater Sounds of Migrating Gray Whales, Eschrichtius glaucus (Cope)." J. Acoust. Soc. Am. Vol. 44, No. 5. 1968. pp 1278-1281.

12. W. C. Cummings, P. O. Thompson, and R. Cook. "Underwater Sounds from the Blue Whale, Balaenoptera musculus." J. Acoust. Soc. Am. Vol. 50, No. 4. 1971. pp 1193-1198.

13. P. O. Thompson and W. C. Cummings. "Sound Production of the Finback Whale, Balaenoptera physalus and Eden's Whale, B. edeni, in the Gulf of California (A)" in Proceedings of the Sixth Annual Conference on Biological Sonar and Diving Mammals. Stanford Research Institute. Stanford, California. 1969. p 109.

14. J. Northrop, W. C. Cummings and P. O. Thompson. "20-Hz Signals Observed in the Central Pacific." J. Acoust. Soc. Am. Vol. 43, No. 2. 1973. pp 383-384.

15. W. E. Schevill. "Classification of Natural Sounds in the Underwater Ambient." JUA. Vol. 16, No. 2. April 1966.

16. D. E. Weston and R. I. Black. "Some Unusual Low-Frequency Biological Noises Underwater." *Deep-Sea Research.* Vol. 12. 1965. pp 295-298.

17. R. D. Rinaldi. "The Probable Distribution of Whales as Sonar Targets in the North Pacific Ocean by Analysis of Whaling Data." Masters Thesis. Naval Postgraduate School. Monterey, California. March 1972.

18. D. Ross, J. Mahler, and L. Solomon. "Navy Interim Shipping Distribution Model." Enclosure to Planning Systems, Inc. Memorandum of 17 Dec 1974. McLean, Virginia.

19. C. E. Davis. "LAMBDA Operational Notes (U)." (Manuscript report.) Naval Undersea Center, San Diego, California. October 1976. SECRET.

20. P. J. Buca. "CHURCH OPAL Exercise: Preliminary Environmental Analysis (U)." (Manuscript report.) Naval Ocean Research and Development Activity. NSTL Station, Mississippi.

21. Bunker Ramo Corporation – Electronic Systems Division. MEDEX Processing System Final Report Volume II: Software. Westlake Village, California. 21 October 1974.

APPENDIX A. LARGE APERTURE MARINE BASIC DATA ARRAY (LAMBDA) (U)

A.1 (U) OVERVIEW

(C) The Large Aperture Marine Basic Data Array (LAMBDA) System is a towed, horizontal line array of acoustic sensors together with certain shipboard electronic equipment. LAMBDA was designed specifically for the collection of acoustic data applicable to undersea surveillance project needs. For descriptive purposes, the LAMBDA system can be subdivided into three basic equipment groupings:

- Wet-end components:
  - A faired tow cable;
  - Vibration-isolation modules (VIMs) both forward and aft of the acoustic array;
  - A compound linear array of hydrophone groups; and
  - A drogue of braided nylon rope (optional).
- Deck handling and storage equipment for the array (i.e., the winch, a level wind assembly, control stations for array deployment/recovery and various items of loose equipment).
- Shipboard electronics
  - Analog signal conditioning equipment;
  - Three-Array Processor (TAP); and
  - Data Analysis Subsystem.

LAMBDA was installed aboard M/V SEISMIC EXPLORER for the duration of the CHURCH OPAL exercise. The winch and level wind assembly were installed near the stern of the ship with the signal processing and data analysis equipment installed in a nearby compartment.

A.2 (U) LAMBDA WET-END COMPONENTS

A.2.1 (U) Physical Description

(U) Mechanically, the LAMBDA wet end consists of the major items listed below and assembled in the sequence shown in Figure A-1.

Item	Length (ft)	Outside Diameter (in.)
Tow Cable	5000	1.9
Forward VIM Assembly (8 modules)	2000	2.9
VL, PDT and RSM Modules (3)	95	3.5
HF Array (4 "C" sections)	505	3.5
RSM (1 module)	50	3.5

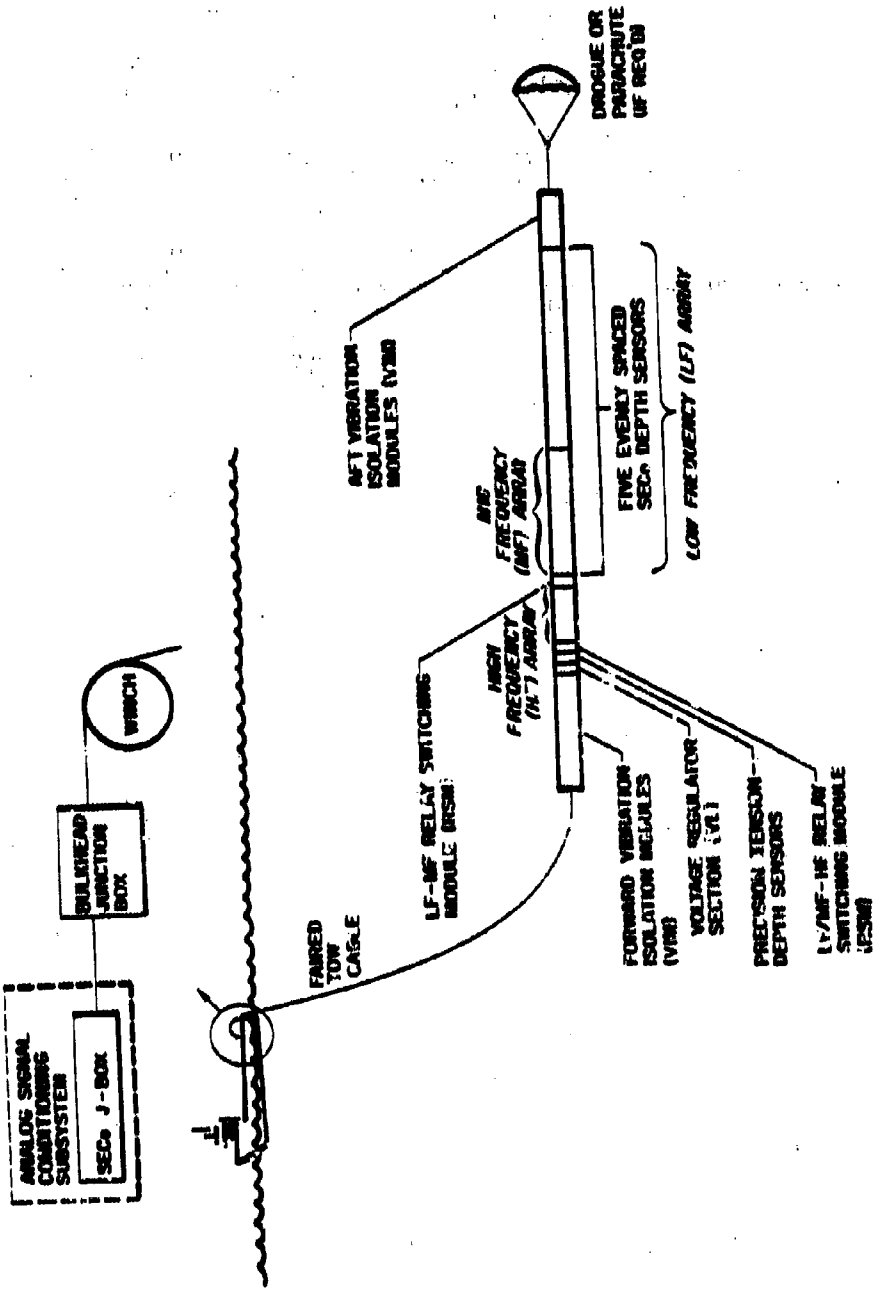

Figure A-1. (C) LAMBDA wet-end configuration. (U)

Item	Length (ft)	Outside Diameter (in.)
MF and LF Arrays (21 "B" sections & 43 "A" sections)	8000	3.5
Aft VIM Assembly (4 modules)	1000	2.9
Drogue	As needed	

As shown in Fig. A-1, five depth sensors were also incorporated in the LAMBDA array configuration deployed during CHURCH OPAL. Five Seismic Engineering Company (SECo) depth sensor modules (each about 5 ft long) were spaced at approximately equal intervals along the length of the LF array. Heading sensors were not included in the LAMBDA wet end configuration deployed during the CHURCH OPAL Exercise.

(C) The active portion of the LAMBDA wet end consists of 68 acoustic sensor modules (4 "C" sections, 21 "B" sections and 43 "A" sections). Each acoustic sensor module is a sealed unit, approximately 125 ft in length, that is filled with a liquid hydrocarbon for buoyancy control and electrical insulation purposes. Long, continuous sections of seamless tubing are joined together to form the outer surface of the module. Polyvinylchloride (PVC) tubing is used throughout the MF and LF arrays ("A" and "B" sections) but the HF modules ("C" sections) use a polyurethane material for the module's outer skin. A pressure bulkhead seals each end of the module and prevents leakage of the fill fluid. Spacers (cylindrical disks) are distributed along the entire length of the module in order to maintain a uniform cylindrical shape and thereby reduce flow noise. Three wire rope strength members run longitudinally through each module and provide the capability to withstand relatively large tensile loads. Consequently, the longitudinal stresses encountered in normal operations result in virtually no deformation of the array in the fore/aft direction. For the most part, the interior of the module is filled with wire harnesses, which also run longitudinally through the module paralleling the strength members.

(U) Vibration-isolation modules (VIMs) attenuate vibratory motion in the direction of the array's longitudinal axis that can result from tow ship motions, cable strum effects, or tail drogue motion. Each VIM module is 250 ft in overall length and is constructed in much the same manner as the acoustic sensor modules. However, three nylon ropes are used as the strength members in the VIMs instead of the wire ropes used elsewhere. Thus, the VIMs are somewhat elastic and can decouple longitudinal vibrations and shocks from the active portion of the array.

(C) An electromechanical tow cable provides the mechanical and electrical linkages between M/V SEISMIC EXPLORER and the acoustic arrays. The LAMBDA tow cable contains 84 twisted pairs of conductors which surround a coaxial cable. The electrical cable is surrounded with a thick layer of insulation. In turn, strength members surround the electrical cable and are double wrapped, in a torque-balancing arrangement. The tow cable "fairing" consists of fabric-reinforced neoprene rubber flags which are attached along nearly all of the tow cable's length in order to suppress cable strum vibrations.

A.2.2 (U) Electroacoustic Characteristics

(S) The LAMBDA wet end contains three distinct arrays of hydrophones (i.e., the HF, MF and LF arrays) arranged in the manner shown in Fig. A-1. The HF array is completely separate from the LF and MF arrays. However, the latter two arrays are "nested" and, thus, share certain common hydrophone groups. Physical and electrical characteristics of the three arrays are summarized in Table A-1 and can be used to gain further understanding of the modular construction arrangement outlined above. Each of 21 "B" sections used in the LF and MF array configuration contains three hydrophone groups per module. Each "A" section used in the LAMBDA array contains one hydrophone group whose center is located 41.67 ft aft of the module connection point. Thus, the MF array consists of all 63 hydrophone groups in the 21 "B" modules and the hydrophone group in the first "A" module. The LF array consists of the first hydrophone group in each "B" module and the hydrophone groups in all 43 "A" sections.

(C) The LAMBDA wet end contains the same type of electronics employed by the manufacturer (Seismic Engineering Company) in its commercial towed arrays intended for geophysical survey applications. A preamplifier is incorporated in the array adjacent to each hydrophone group, with the output from each hydrophone group transformer coupled to the preamplifier's input terminals. The amplified, but still low-level, analog signal is then transmitted to the tow ship on an individual twisted pair of conductors. However, due to the limited number of electrical conductors in the two cable, only one 64-element LAMBDA array can be monitored aboard ship at any given time. Two Relay Switching Modules (RSMs) are provided in the LAMBDA wet-end configuration in order to connect the 64 acoustic data channels in the tow cable to the desired 64-element array. Array selection is controlled manually by the operator aboard ship.

(S) Specific electroacoustic characteristics of the LAMBDA hydrophone groups are as follows:

Hydrophone group sensitivity:	
MF and LF arrays	-185 dBV re 1 μPa
HF array	-187 dBV re 1 μPa
Frequency response:	Flat to 1 kHz
Hydrophone group capacitance:	
MF and LF arrays	8.8 μF
HF array	2.2 μF
Hydrophone group sensitivity variation with depth changes:	0.5 dB per 1000 ft
Hydrophone crush depth:	6000 ft.

A.3 (U) SHIPBOARD ELECTRONICS

A.3.1 (U) Introduction

(C) Signal conditioning, recording, and data processing equipment installed aboard M/V SEISMIC EXPLORER for the CHURCH OPAL exercise are shown in Figs. A-2 and A-3.

Table A-1. (S) LAMBDA array characteristics. (U)

	LF Array	MF Array	HF Array
Hydrophone Type (Multidyne™)	MD-3	MD-3	MD-3
No. of Hydrophones per Group	20	20	4
Hydrophone Spacing (See Note 2)	1.095 ft (0.334 m)	1.095 ft (0.334 m)	0.24 ft (0.378 m)
No. of Hydrophone Groups	64	64	64
Average Hydrophone Group Center-To-Center Spacing (See Note 3)	125 ft (38.10 m)	41.67 ft (12.70 m)	7.42 ft (2.26 m)
Hydrophone Group Length	20.8 ft (6.34 m)	20.8 ft (6.34 m)	3.71 ft (1.13 m)
Acoustic Aperture (See Note 5)	7896 ft (2407 m)	2645 ft (806 m)	470 ft (143 m)
Frequency Response (Hydrophone & Preamplifier			
±0.5 dB	4-100 Hz	4-100 Hz	52-320 Hz
-3.0 dB	2-500 Hz	2-500 Hz	40-350 Hz
Operating Depth	100 ft to 4000 ft (30.5 m to 1219 m)		
Survival Depth	6000 ft (1829 m)		
Preamplifier Gain	28 dB		
Preamplifier Output Impedance	100 ohms		
Streamer O.D.	3.5 in. (8.89 cm)		
Forward VIM Length & O.D.	2000 ft & 2.9 in. (610 m & 7.37 cm)		
Aft VIM Length & O.D.	1000 ft & 2.9 in. (305 m & 7.37 cm)		
Tow Cable Length & O.D.	5000 ft & 1.9 in. (1524 m & 4.83 cm)		

Notes:

1) Array dimensions and other characteristics were obtained from the Seismic Engineering Company documents entitled "Instructions Manual LAMBDA VIII Array" and "High Frequency Array, LAMBDA VIII Array" (both undated).
2) Actual hydrophone group lengths and spacings in the MF array vary somewhat. Average spacing given here was calculated from the nominal hydrophone group length.
3) Average hydrophone group center-to-center spacing given for MF array varies somewhat; consult the SECo drawings for more detail.
4) HF Array construction is unique. Module length = 17 x (hydrophone group center-to-center spacing). A hydrophone group is not included at the module coupling location; hence, each coupling location is a "dead phone". Physically, the HF array is 67 elements long with 3 "dead phones".
5) Acoustic aperture calculated by the following:

   Acoustic aperture = 63 (hydrophone group center-to-center spacing) + 1 (hydrophone group length).

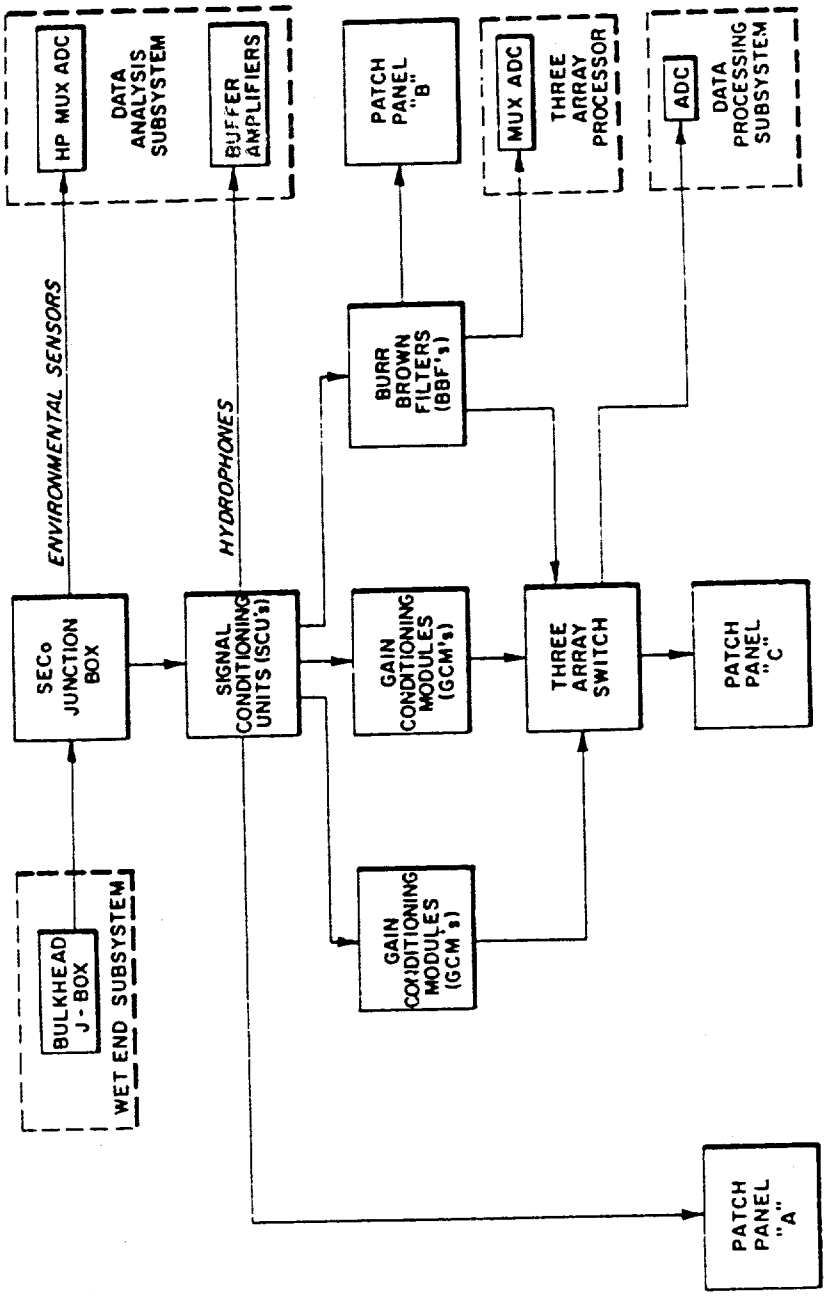

Figure A-2. (U) Functional block diagram of LAMBDA signal processing equipment. (U)

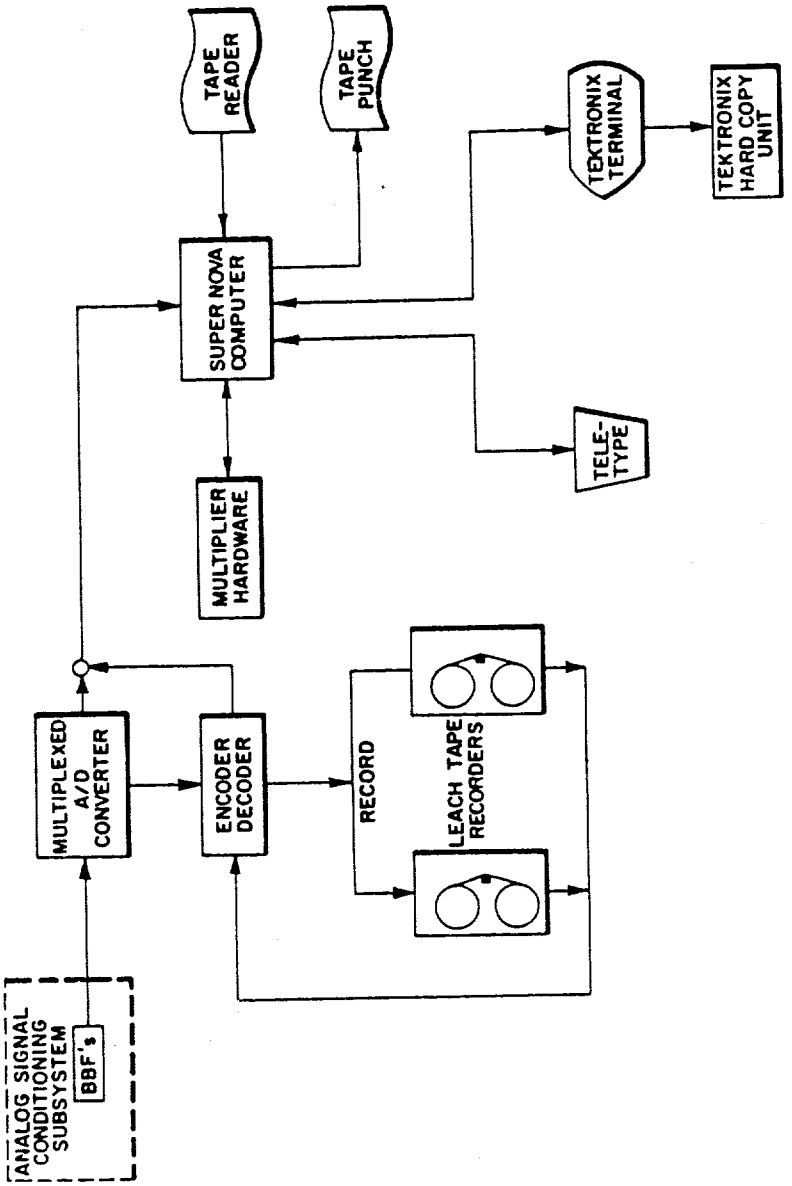

Figure A-3. (U) Three array processor (TAP) block diagram. (U)

The remainder of this section presents brief descriptions of the three equipment groupings used for the acquisition and analysis of ambient noise data.

- Analog signal conditioning equipment (see Fig. A-2)
- Three-Array Processor (see Fig. A-3)
- Data Analysis Subsystem

A.3.2 (U) Analog Signal Conditioning Equipment

(C) As stated, 64 low-level analog outputs from the selected array are transmitted on separate conductor pairs to the tow ship. Upon receipt aboard ship, the input signal from each LF or MF hydrophone group is applied to an RC circuit which is used to adjust the phase of the data channel. Since the transmission line lengths for the MF and LF arrays vary by a substantial amount, equalization of the phase shift in all 64 signal channels is mandatory for proper beamforming. Equalization of the gain in each channel is also accomplished at this point through the use of resistive divider networks.

(S) Each signal channel is then routed to a signal conditioning unit, (SCU) which contains a variable-gain amplifier and both high-pass and low-pass filters. Specifications for the Data Control Systems (DCS) SCU-3G units are presented below:

High-pass filter:	3-pole Butterworth, -3 dB point at 4.5 Hz
Low-pass filter:	6-pole Bessel, -3 dB point at 1000 Hz
Gain:	0 to 90 dB in 6 dB increments

Outputs from the SCU-3G units are then routed to anti-aliasing filters and prewhitening circuits (HF array only) prior to beamforming. In addition, the SCU outputs are also available for monitoring, spectral analysis and recording operations with the Data Analysis Subsystem.

(S) Gain conditioning modules (GCMs) provide anti-aliasing filters for the LF and MF acoustic data channels. Specifications for the Data Control Systems GCM-1 units are as follows:

LF array low-pass filter:	9-pole elliptic, -3 dB point at 26.5 Hz
MF array low-pass filter:	9-pole elliptic, -3 dB point at 53 Hz
Gain:	0 to 90 dB in 6-dB increments

(S) Anti-aliasing filters and prewhitening circuits for the HF acoustic data channels are provided by the Burr Brown filters (BBFs). Specifications for the active filters and prewhitening units (Burr Brown model ATF76-L8MB-3200/16) are listed below:

HF array prewhitening:	2-pole Butterworth, +3 dB point at 56 Hz
HF array low-pass filter:	8-pole Butterworth, -3 dB point at 320 Hz
Gain:	0 to 40 dB

A.3.3 (U) Three-Array Processor

(C) Although originally intended as a backup system, the TAP was the primary equipment used for beamforming and spectral analysis operations during the CHURCH OPAL Exercise. Since the capabilities of the TAP are somewhat limited, the quantity of data that could be acquired was correspondingly less than originally planned. TAP characteristics affecting the ambient noise analyses are listed below:

- Spectral Analysis
  - Discrete Fourier transform (DFT) algorithm limited power spectra calculations to one analysis frequency and bandwidth at any given time;
  - Transform length varied as a function of the array used (sampling rate) and spectral analysis bandwidth;
  - Hann window used to amplitude weight FFT inputs.
    Note: Rectangular and WAG windows were also selectable by the operator but were not used for the work reported herein (see Ref. 21);
  - Maximum of 8 analysis frequencies allowed per run (see Table 2 for spectral analysis frequencies and bandwidths actually used).
- Beamforming
  - Full azimuthal coverage using 64 beams, spaced in equal increments of sin θ_s (see Fig. 3);
  - Hann window used for amplitude weighting (spatial shading) across the acoustic aperture.
    Note: Spatial shading coefficients were hand-entered by the operator into specific storage locations (tables) provided within the TAP software (three shading tables were available per array).
- Averaging

(U) For ambient noise analyses, the most severe drawback of the TAP is the inability to obtain simultaneous power level measurements at several analysis frequencies. Since the DFT algorithm provided Fourier coefficients for only one analysis frequency and bandwidth at any given time, beam noise levels could only be measured sequentially, one analysis frequency at a time. The results shown in the body of the report (see Fig. 2) illustrate the TAP measurement and analysis cycle. The averaged beam power levels of samples used in this average is selected by the operator and is listed in the legend above the plot (e.g., SAMPLE SIZE/FREQ = 12 in Fig. 2). As the information presented in Fig. 2 implies, the TAP made three complete cycles through the set of five MF array analysis frequencies during this particular run. The most recent data plotted are available within the computer and can be listed in the manner shown in Fig. 3. In addition, cumulative results from all the measurements, indexed according to frequency and steering angle, are available in a master accumulator table. The master accumulator table is output in almost the identical format as Fig. 3; only the title and number of updates are different. The average (mean) beam power levels contained in the master accumulator table were taken as representative values for each (15-min) CHURCH OPAL ambient noise measurement interval. It is these values that were used in subsequent processing actions for horizontal directionality and azimuthal anisotropy assessments.

(U) The TAP hardware suite consisted of the following units interconnected in the manner shown in Fig. A-3.

- Multiplexed analog to digital converter (Analogic)
- SUPERNOVA computer (Data General Corporation)
- Hardwired multiplier unit for amplitude shading product calculations
- CRT terminal and hard copy unit (Tektronix)
- Assorted peripherals (e.g., tape recorders, teletypewriter, tape reader and tape punch).

A.3.4 (U) Data Analysis Subsystem

(U) The LAMBDA Data Analysis Subsystem consisted of an HP 2100A minicomputer, the computer peripherals listed below as well as various other equipment items.

- HP 7900A moving-head disc memory
- HP 7970B (9-track, digital) magnetic tape recorder/reproducer
- Tektronix 4010 computer terminal
- Tektronix 4610 Hard Copy Unit
- COMPLOT plotter
- Line printer (132-column)
- Teletypewriter
- Paper tape reader
- Paper tape punch

As the name implies, the Data Analysis Subsystem is intended for timely analysis of acoustic and non-acoustic data collected during at-sea operations. Its primary use in support of the CHURCH OPAL ambient noise objectives was to execute ambiguity resolution algorithms. In this manner, an initial assessment of the ambient noise field's horizontal directionality properties could be obtained shortly after the measurements were collected.

APPENDIX B. ENVIRONMENTAL DATA (U)

(U) The prevailing environmental conditions during the CHURCH OPAL Exercise were very nearly the same as the predicted conditions for the Northeast Pacific operating area during the late summer or early fall. The figures presented in this appendix were extracted from Ref. 20 and are intended as a summary description only. For a more complete description, the interested reader should consult Refs. 3 and 20.

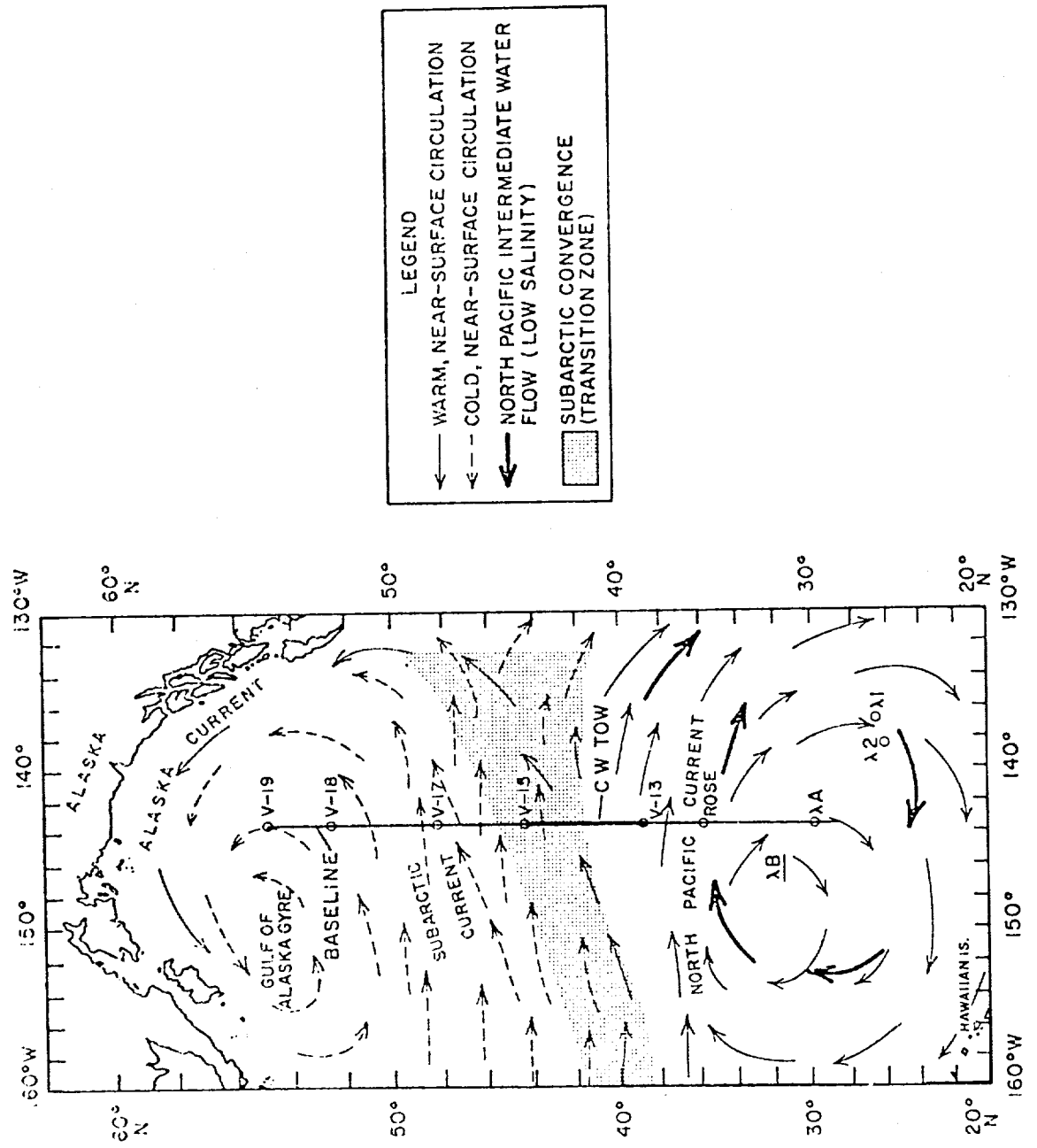

Figure B-1. (U) Generalized ocean circulation in the CHURCH OPAL Exercise area. (U)

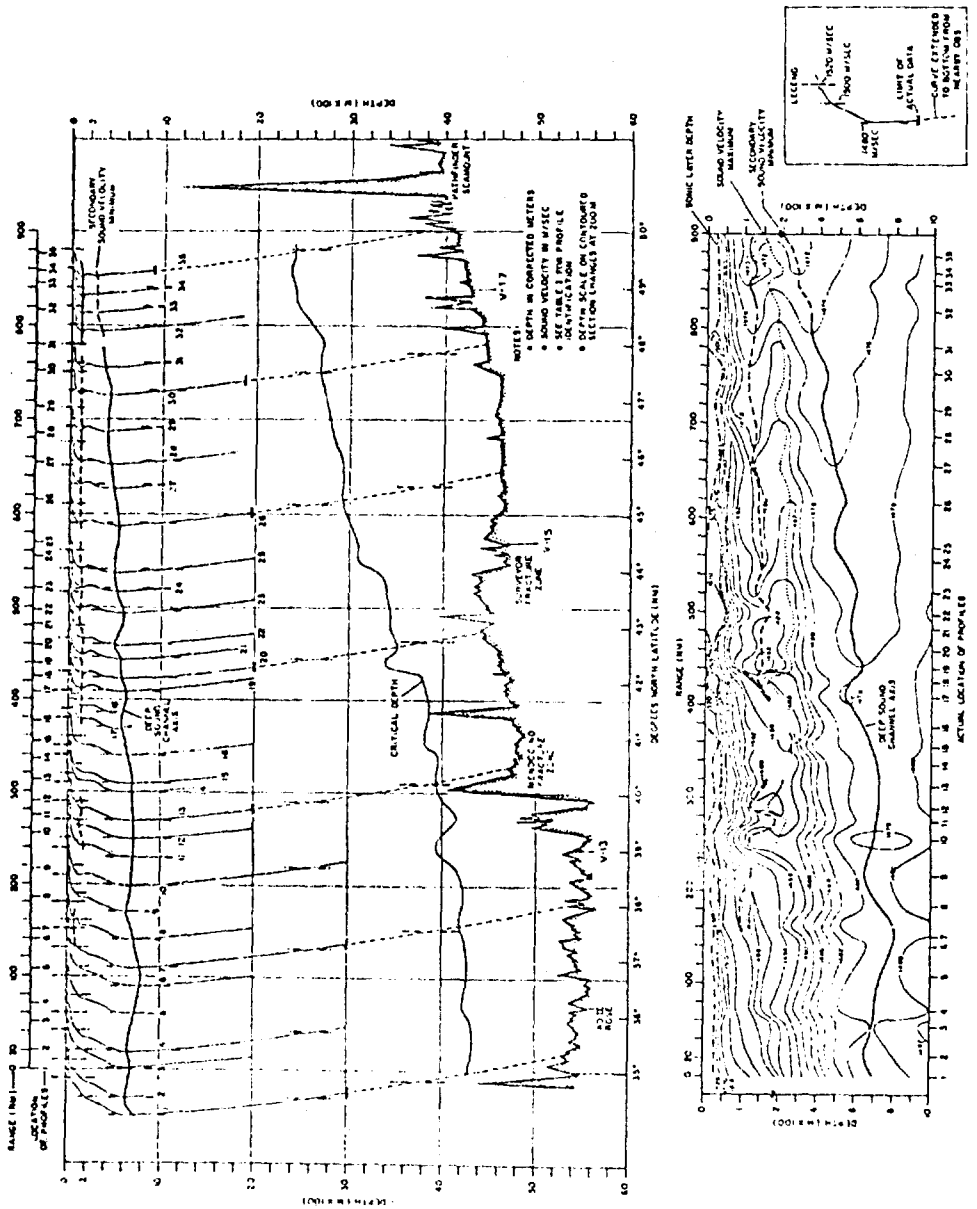

Figure B-2. (U) Sound-speed structure along the CHURCH OPAL Exercise baseline (143° 30'W) during the September 11-30, 1975 time frame. (U)

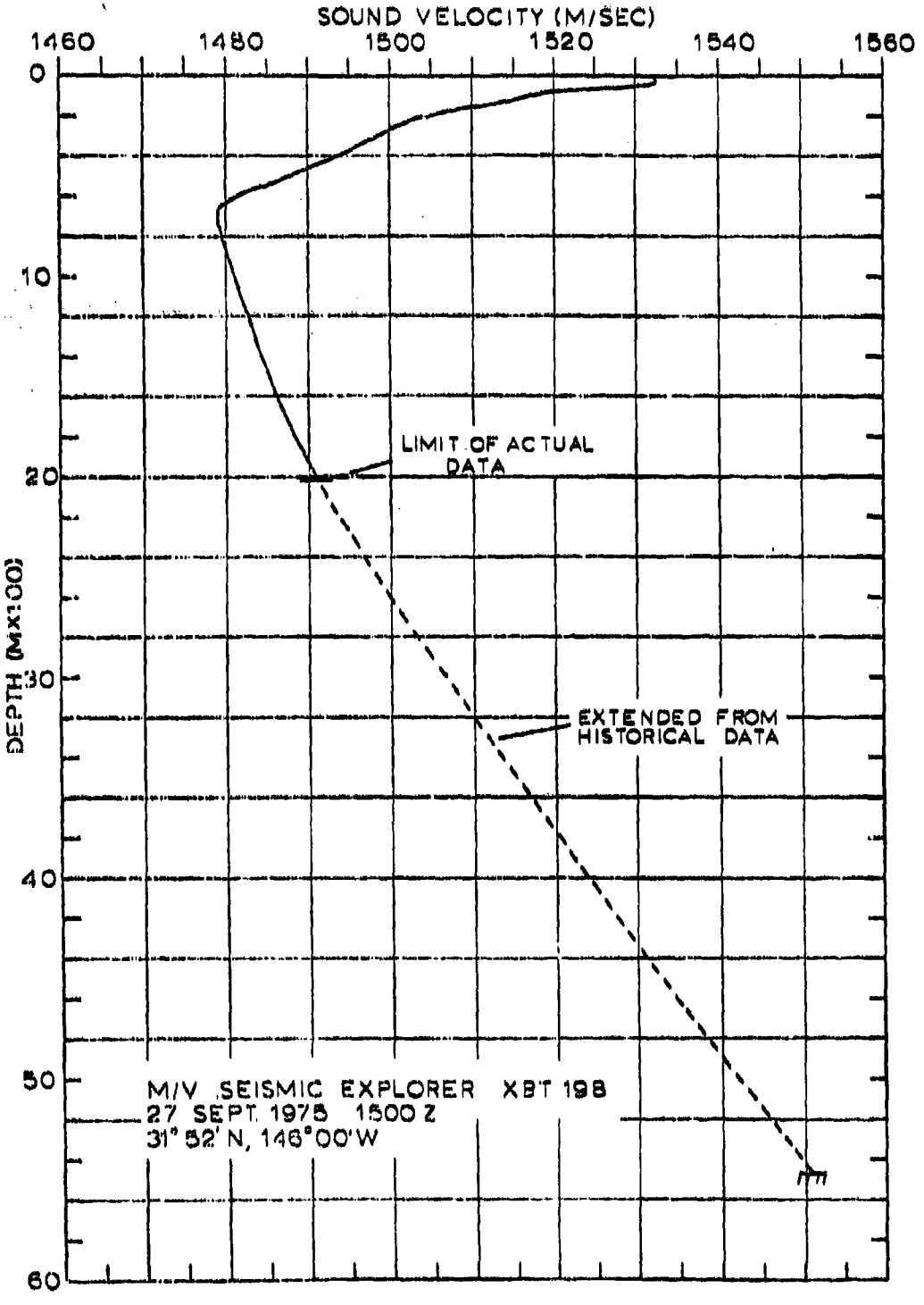

Figure B-3. (U) Sound-speed profile in the vicinity of Site λB. (U)

APPENDIX C. AZIMUTHAL ANISOTROPY AND NOISE GAIN IMPROVEMENT (U)

(C) Azimuthal variations of 11, 19, 50 and 100 Hz ambient noise levels for various beam or sector widths are presented in this appendix. The ambient noise analysis results presented herein complement and extend the azimuthal anisotropy results presented in the body of the report (see Section 4.6). Data analysis procedures and the methods used for presentation of results are the same as described in the body of the report and will not be repeated here. However, it is important to emphasize that:

a. Azimuthal anisotropy and noise gain improvement results presented in this appendix were computed from all noise polygon measurements. Thus, the input data have not been limited to any particular true bearing sector or azimuthal orientation (i.e., such as north/south or east/west orientations).

b. Left-right ambiguities in the data have not been removed and, consequently, the results are applicable only for horizontal arrays with similar ambiguities in the beam patterns.

c. The data processing algorithms used for this analysis attempted to remove spatial smoothing effects produced by the measurement array and also attempted to eliminate contributions from the side lobes. However, greater uncertainties in the results should be expected for the lowest beam noise levels since these levels are subject to the largest measurement and data processing errors. For example, the lowest beam levels measured by the LAMBDA arrays are undoubtedly contaminated to some extent by the individual array's sidelobe structure (see Appendix A) and, thus, are probably not the lowest levels which would be measured by a "perfect" array.

Nonetheless, the results provide an adequate description of the noise field for those surveillance system performance investigations which focus on beamwidth considerations.

(C) Azimuthal anisotropy of the beam noise levels (in one frequency band) at a particular site is presented in the form of a cumulative distribution function. The ordinate of the plot is the horizontal aperture of the main lobe (i.e., sector width or beamwidth. To be exact, the sector width shown is the width of an ideal beam pattern for a horizontal line array (i.e., a cone-shaped beam pattern with a uniform response across the main lobe and complete suppression of all side lobes). The abscissa yields the relative number of azimuthal orientations (in percent) for which the beam output would be less than the noise level corresponding to the plotted curve. Using Figure C-1 as an example, a horizontal line array with an ideal beamwidth of 4 deg (at 11 Hz) would measure beam noise levels of less than 64.3 dB on 50% of all possible beam orientations when towed at Site λ_B at a depth of approximately 180 m.

(C) Noise gain improvement (NGI) results are also presented in terms of a cumulative distribution function with the ideal sector width (or beamwidth) used as a parameter. It should be emphasized that noise gain improvement results indicate the statistical relationship between beam noise levels and omnidirectional noise levels. Since the input data have not been screened or selected on the basis of array heading values, the results combine the effects

of spatial variations in the ambient noise field together with temporal variations in the ambient noise field. At 11 Hz, for example, the NGI will be less than 20 dB for 50% of the possible samples if

- A 4.5-deg sector width is employed at a depth of 180 m (from Fig. C-2)
- A 3.2-deg sector width is employed at a depth of 500 m (from Fig. C-4).

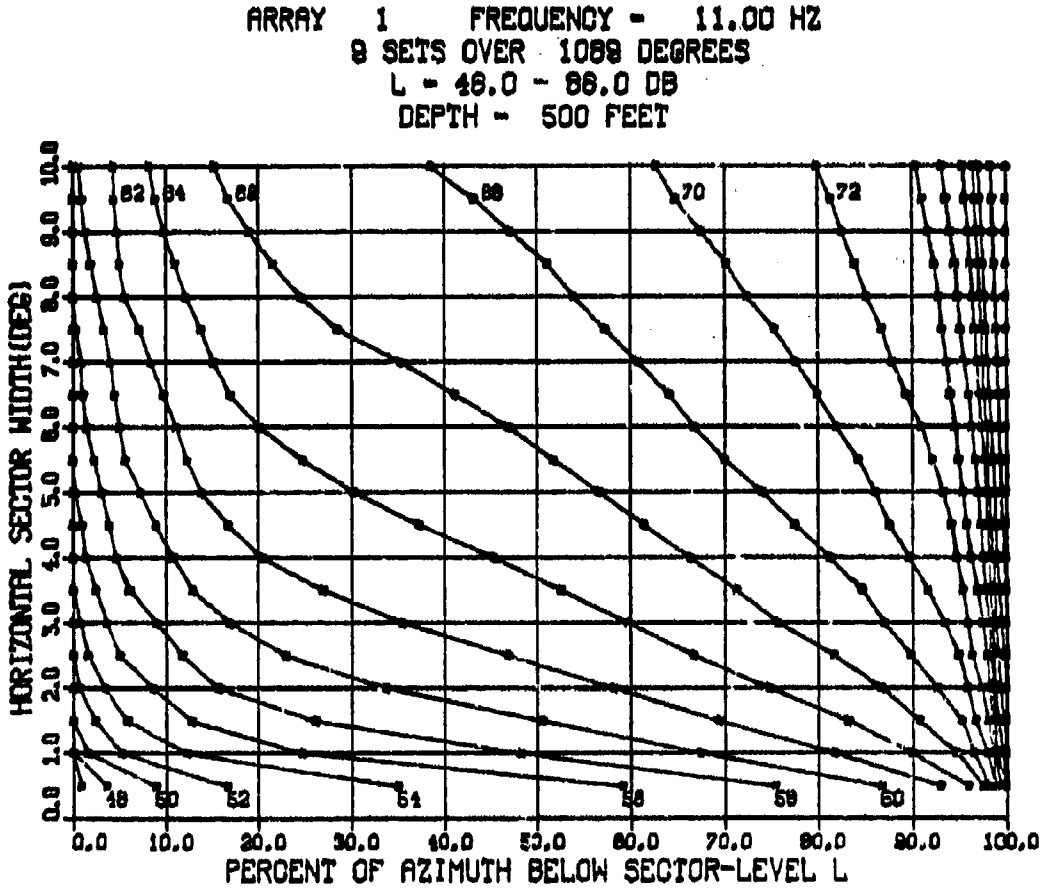

Figure C-1. (C) Azimuthal anisotropy characteristics for 11-Hz ambient noise measurements at a depth of 180 m. (U)

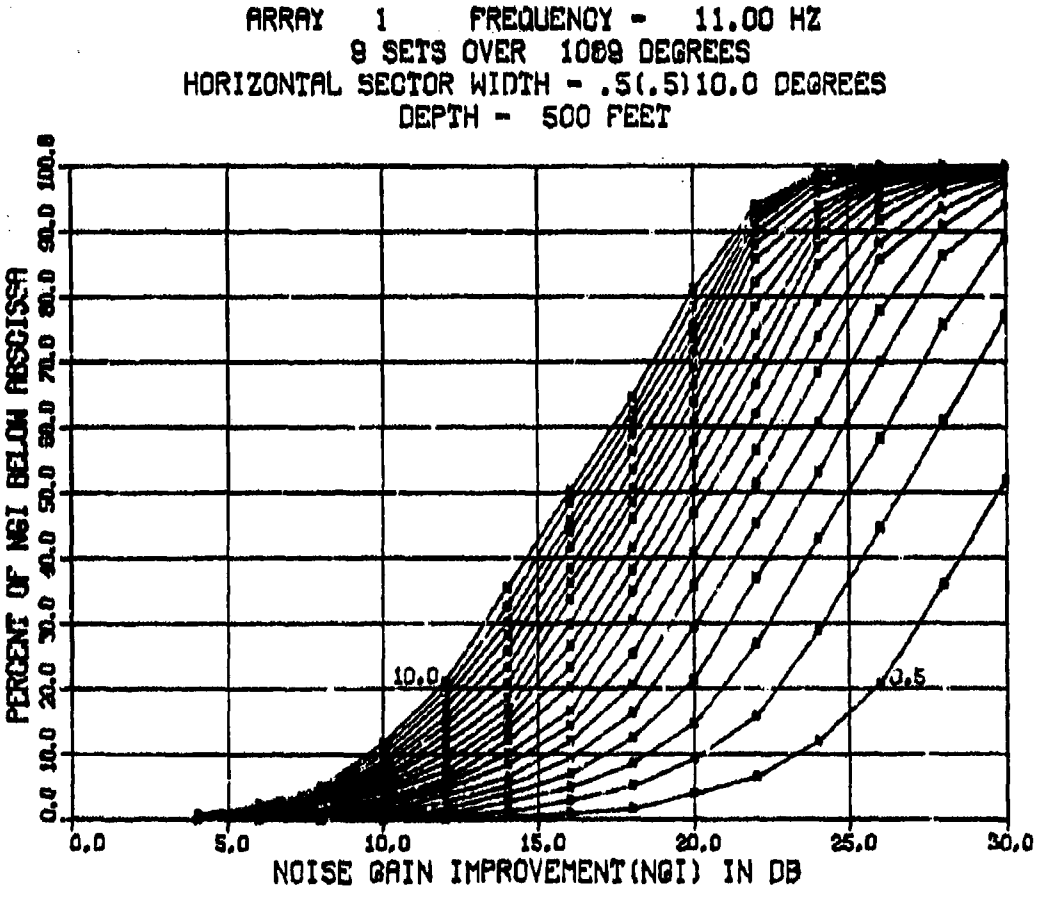

Figure C-2. (C) Noise gain improvement characteristics for 11-Hz ambient noise measurements at a depth of 180 m. (U)

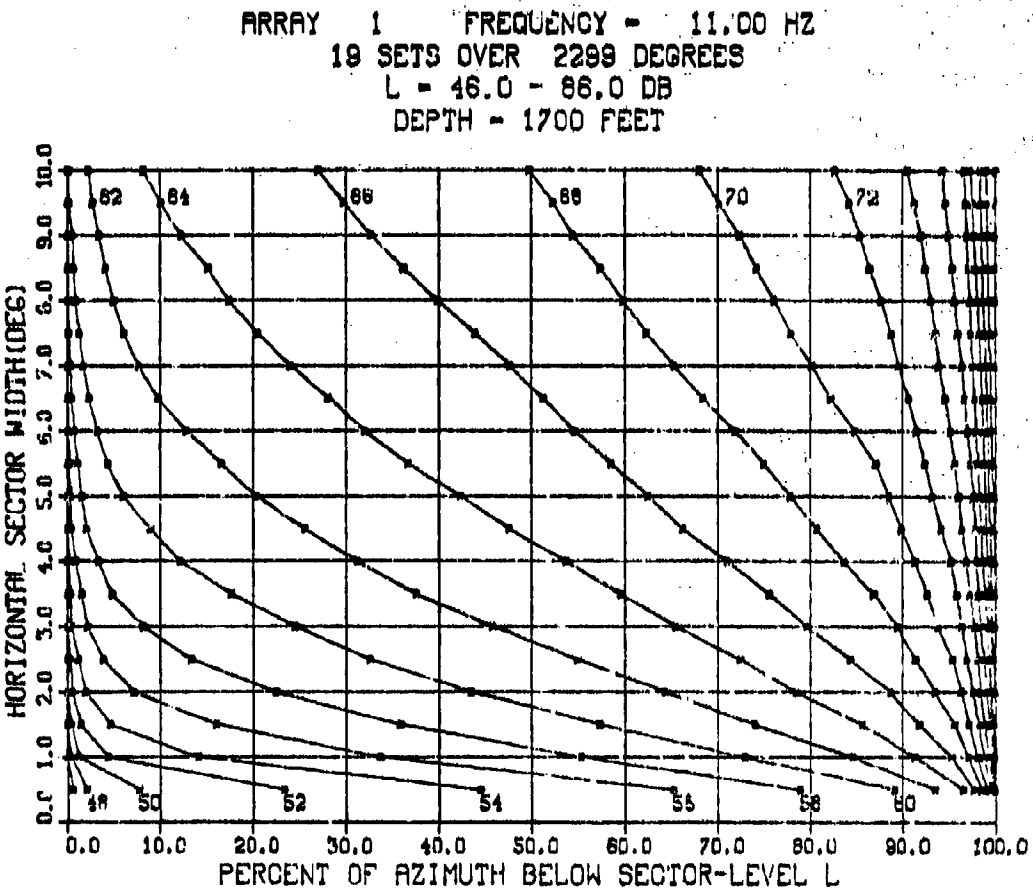

Figure C-3. (C) Azimuthal anisotropy characteristics for 11-Hz ambient noise measurements at a depth of 500 m. (U)

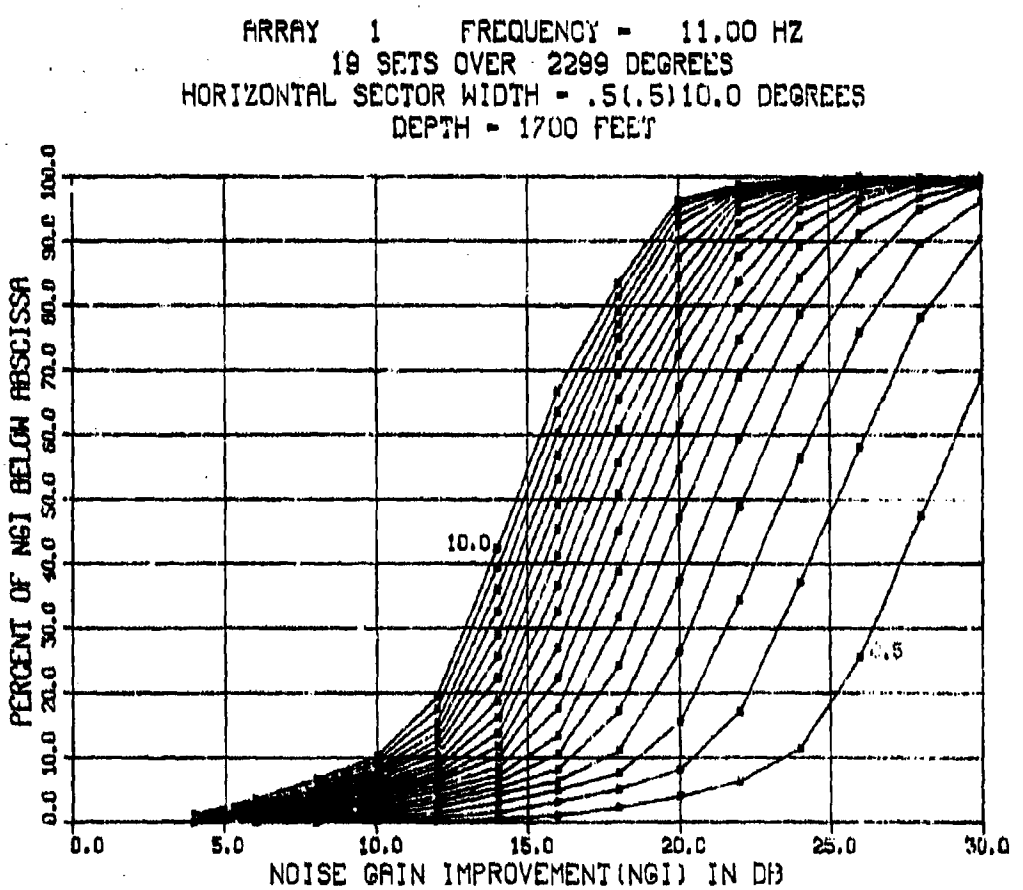

Figure C-4. (C) Noise gain improvement characteristics for 11-Hz ambient noise measurements at a depth of 500 m. (U)

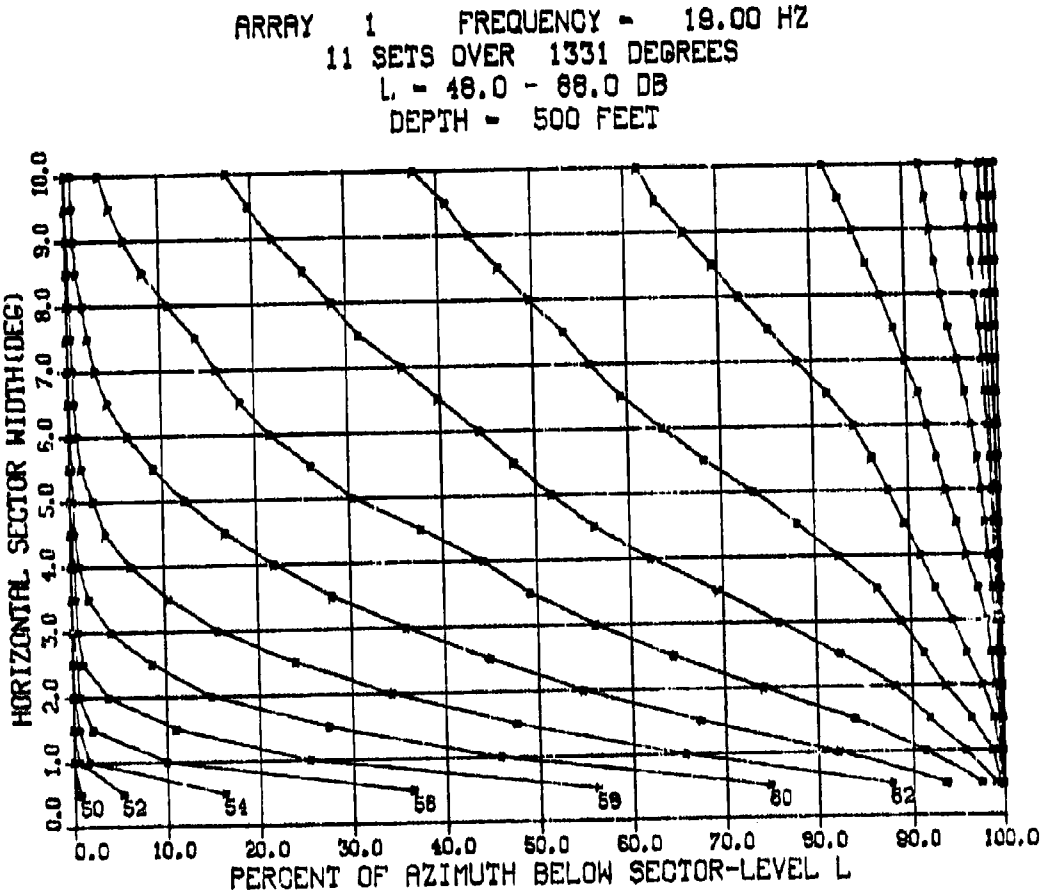

Figure C-5. (C) Azimuthal anisotropy characteristics for 19-Hz ambient noise measurements at a depth of 180 m. (U)

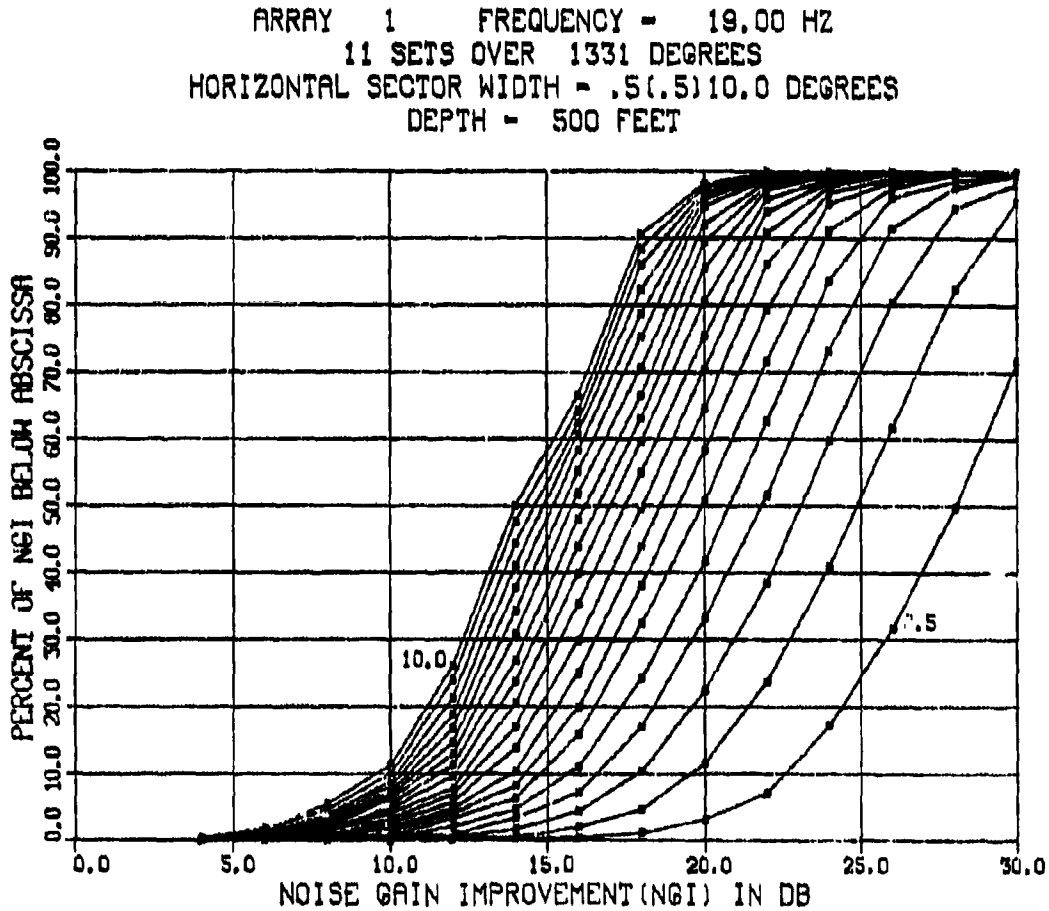

Figure C-6. (C) Noise gain improvement characteristics for 19-Hz ambient noise measurements at a depth of 180 m. (U)

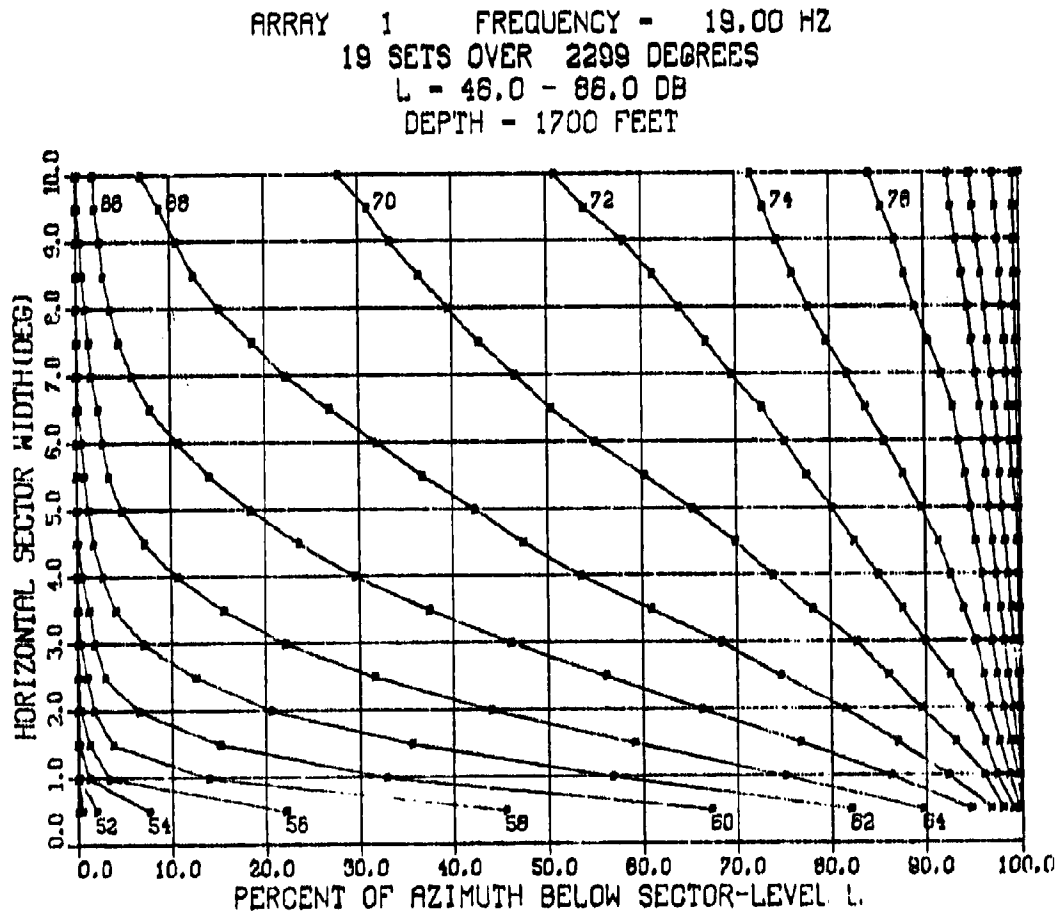

Figure C-7. (C) Azimuthal anisotropy characteristics for 19-Hz ambient noise measurements at a depth of 500 m. (U)

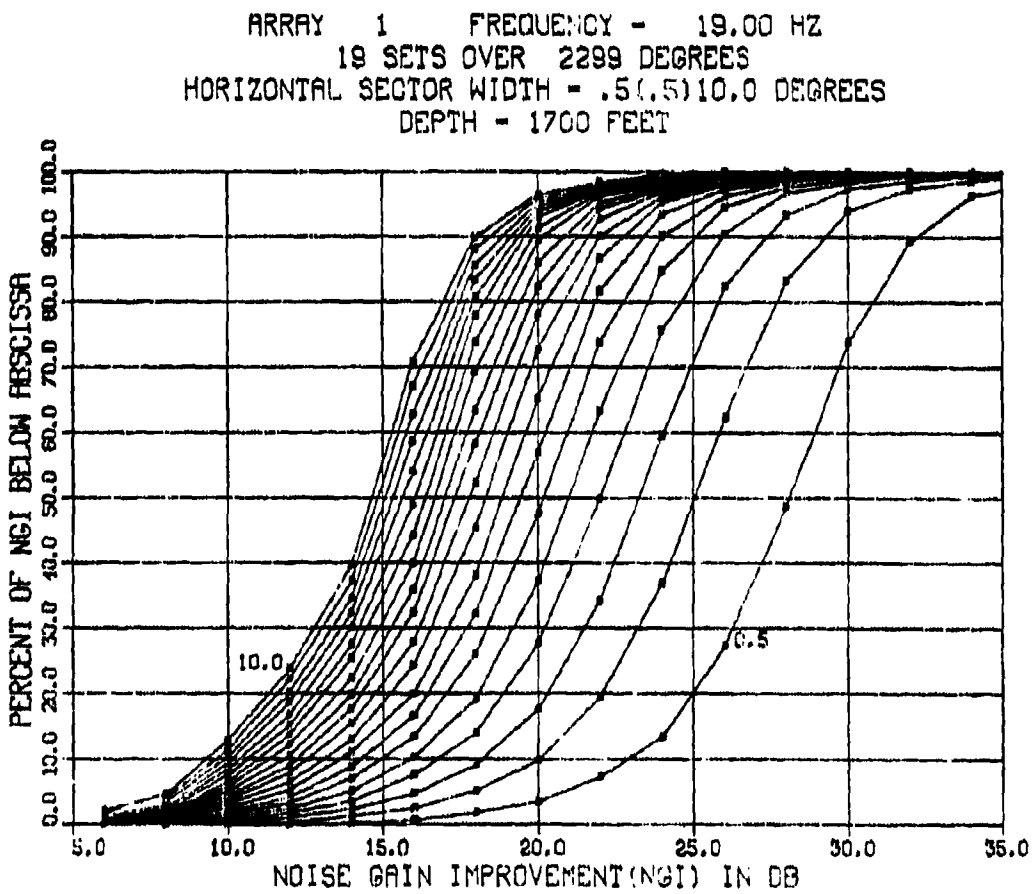

Figure C-8. (C) Noise gain improvement characteristics for 19-Hz ambient noise measurements at a depth of 500 m. (U)

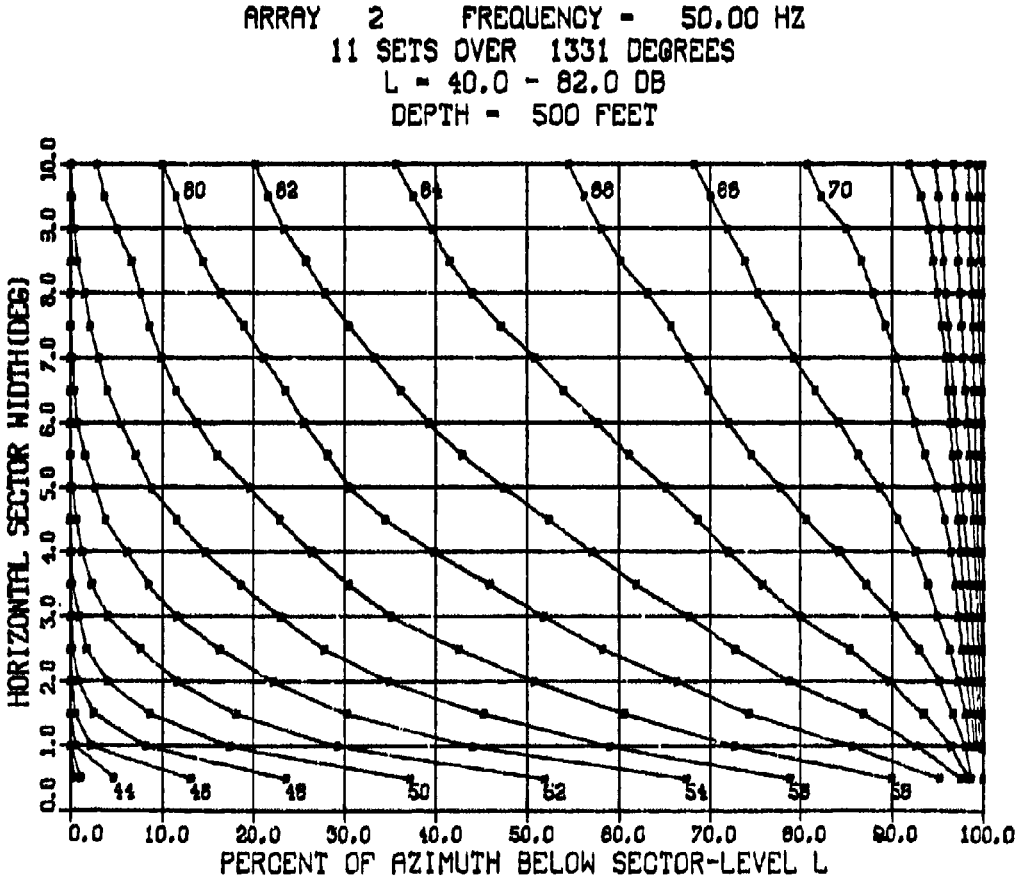

Figure C-9. (C) Azimuthal anisotropy characteristics for 50-Hz ambient noise measurements at a depth of 180 m. (U)

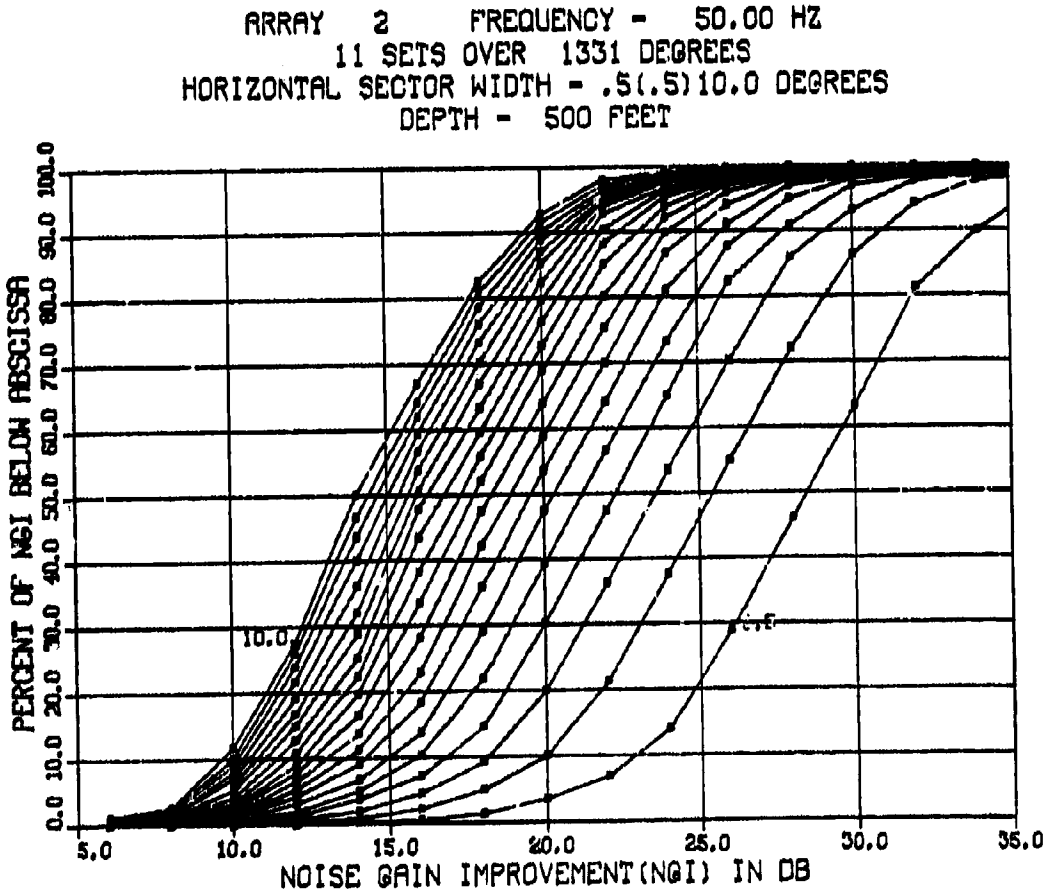

Figure C-10. (C) Noise gain improvement characteristics for 50-Hz ambient noise measurements at a depth of 180 m. (U)

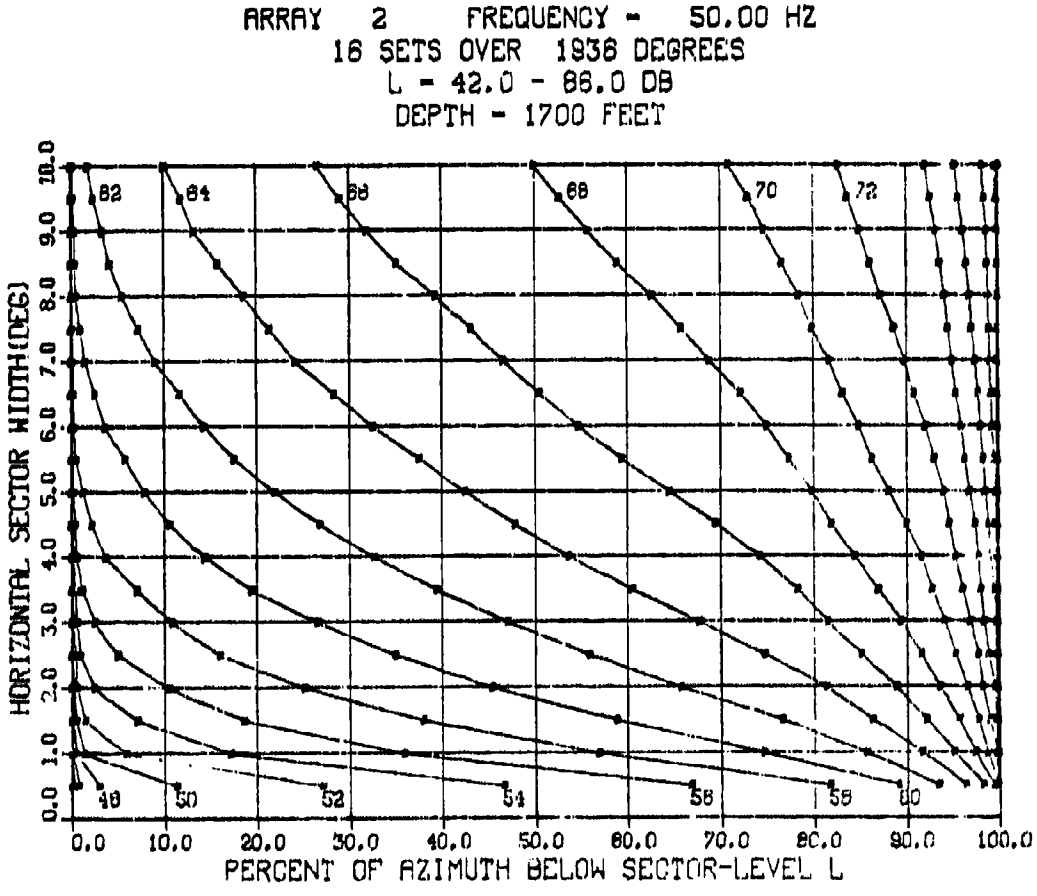

Figure C-11. (C) Azimuthal anisotropy characteristics for 50-Hz ambient noise measurements at a depth of 500 m. (U)

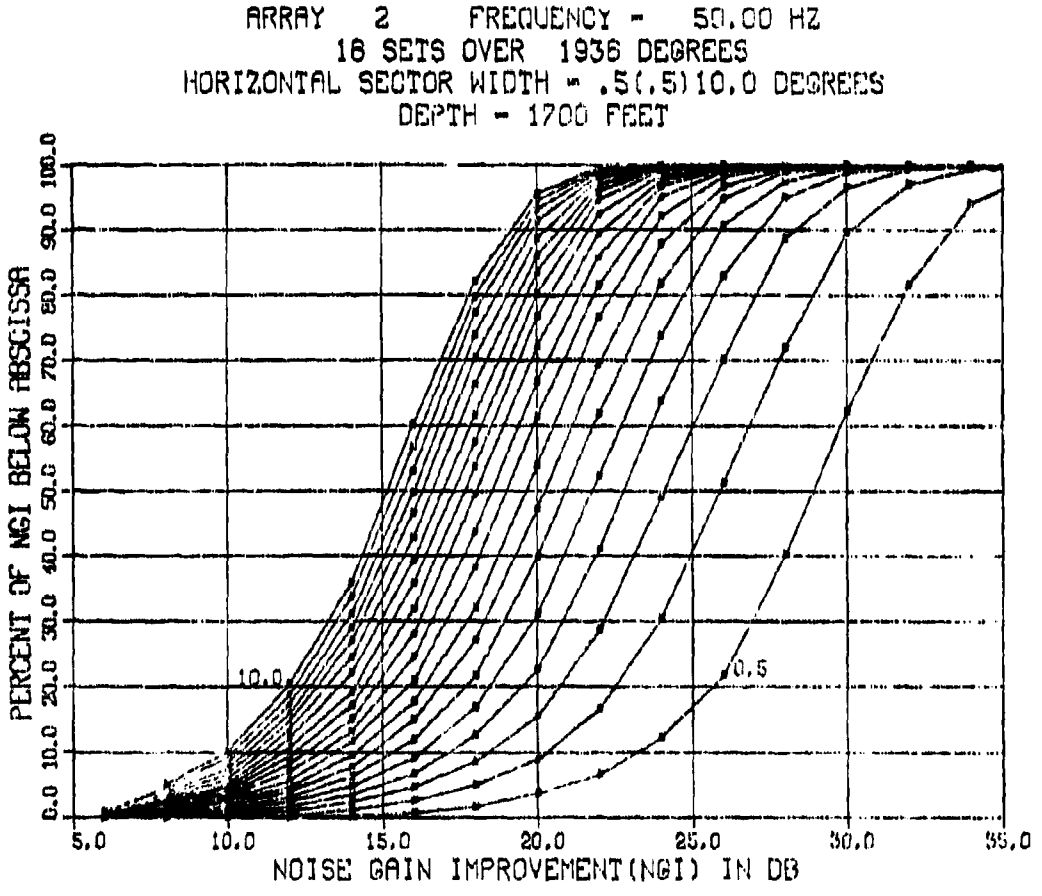

Figure C-12. (C) Noise gain improvement characteristics for 50-Hz ambient noise measurements at a depth of 500 m. (U)

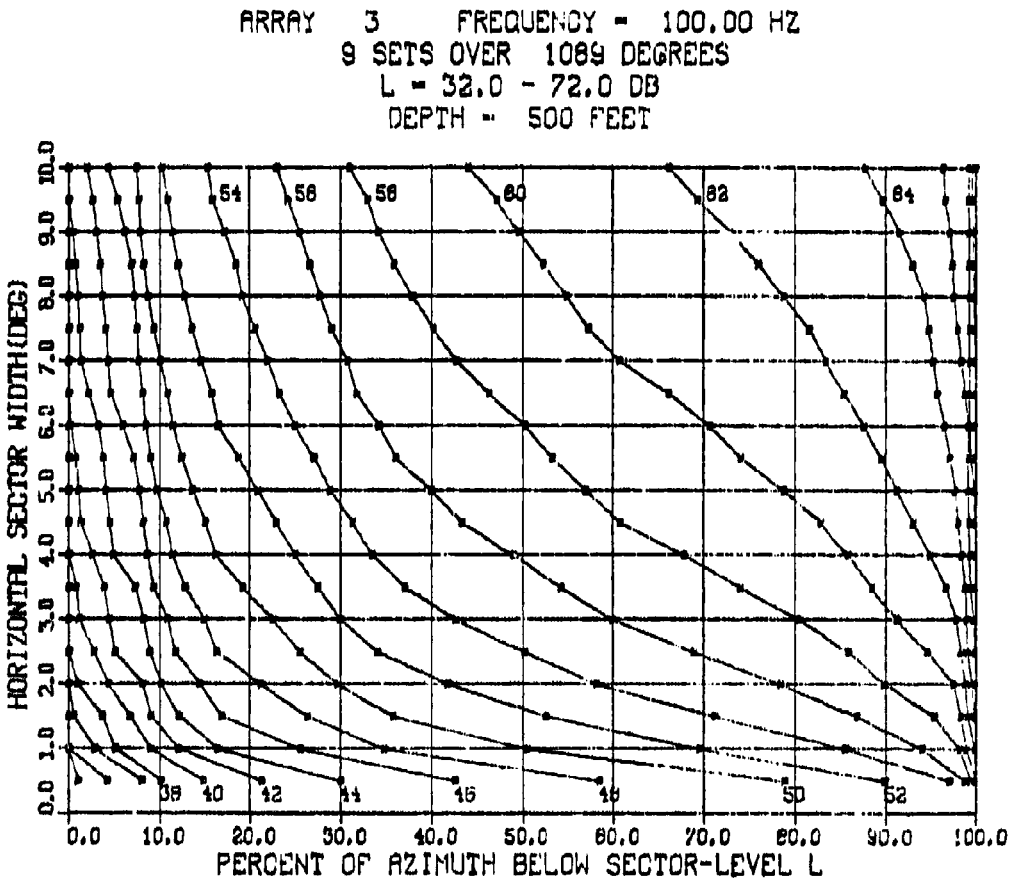

Figure C-13. (C) Azimuthal anisotropy characteristics for 100-Hz ambient noise measurements at a depth of 180 m. (U)

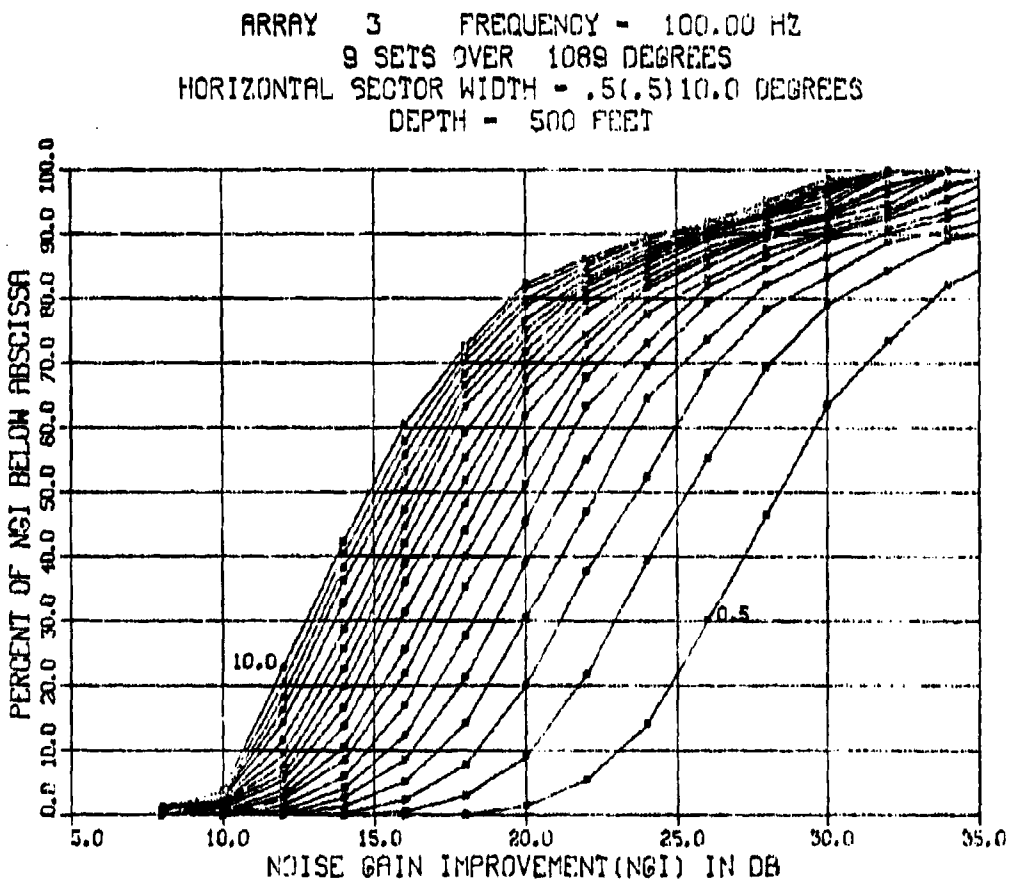

Figure C-14. (C) Noise gain improvement characteristics for 100-Hz ambient noise measurements at a depth of 180 m. (U)

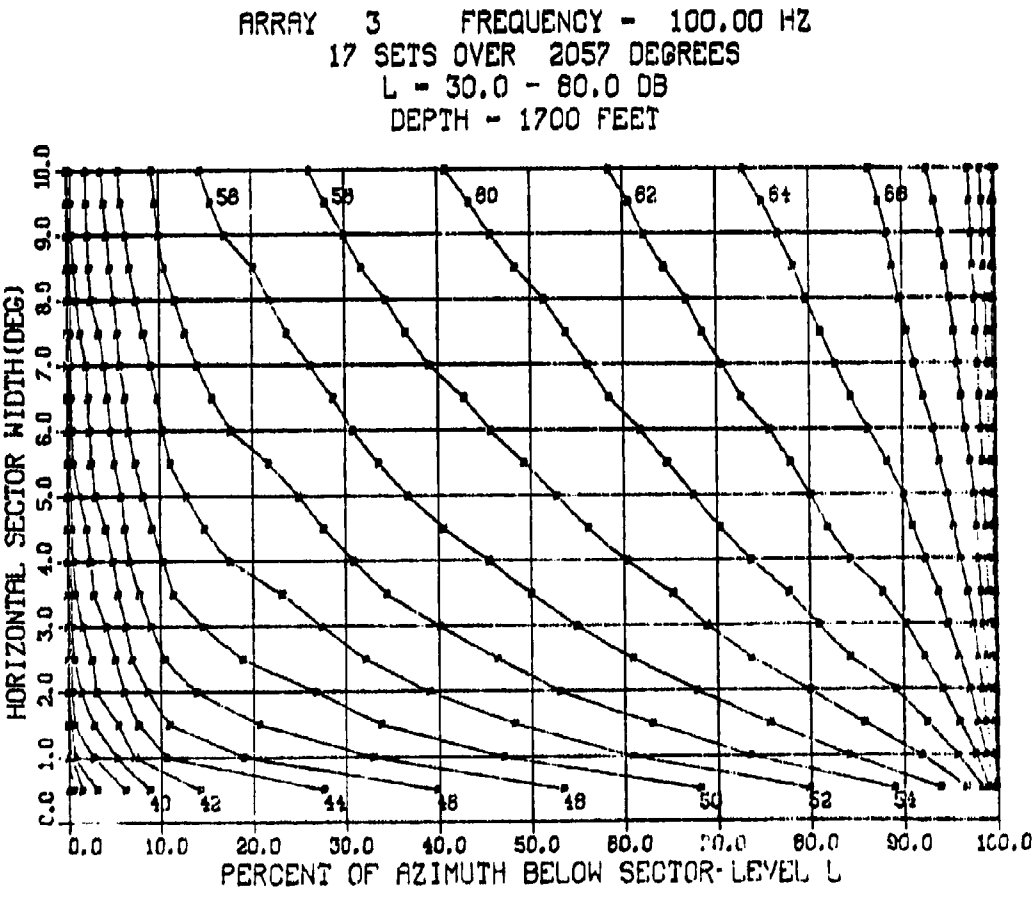

Figure C-15. (C) Azimuthal anisotropy characteristics for 100-Hz ambient noise measurements at a depth of 500 m. (U)

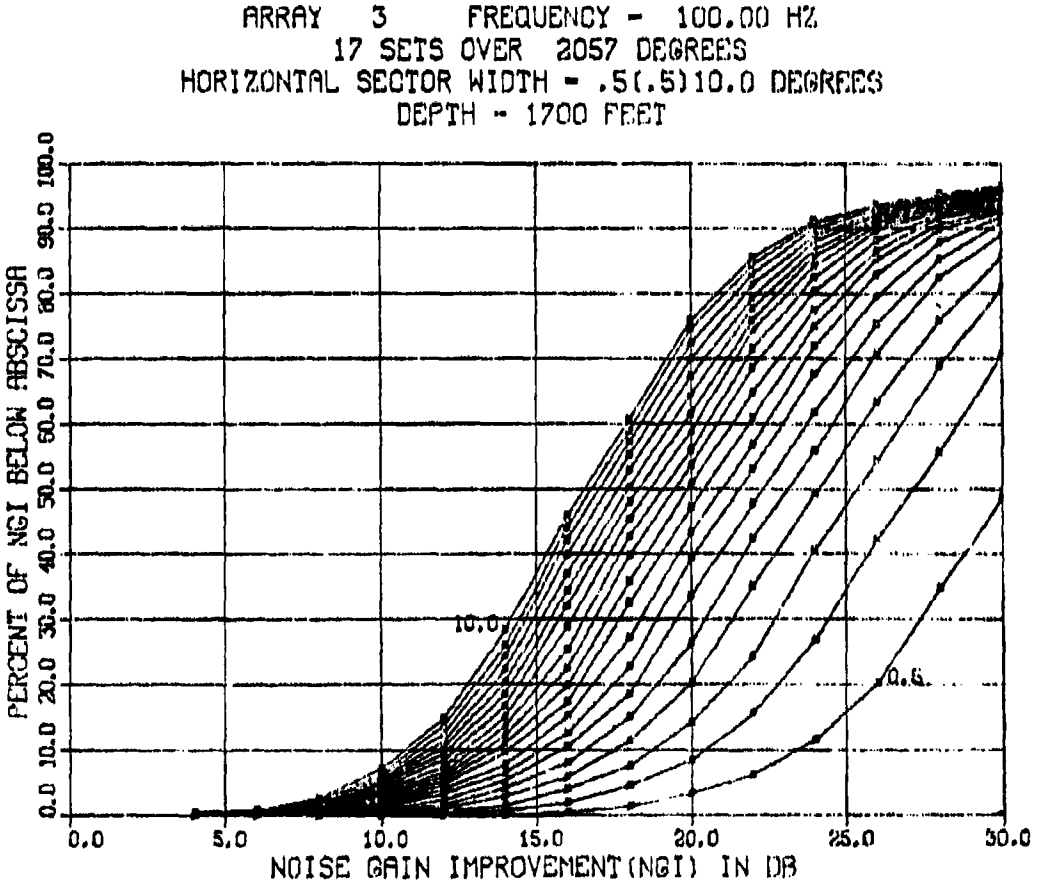

Figure C-16. (C) Noise gain improvement characteristics for 100-Hz ambient noise measurements at a depth of 500 m. (U)

DEPARTMENT OF THE NAVY
OFFICE OF NAVAL RESEARCH
800 NORTH QUINCY STREET
ARLINGTON, VA 22217-5660

IN REPLY REFER TO
5510/1
Ser 43/885
03 Dec 03

MEMORANDUM FOR DISTRIBUTION LIST

Subj: DECLASSIFICATION OF CHURCH OPAL DOCUMENTS

Ref: (a) SECNAVINST 5510.36

Encl: (1) Partial List of CHURCH OPAL Documents

1. In accordance with reference (a), a declassification review has been conducted on a number of classified CHURCH OPAL documents.

2. The CHURCH OPAL documents listed in Part 1 of enclosure (1) have been downgraded to UNCLASSIFIED and have been approved for public release. These documents should be remarked as follows:

Classification changed to UNCLASSIFIED by authority of the Chief of Naval Operations (N774) letter N774D/3U630173, 11 September 2003.

DISTRIBUTION STATEMENT A: Approved for Public Release; Distribution is unlimited.

3. If other CHURCH OPAL documents are located in your repositories, their markings should be changed and a copy of the title page and a notation of how many pages the documents contained should be provided to Chief of Naval Research (ONR 43) 800 N. Quincy Street, Arlington, VA 22217-5660. This will enable me to maintain a master list of downgraded/declassified CHURCH OPAL reports.

4. Questions may be directed to the undersigned on (703) 696-4619, DSN 426-4619.

Peggy Lambert

PEGGY LAMBERT
By direction

DISTRIBUTION LIST:
See page 2

Subj: DECLASSIFICATION OF CHURCH OPAL DOCUMENTS

DISTRIBUTION LIST:
NAVOCEANO (Code N121LC - Jaime Ratliff)
NRL Washington (Code 5596.3 - Mary Templeman)
PEO LMW Det San Diego (PMS 181-1) (LTJG Ken Larson, USN)
DTIC-OCQ (Larry Downing)
ARL, U of Texas (David Knobles)
BlueSea Corporation (Roy Gaul)
ONR 32B (CAPT Houtman)
ONR 321 (Dr. Livingston)
ONR 03B (Mr. Lackie)

Title: CHURCH OPAL ENVIRONMENTAL ACOUSTIC SUMMARY
Formerly SECRET
Author: Unknown
Originator: Naval Ocean R&D Activity
Ref. No.: LRAPP RS 77-002 Date: April 1977
Available at NRL (529148), MC/NAVOCEANO (85006869) and ARL:UT (51577)

Title: CHURCH OPAL EXERCISE OPERATIONS SUMMARY AND DATA INVENTORY
Formerly SECRET
Author: Unknown
Originator: Xonics, Inc.
Ref. No.: Xonics 1099
Date: October 1976
Available at MC/NAVOCEANO (85028383)

Title: HORIZONTAL DIRECTIONALITY OF AMBIENT NOISE DURING THE CHURCH OPAL EXERCISE
Formerly SECRET
DTIC No.: AD C017 835
Author: Wagstaff, R. A.
MCS No.: 85007295
Originator: Naval Ocean Systems Center
Ref. No.: NOSC TR394
Date: October 1978
Available at MC/NAVOCEANO (85007295)

Title: OTH RADAR SURVEILLANCE AT WARF DURING THE LRAPP CHURCH OPAL EXERCISE
Formerly SECRET
DTIC No.: AD CO10 483
Author: Barnum, J. R.
MCS No.: 85010085
Originator: Stanford Research Institute
Ref. No.: TR39S231
Date: March 1977
Available at MC/NAVOCEANO (85010085) and NRL (528986)

Title: CHURCH OPAL Exercise Summary, 1 September 1975 - Xonics, Inc
Formerly CONFIDENTIAL
DTIC No.: AD C004 343
Available at NRL (516165), ARL:UT (??) and MC/NAVOCEANO (??)

Title: CHURCH OPAL EXERCISE PLAN
Formerly SECRET
Author: none
Originator: Xonics, Inc and Office of Naval Research
Ref No: Xonics 1101
Date: August 1975
Available at NRL (521309), ARL:UT (55397) and MC/NAVOCEANO (??)